Electronic Supplementary Material (ESI) for Dalton Transactions.
This journal is © The Royal Society of Chemistry 2015

Supporting Information

Mononuclear iron(II) complex: cooperativity, kinetics and activation energy of solvent-dependent spin transition

Mark B. Bushuev,*[a,b] Denis P. Pishchur,[a] Vladimir A. Logvinenko,[a,b] Yuri V. Gatilov,[b,c] Ilya V. Korolkov,[a,b] Inna K. Shundrina,[b,c] Elena B. Nikolaenkova[c] and Viktor P. Krivopalov[c]

[a]Nikolaev Institute of Inorganic Chemistry, Siberian Branch of Russian Academy of Sciences, 3, Acad. Lavrentiev Ave., Novosibirsk, 630090, Russia
[b]Novosibirsk State University, 2, Pirogova str., Novosibirsk, 630090, Russia
[c]N. N. Vorozhtsov Novosibirsk Institute of Organic Chemistry, Siberian Branch of Russian Academy of Sciences, 9, Acad. Lavrentiev Ave., Novosibirsk, 630090, Russia

Contents

1. CHEMISTRY

General

The synthesis was carried out in deoxygenated EtOH under an inert atmosphere of argon using standard glovebox techniques. The ligand L was prepared according to the procedure previously reported.[S1] All other reagents and solvents were commercially available and were used without additional purification. Elemental analysis (C, H, N) was performed with a EuroEA3000 analyzer using standard technique.

S1 M. B. Bushuev, Y. V.Gatilov, E. B. Nikolaenkova, V. G. Vasiliev and V. P. Krivopalov, *Inorg. Chim. Acta*, 2013, **395**, 95.

Synthesis of $[FeL_2](BF_4)_2 \cdot EtOH \cdot H_2O$, ($1^{LS} \cdot EtOH \cdot H_2O$) and $[FeL_2](BF_4)_2 \cdot xH_2O$ (β-$1^{LS} \cdot xH_2O$)

A solution of L (0.040 mmol, 10.6 mg) in EtOH (0.7 mL) was added to a solution of $Fe(BF_4)_2 \cdot 6H_2O$ (0.020 mmol, 6.8 mg) in EtOH (0.7 mL). The solution turned dark red. Dark red needle crystals began to form in ca. 1 min. The formation of a new crystalline phase (prismatic well shaped dark red crystals) was detected in 2 – 3 days. Transformation of needle crystals into prismatic ones took ca. 2 weeks. After that, the prismatic crystals were filtered off, washed with EtOH, and dried in the ambient air. Yield: 14.0 mg (86%). Elemental analysis for a freshly prepared sample (%), calcd for $C_{32}H_{38}N_{10}B_2F_8FeO_2$ ($[FeL_2](BF_4)_2 \cdot EtOH \cdot H_2O$, 824.18): C 46.6, H 4.4, N 17.0; found C 46.9, H 4.4, N 16.8.

In the ambient air the crystals of $\mathbf{1^{LS} \cdot EtOH \cdot H_2O}$ lose the solvent molecules transforming into the phase $\mathbf{[FeL_2](BF_4)_2 \cdot xH_2O}$ ($\mathbf{\beta\text{-}1^{LS} \cdot xH_2O}$). Elemental analysis for a sample after staying at room temperature in the ambient air for four days (%), calcd for $C_{32}H_{37}N_{10}B_2F_8FeO$ ($[FeL_2](BF_4)_2 \cdot H_2O$, 778.11): C 46.3, H 4.1, N 18.0; found C 46.7, H 4.3, N 17.8. Elemental analysis for a sample after staying at room temperature in the ambient air for a month (%), calcd for $C_{32}H_{37}N_{10}B_2F_8FeO$ ($[FeL_2](BF_4)_2 \cdot H_2O$, 778.11): C 46.3, H 4.1, N 18.0; found C 46.4, H 4.0, N 18.1. This tendency shows that EtOH molecules easily evaporate even at room temperature.

2. CRYSTAL STRUCTURES

Experimental details

The data were collected with crystals of $[FeL_2](BF_4)_2 \cdot EtOH \cdot H_2O$, $[FeL_2](BF_4)_2$ and $[FeL_2](BF_4)_2 \cdot y EtOH \cdot zH_2O$ (y = 0.41, z = 0.40) with a Bruker APEX II CCD diffractometer using graphite monochromated Mo-$K\alpha$ radiation ($[FeL_2](BF_4)_2 \cdot EtOH \cdot H_2O$ T = 200 K, $[FeL_2](BF_4)_2$ T = 296 K, $[FeL_2](BF_4)_2 \cdot y EtOH \cdot zH_2O$ (y = 0.41, z = 0.40) T = 296 K; λ = 0.71073 Å). The structures were solved by direct methods and the refinement on F^2 and all further calculations were carried out with the SHELX suite.[S2] All non-hydrogen and major parts of disordered atoms were refined anisotropically. All disordered parts were refined with restraints. Hydrogen atoms were placed geometrically on their carrier atoms and were refined with a riding model.

S2 G. M. Sheldrick, *Acta Crystallogr*., 2015, **C71**, 3 – 8.

Crystallographic data for $[FeL_2](BF_4)_2 \cdot EtOH \cdot H_2O$ ($\mathbf{1^{LS} \cdot EtOH \cdot H_2O}$)

Formula $C_{32}H_{38}B_2F_8FeN_{10}O_2$, M = 824.19, monoclinic, space group $P2/c$, a = 16.9811(4), b = 11.3326(3), c = 20.1037(6) Å, β = 105.433(1)°, V = 3729.26(17) Å^3, Z = 4, D_{calc} = 1.468 g·cm^{-3}, μ = 0.490 mm^{-1}, min/max transmission = 0.916/0.954, θ_{max} = 27.9°, measured 70474, unique 8911 (R_{int} = 0.0351), observed [I_o>2 σ(I)] 7290 reflections, R_1 = 0.0513 (I_o), wR_2 = 0.1744 (all), Gof = 0.959, $\Delta\rho_{max}$ = 1.17, $\Delta\rho_{min}$ = -0.58 e·Å^{-3}, CCDC 1409266.

One tetrafluoroborate ion is disordered over two positions with occupancies 0.745(7):0.255(7). The ethanol molecules and water molecules (O2 and O3) are also disordered with occupancies 0.5:0.5. Hydrogen atoms of water molecules could not be found and were omitted in the structural model.

Crystallographic data for $[FeL_2](BF_4)_2$ ($\mathbf{1^{A/LS}}$)

After the thermal cycling of the samples **1**, **14** and **15** (high m/V ratio, parent phase $\mathbf{1^{LS} \cdot EtOH \cdot H_2O}$, see below) had been done we found that the samples looked like bunches of single crystals and managed to find one suitable for X-ray single crystal analysis. The single crystal which appeared to be that one of the phase $\mathbf{1^{A/LS}}$ was taken from the sample **14**.

Formula $C_{30}H_{30}B_2F_8FeN_{10}$, M = 760.11, orthorhombic, space group $Pbca$, a = 12.8079(14), b = 19.1932(19), c = 27.373(3) Å, V = 6729.1(12) Å^3, Z = 8, D_{calc} = 1.501 g·cm^{-3}, μ = 0.532 mm^{-1}, min/max transmission = 0.605/0.970, θ_{max} = 25.4°, measured 61787, unique 6143 (R_{int} = 0.1356), observed [I_o>2 σ(I)] 3840 reflections, R_1 = 0.0653 (I_o), wR_2 = 0. 2179 (all), Gof = 0.901, $\Delta\rho_{max}$ = 0.74, $\Delta\rho_{min}$ = –0.51 e·Å^{-3}, CCDC 1409267.

Both tetrafluoroborate ion are disordered over two positions with occupancies 0.61(1):0.39(1) and 0.613(9):0.387(9).

Crystallographic data for $[FeL_2](BF_4)_2 \cdot y$EtOH $\cdot z H_2O$ ($1^{E/LS} \cdot y$EtOH $\cdot z H_2O$)

A single crystal of the phase $\mathbf{1^{E/LS} \cdot}$ ***y*EtOH** $\cdot$ $\boldsymbol{zH_2O}$ (y = 0.41, z = 0.40) suitable for X-ray analysis was taken from the sample **21** after thermal cycling.

Formula $C_{30.82}H_{33.26}B_2F_8FeN_{10}O_{0.81}$, M = 786.20, monoclinic, space group $C2/c$, a = 46.241(3), b = 8.2140(5), c = 18.5849(10) Å, β = 93.444(4)°, V = 7046.3(7) Å^3, Z = 8, D_{calc} = 1.482 g·cm^{-3}, μ = 0.512 mm^{-1}, min/max transmission = 0.831/0.912, θ_{max} = 25.4°, measured 50445, unique 6402 (R_{int} = 0.0475), observed [I_o>2 σ(I)] 5086 reflections, R_1 = 0.0715 (I_o), wR_2 = 0.1968 (all), Gof = 1.133, $\Delta\rho_{max}$ = 0.78, $\Delta\rho_{min}$ = –0.46 e·Å^{-3}, CCDC 1409268.

One tetrafluoroborate ion, ethanol and water molecules are disordered over two positions with occupancies 0.37(2):0.63(2), 0.41(1):0.41(1), 0.40(1):0.40(1) accordingly.

Table S1

Selected bond lengths (Å) and angles (°) in the crystal structures of $[FeL_2](BF_4)_2 \cdot EtOH \cdot H_2O$, $[FeL_2](BF_4)_2$ and $[FeL_2](BF_4)_2 \cdot 0.41EtOH \cdot 0.4H_2O$.

Bond length	$\mathbf{1^{LS} \cdot EtOH \cdot H_2O}$	$\mathbf{1^{A/LS}}$	$\mathbf{1^{E/LS} \cdot 0.41EtOH \cdot 0.4H_2O}$
Fe(1)–N(2)	1.8882(18)	1.884(4)	1.889(3)
Fe(1)–N(3)	1.9869(19)	1.981(3)	1.983(4)
Fe(1)–N(5)	1.998(2)	1.982(4)	2.005(4)
Fe(1)–N(7)	1.8860(18)	1.882(4)	1.888(3)
Fe(1)–N(8)	1.983(2)	1.984(4)	1.982(4)
Fe(1)–N(10)	1.998(2)	1.992(4)	1.998(4)
Angle			
N(2)–Fe(1)–N(3)	80.80(8)	80.75(15)	80.68(15)
N(2)–Fe(1)–N(5)	79.28(8)	79.69(15)	79.06(14)
N(2)–Fe(1)–N(7)	178.46(8)	178.53(16)	179.21(15)
N(2)–Fe(1)–N(8)	100.53(8)	100.78(15)	99.47(15)
N(2)–Fe(1)–N(10)	99.13(8)	98.84(15)	100.51(15)
N(3)–Fe(1)–N(5)	160.00(8)	160.43(16)	159.64(14)
N(3)–Fe(1)–N(7)	98.44(8)	99.96(15)	98.63(15)
N(3)–Fe(1)–N(8)	90.70(8)	92.29(15)	93.29(15)
N(3)–Fe(1)–N(10)	92.34(8)	88.74(15)	89.38(15)
N(5)–Fe(1)–N(7)	101.52(8)	99.59(15)	101.65(15)
N(5)–Fe(1)–N(8)	91.24(8)	91.85(16)	88.20(15)
N(5)–Fe(1)–N(10)	92.50(8)	93.74(14)	96.13(15)
N(7)–Fe(1)–N(8)	80.80(8)	80.50(16)	80.91(15)
N(7)–Fe(1)–N(10)	79.54(8)	79.91(15)	79.10(15)
N(8)–Fe(1)–N(10)	160.34(8)	160.26(16)	160.01(15)

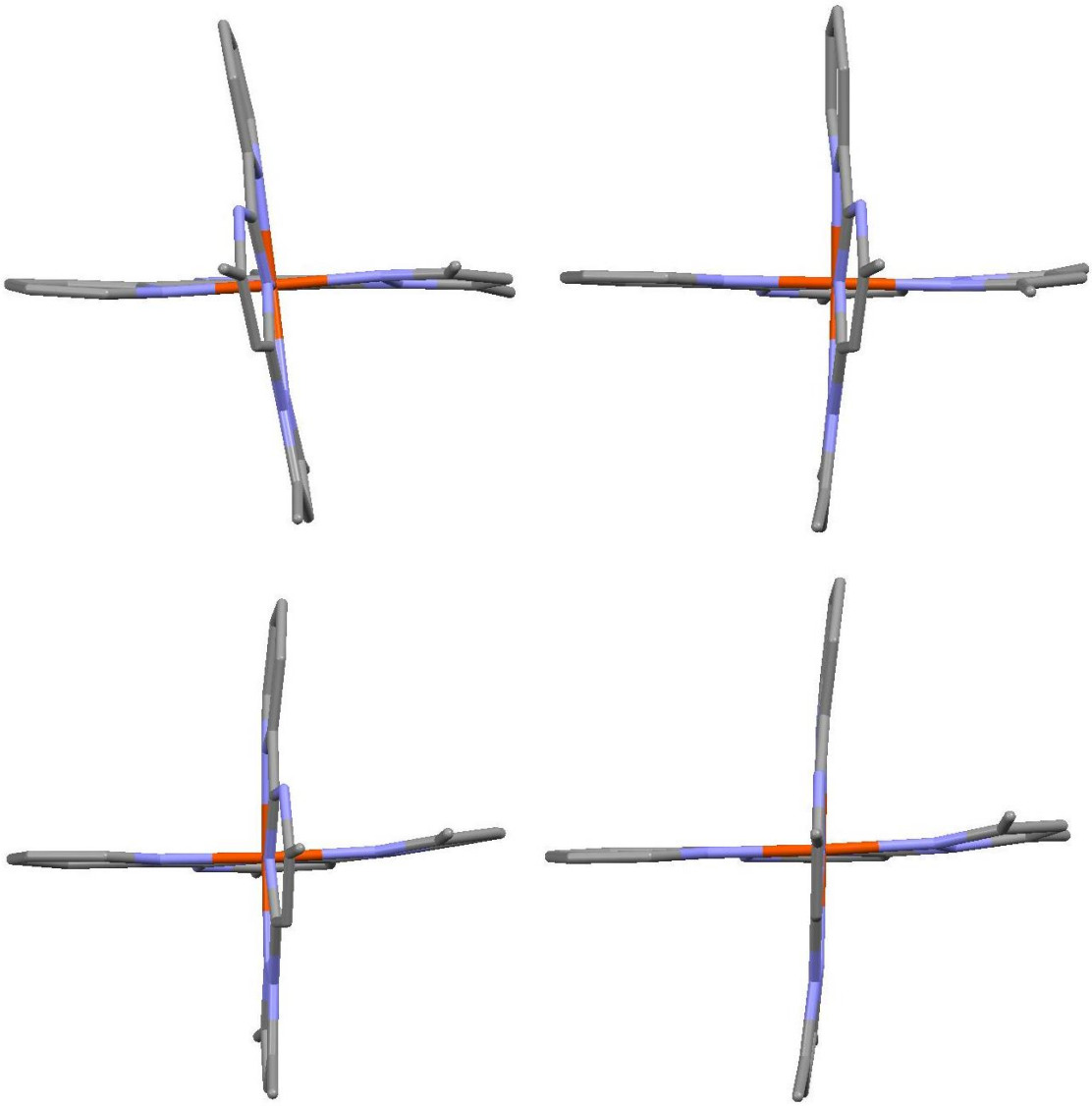

Figure S1. Structural distortions exhibited by $[FeL_2]^{2+}$ in the phases **α-1^{LS}·*x*H$_2$O** (top, left, φ = 177.4°, θ = 82.1°), **1^{LS}·EtOH·H$_2$O** (top, right, φ = 178.5°, θ = 88.0°), **1$^{A/LS}$** (bottom, left, φ = 178.6°, θ = 86.0°) and **1$^{E/LS}$**·***y*EtOH**·***z*H$_2$O** (bottom, right, φ = 179.2°, θ = 83.3°) . Hydrogen atoms are omitted for clarity.

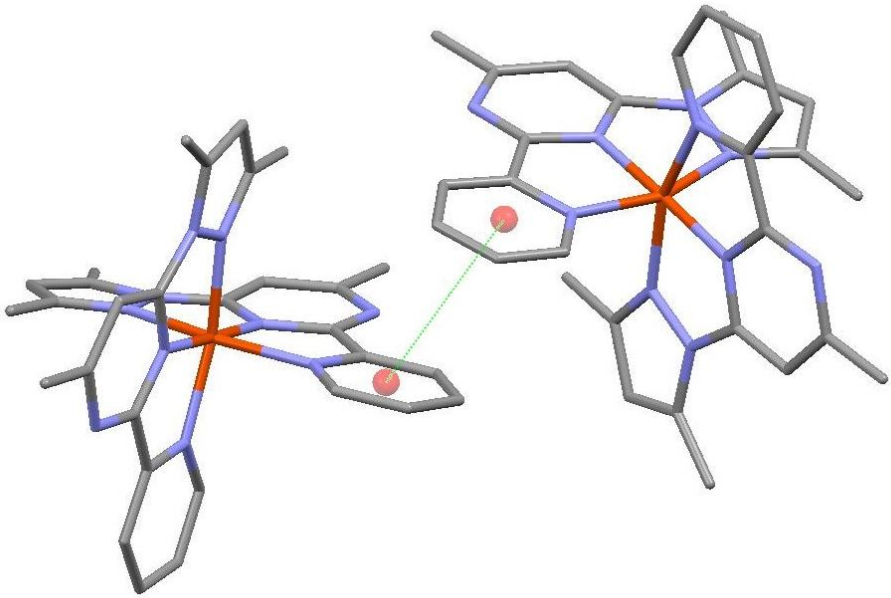

Figure S2. π-π stacking interactions between N3C6–C10 pyridine rings of neighboring FeL_2 units in the structure of $\mathbf{1^{LS}\cdot EtOH\cdot H_2O}$. Hydrogen atoms are omitted for clarity. Cg···Cg = 3.8829(16) Å, α = 15°, β = γ = 23.91°, where α is the dihedral angle between the planes I and J, β is the angle between the Cg(I)→Cg(J) vector and the normal to the plane I, γ is the angle between the Cg(I)→Cg(J) vector and the normal to the plane J.

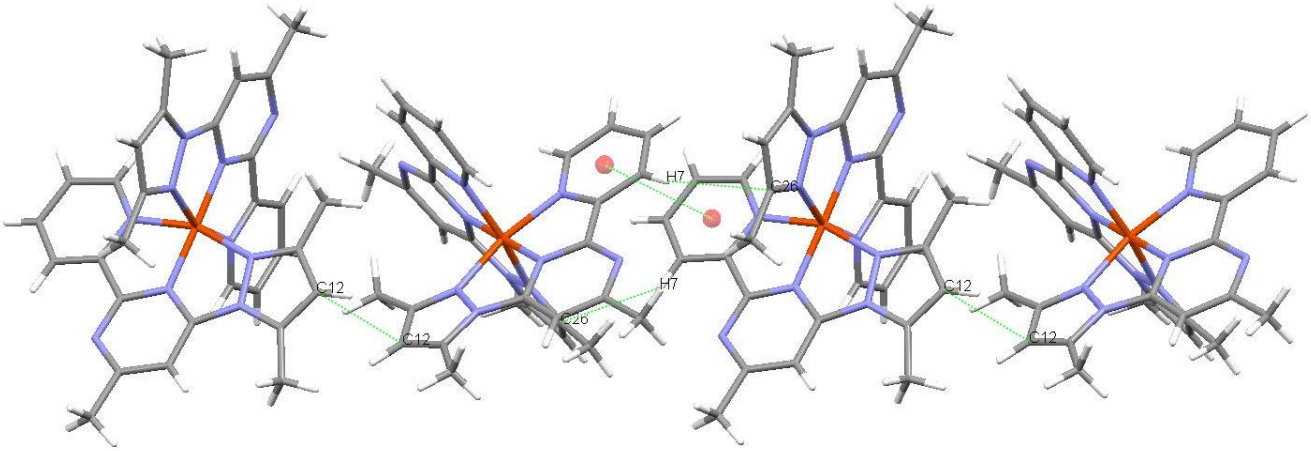

Figure S3. 1D-chain in the structure of $\mathbf{1^{LS}\cdot EtOH\cdot H_2O}$ (C12···C12 3.34 Å, H7···C26 2.85 Å).

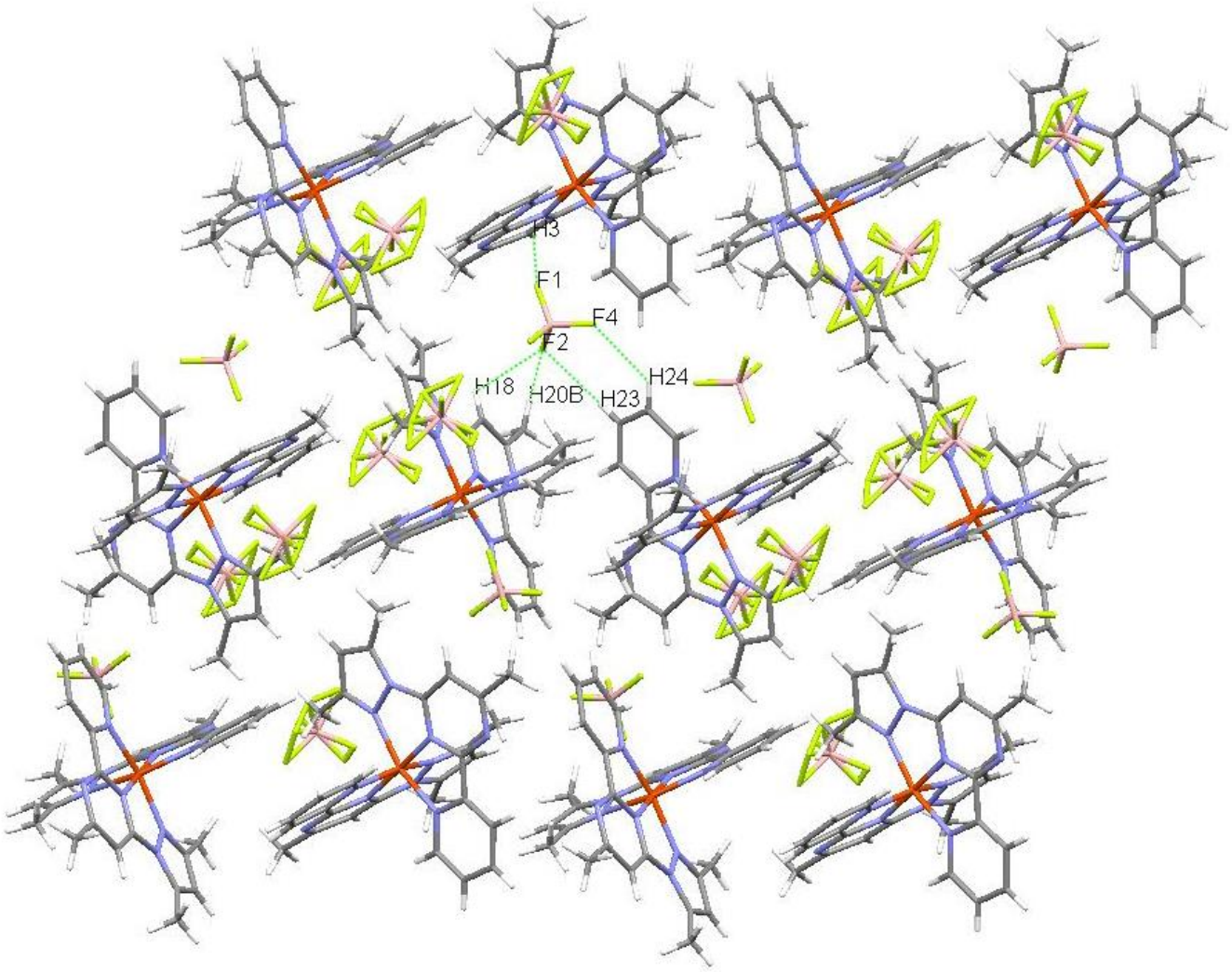

Figure S4. Packing of 1D chains in the structure of $\mathbf{1^{LS}\cdot EtOH\cdot H_2O}$. Short F···H contacts between the $[FeL_2]^{2+}$ cation and the non-disordered anion are shown (H3···F1 2.54 Å, H20B···F2 2.63 Å, H18···F2 2.62 Å, H23···F2 2.63 Å, H24···F4 2.66 Å).

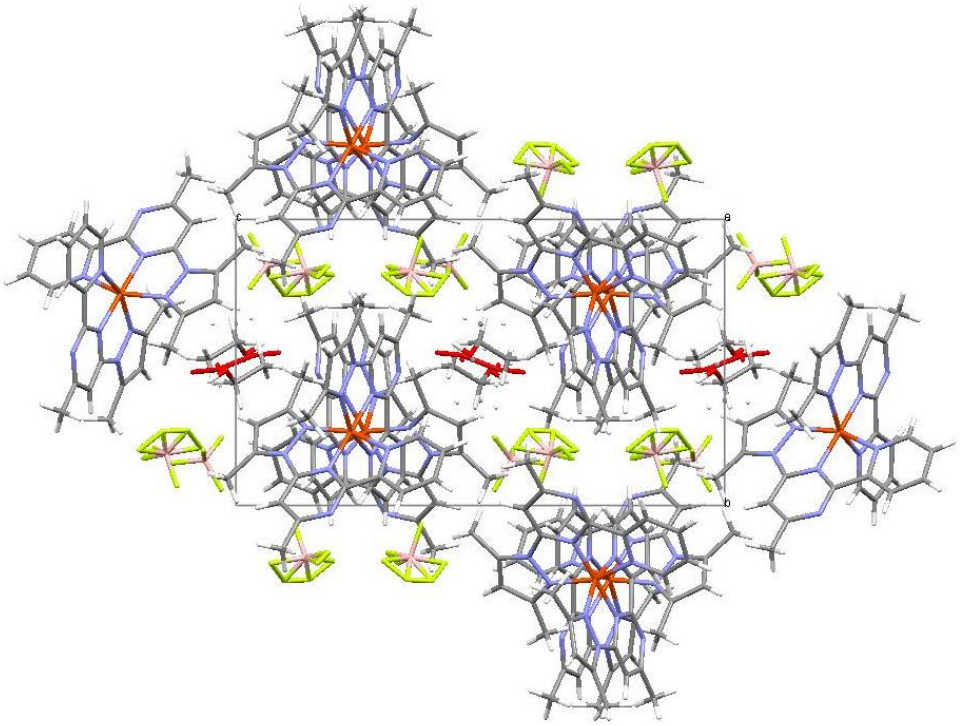

Figure S5. Packing diagram for $\mathbf{1^{LS}\cdot EtOH\cdot H_2O}$. View along the *a* axis.

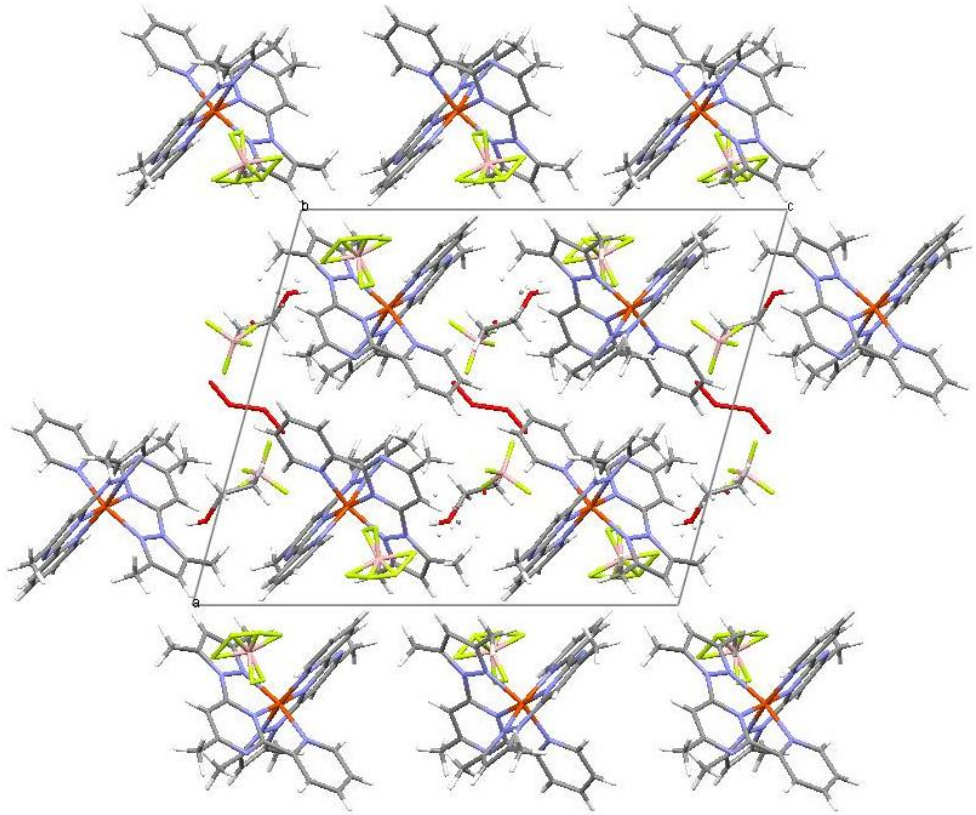

Figure S6. Packing diagram for $\mathbf{1^{LS}\cdot EtOH\cdot H_2O}$. View along the *b* axis.

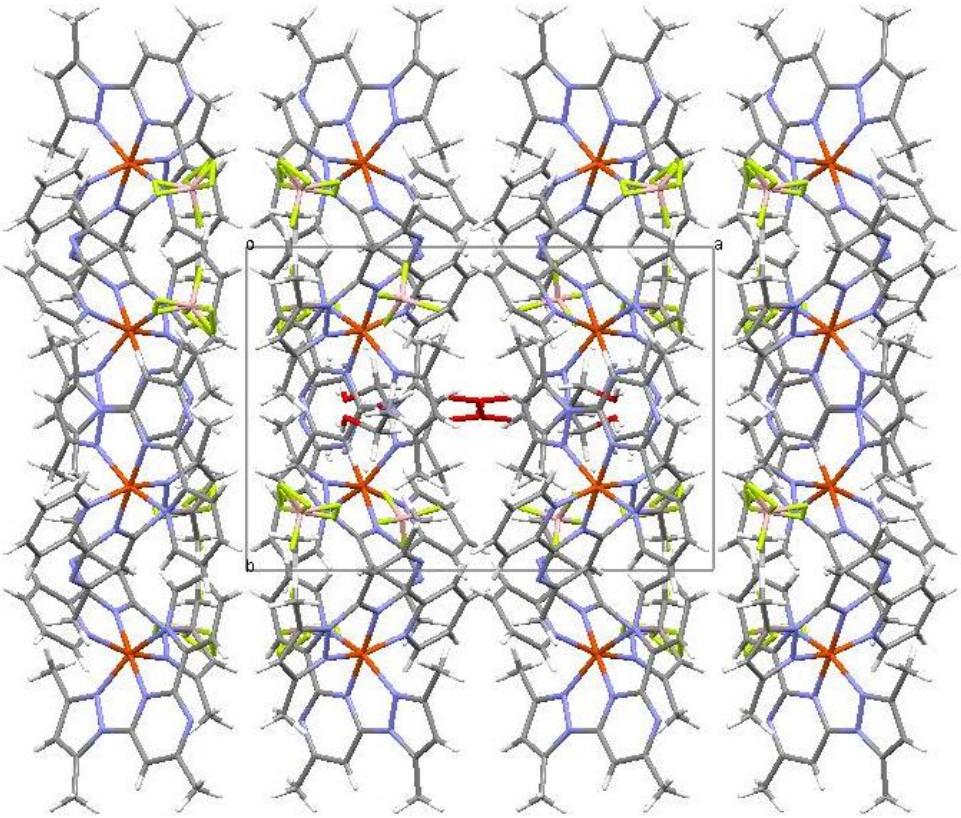

Figure S7. Packing diagram for $\mathbf{1^{LS}\cdot EtOH\cdot H_2O}$. View along the *c* axis.

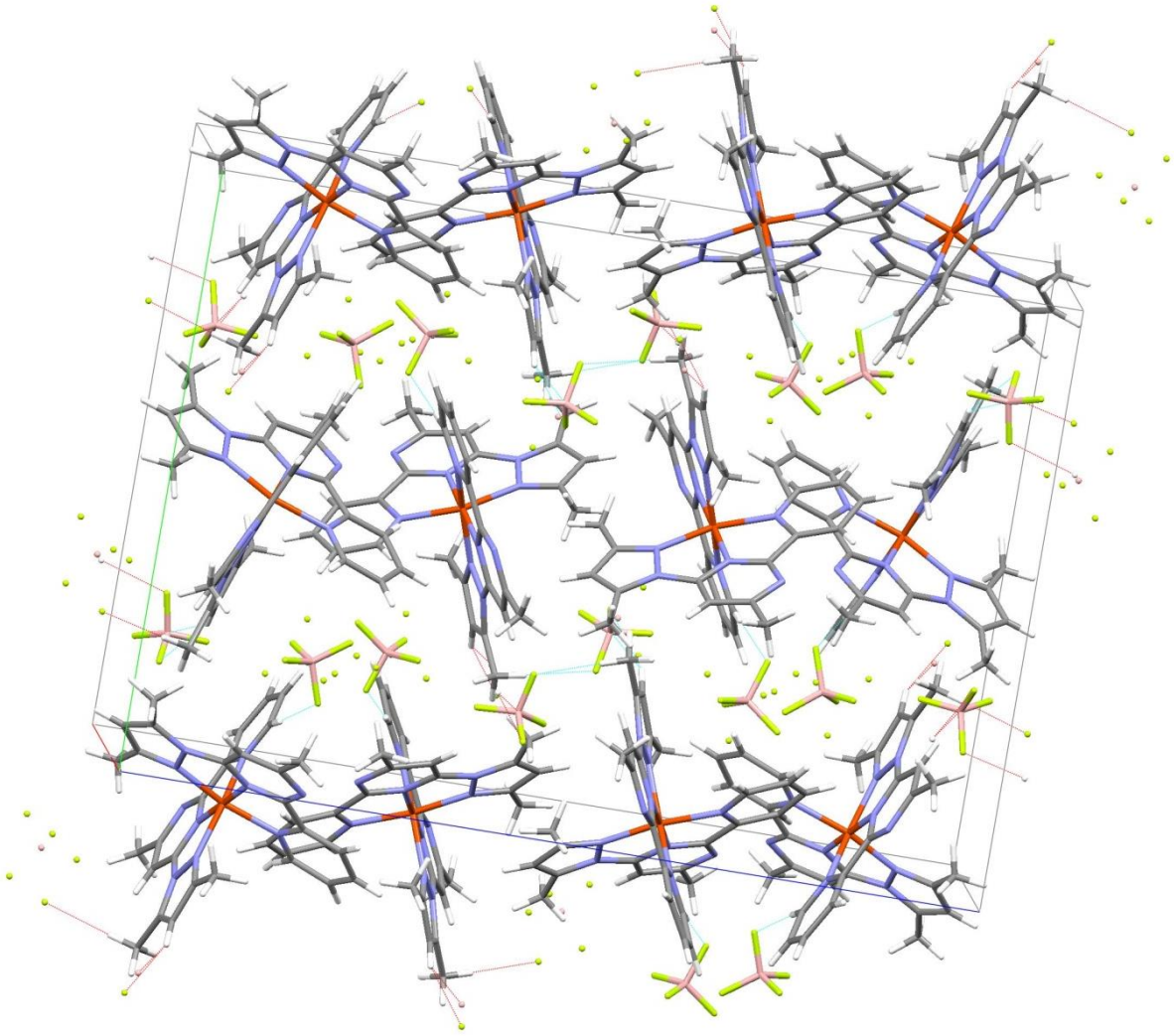

Figure S8. Packing diagram for $\mathbf{1}^{\mathbf{A/LS}}$. View along the *a* axis. Short contacts (less than sum of VDW radii by 0.2 Å) are also displayed.

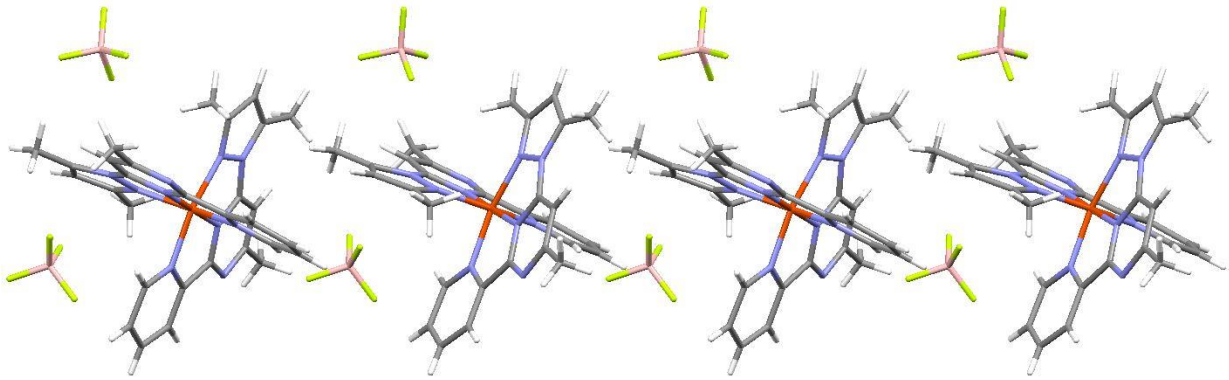

Figure S9. 1D chain in the structure of $\mathbf{1}^{\mathbf{A/LS}}$ (only one orientation for each disordered anion is shown).

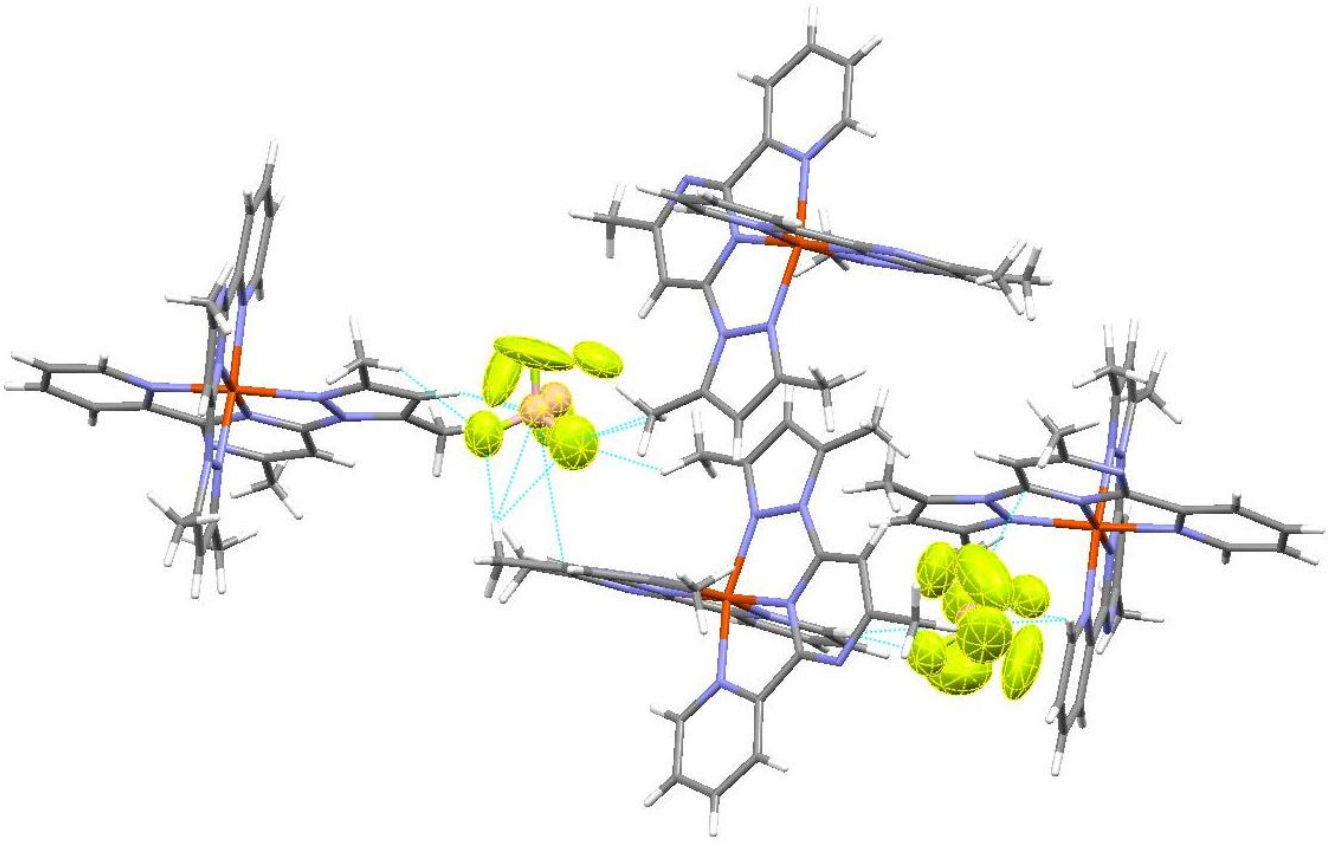

Figure S10. Disordered BF_4^- anions in the structure of $\mathbf{1}^{\mathbf{A/LS}}$.

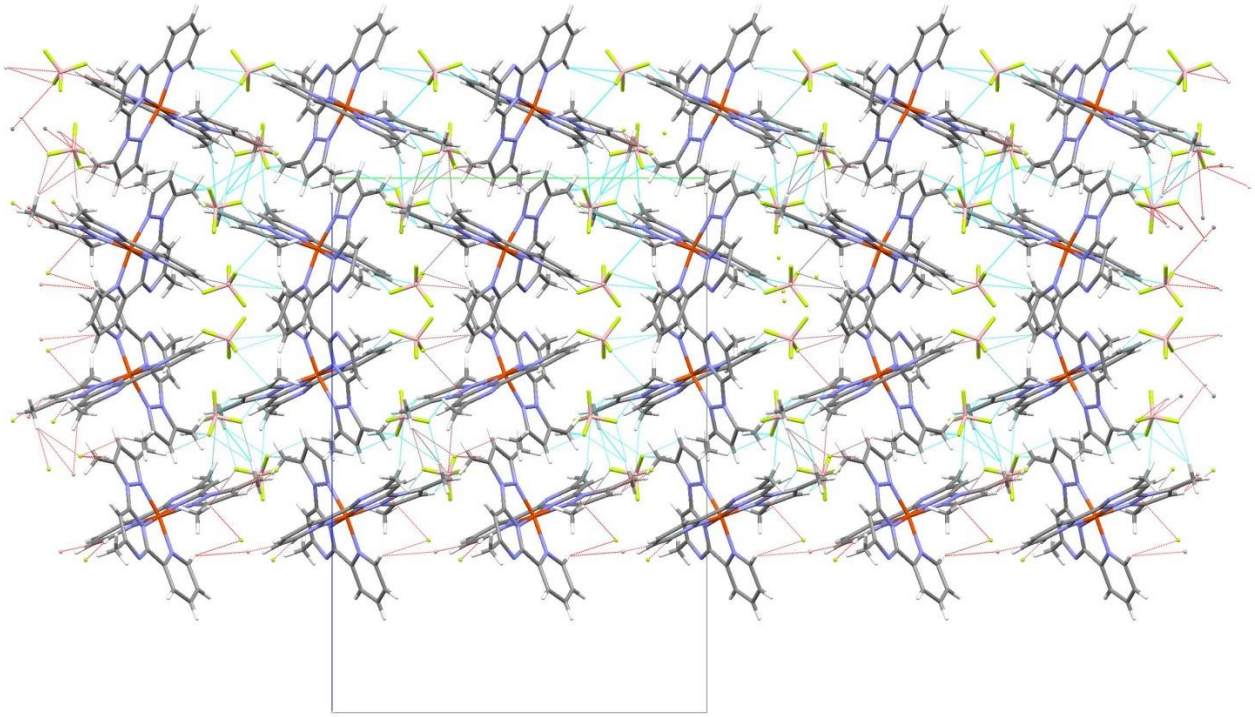

Figure S11. Projection of the crystal structure of **1**$^{A/LS}$ on the *bc*-plane. Side view of two 2D corrugated layers running into the opposite direction. Short contacts (< sum of VDW radii) within layers are shown.

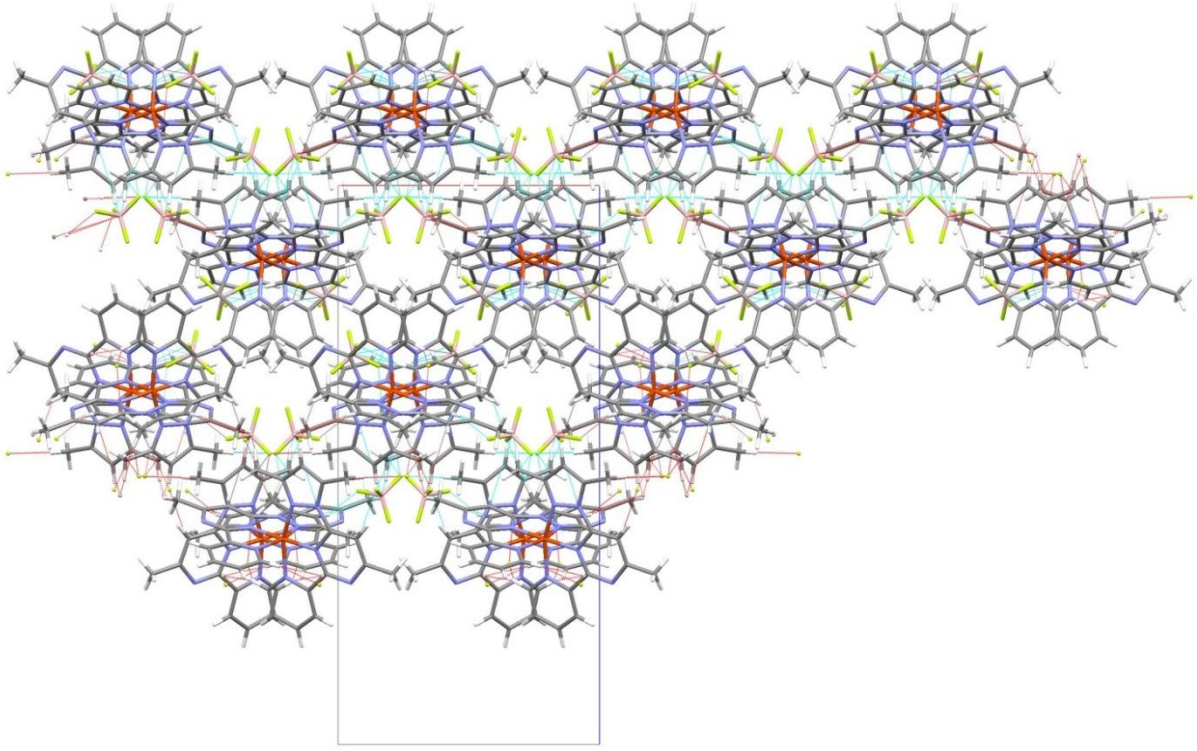

Figure S12. Projection of the crystal structure of **1**$^{A/LS}$ on the *ac*-plane (front view along 1D chains forming corrugated layers).

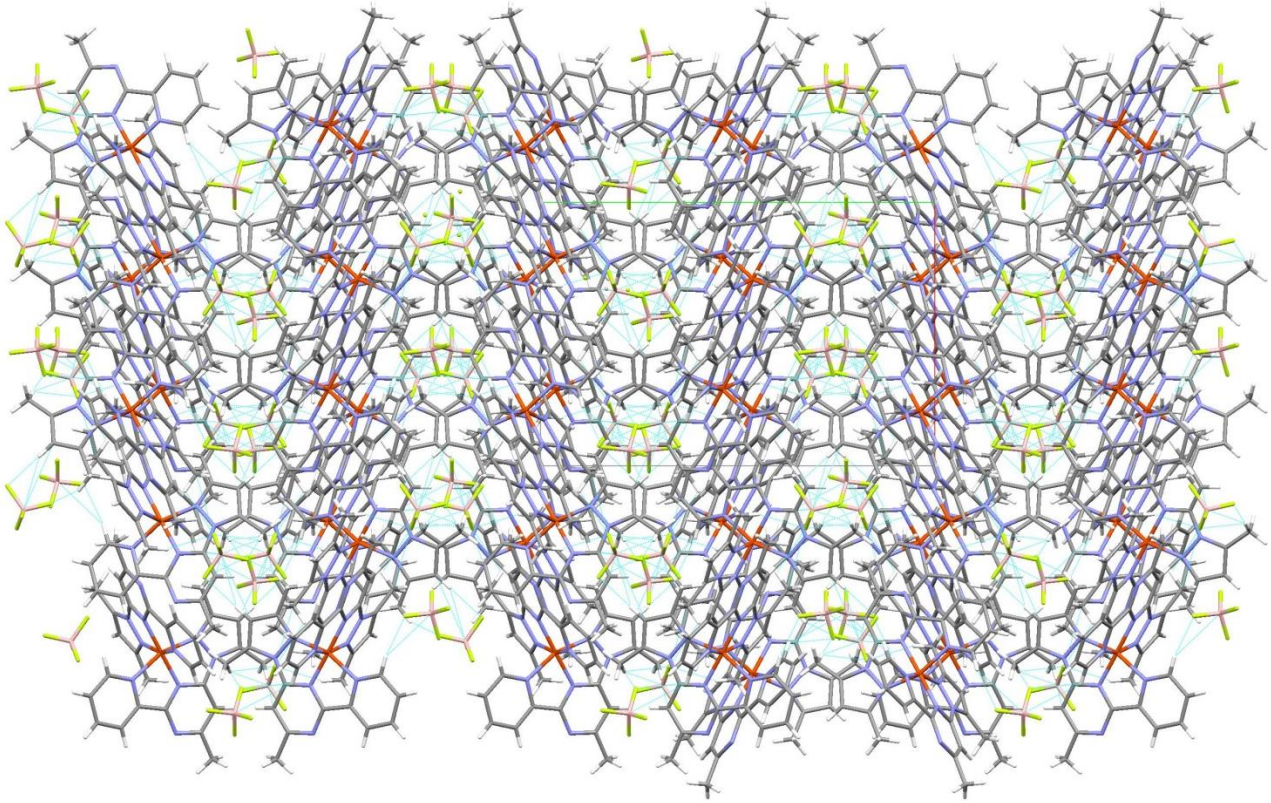

Figure S13. Projection of the crystal structure of $\mathbf{1}^{\mathbf{A/LS}}$ on the *ab*-plane.

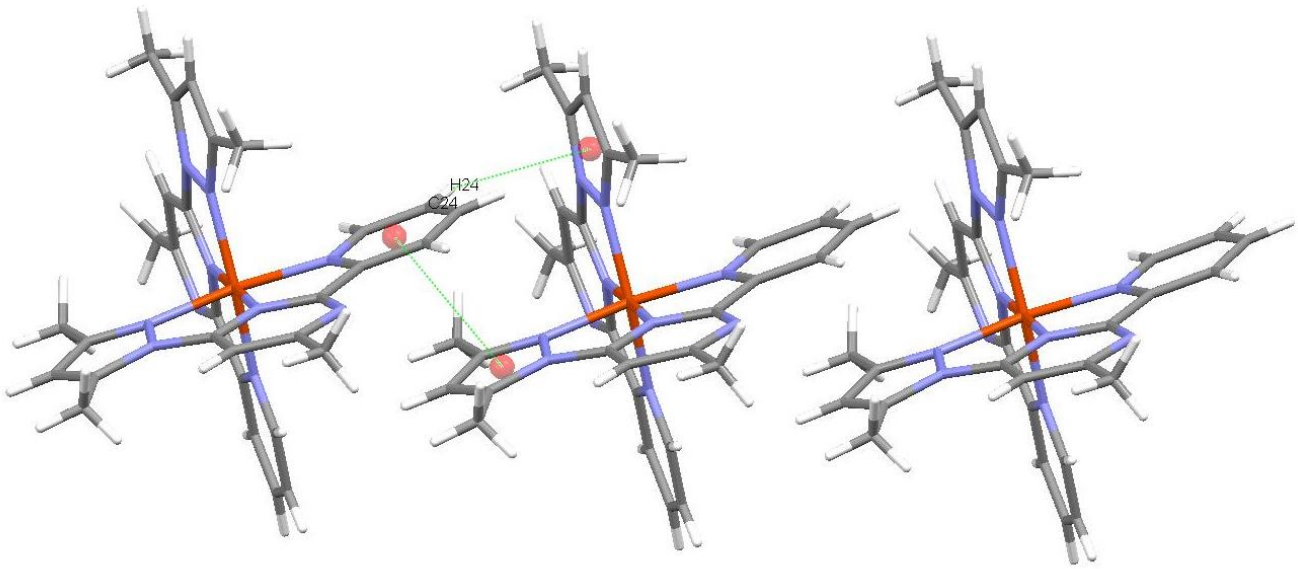

Figure S14. CH···π interactions and π-π stacking in the structure of $\mathbf{1}^{\mathbf{E/LS}}\cdot y\mathbf{EtOH}\cdot z\mathbf{H_2O}$. C–H···π, C24-H24···Cg 2.98 Å, γ = 5.38°, C-H···Cg 139°; π-π, Cg···Cg = 3.544(3) Å, α = 2.8(3)°, β = 16.35, γ = 16.46°.

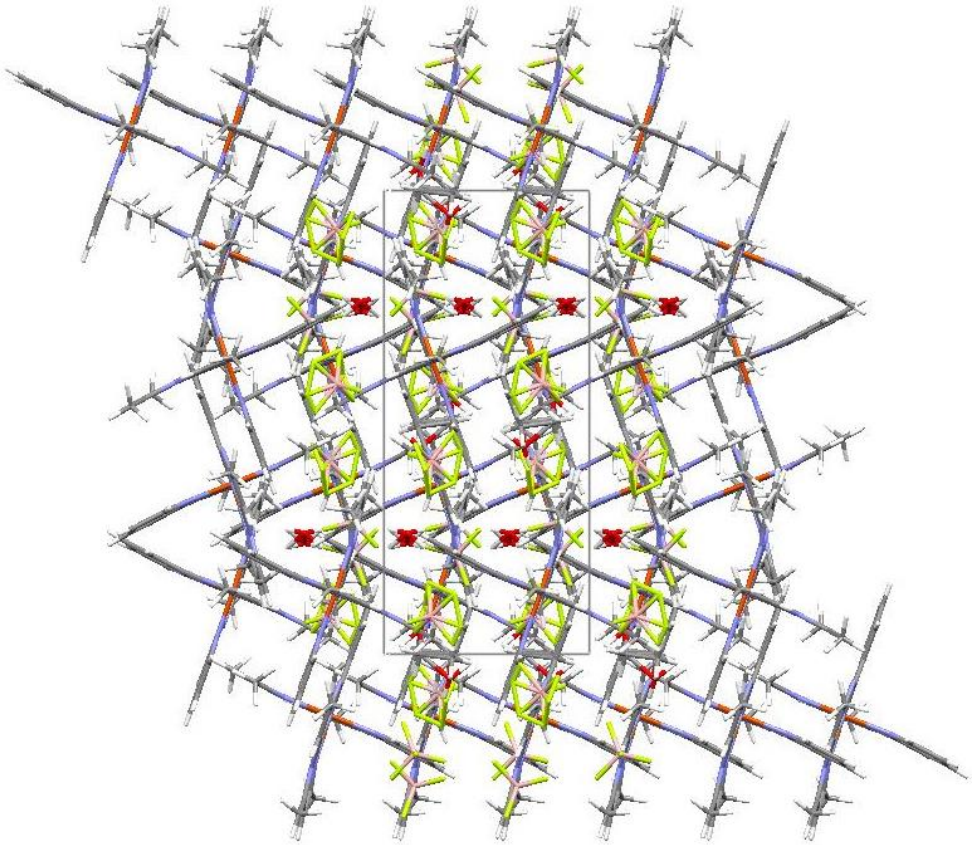

Figure S15. Packing diagram for $\mathbf{1}^{\mathbf{E/LS}}\cdot y\mathbf{EtOH}\cdot z\mathbf{H_2O}$. View along the *a* axis.

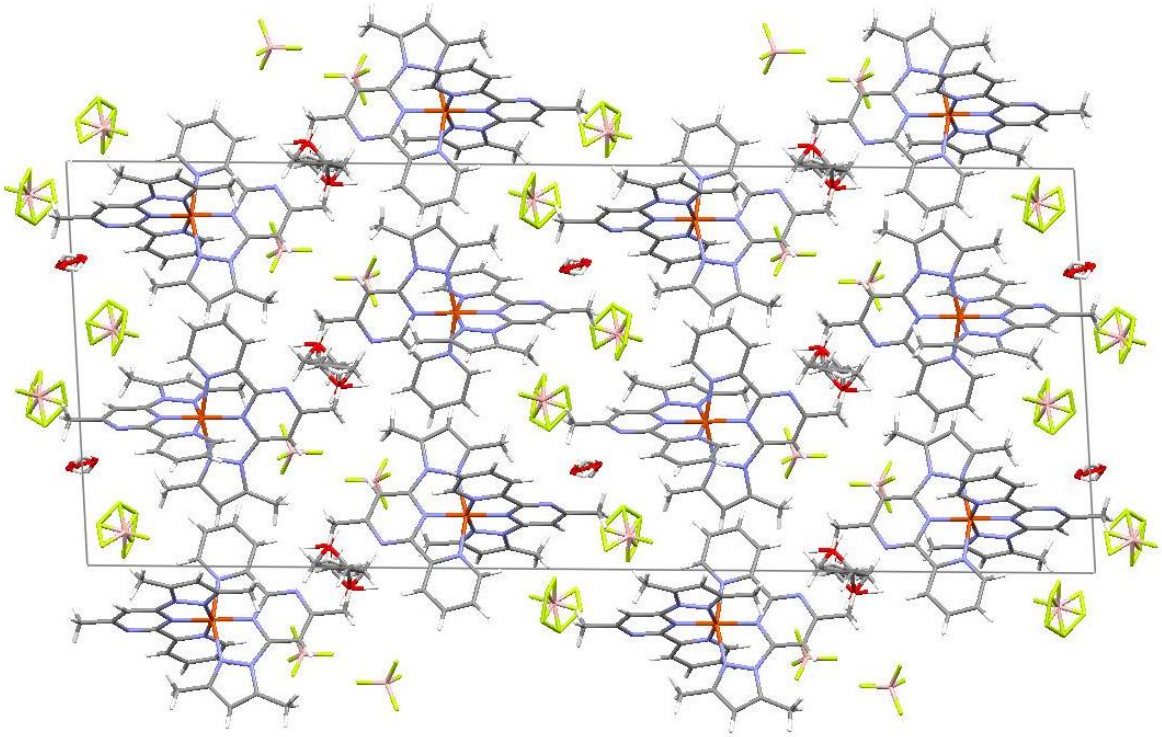

Figure S16. Packing diagram for $\mathbf{1}^{\mathbf{E/LS}}\cdot y\mathbf{EtOH}\cdot z\mathbf{H_2O}$. View along the *b* axis. Side view of two 2D double layers.

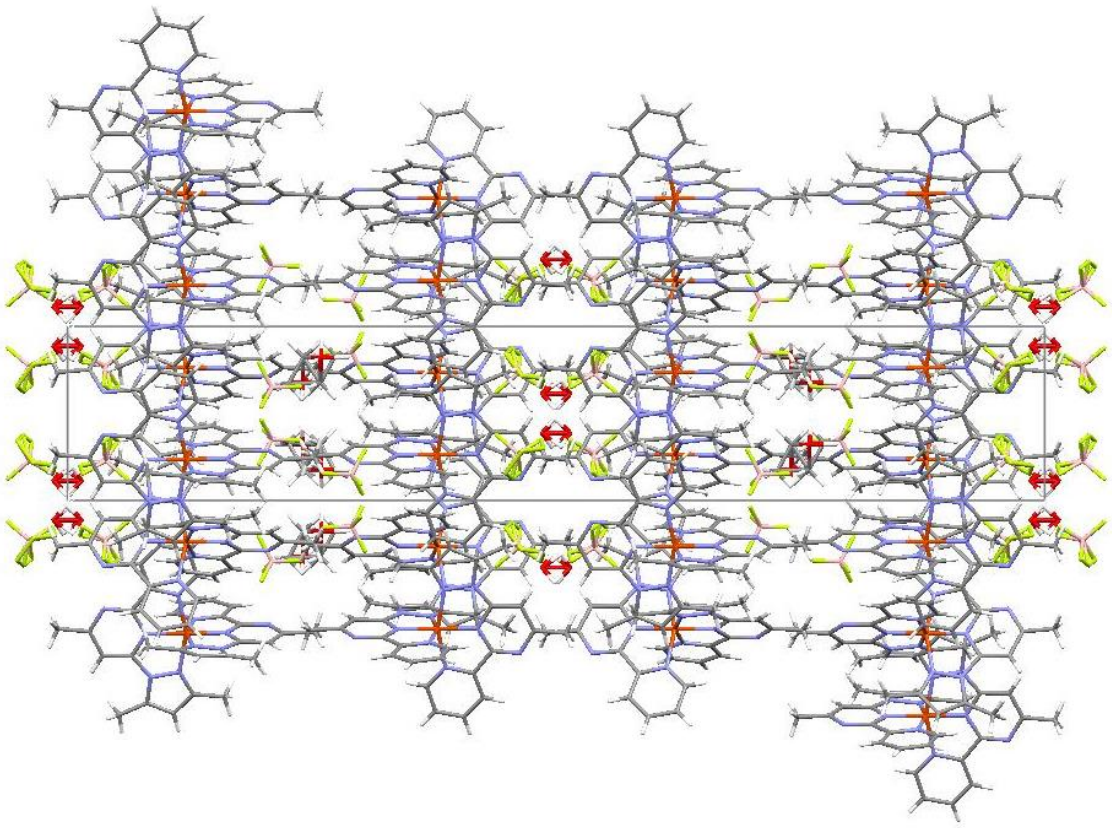

Figure S17. Packing diagram for $\mathbf{1}^{\mathbf{E/LS}}\cdot y\mathbf{EtOH}\cdot z\mathbf{H_2O}$. View along the *c* axis. Side view of two 2D double layers.

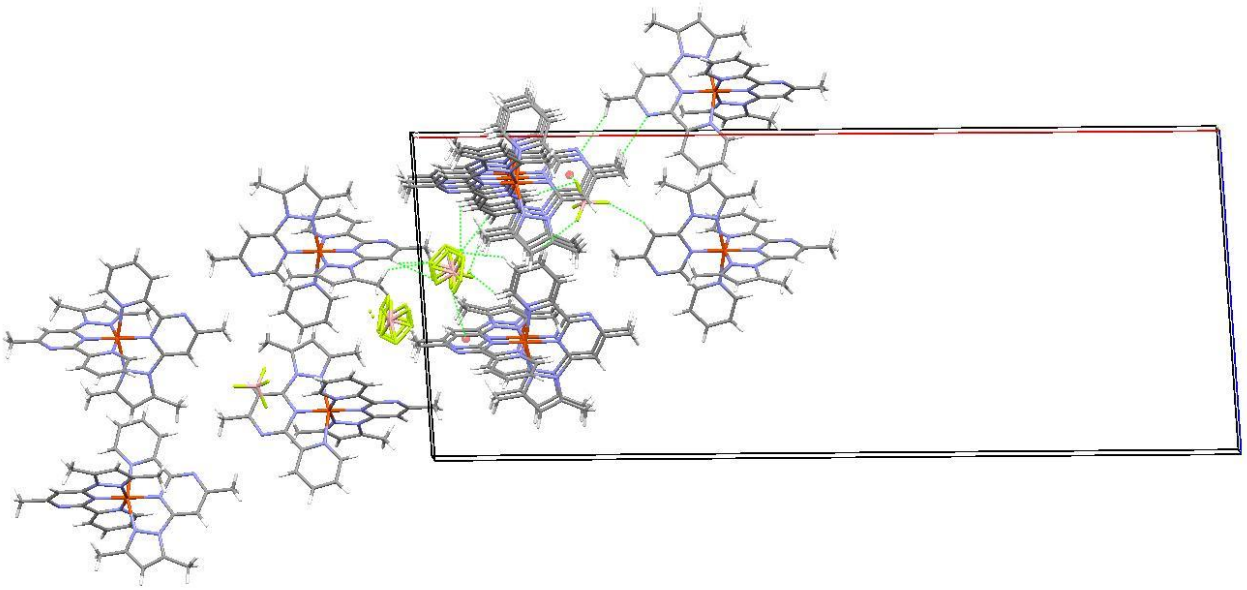

Figure S18. Supramolecular 3D structure of $\mathbf{1}^{\mathbf{E/LS}}\cdot y\mathbf{EtOH}\cdot z\mathbf{H_2O}$ formed due to BF···HC hydrogen bonds and lone pair – π interactions (two 2D double layers are shown, disordered solvent molecules are omitted for clarity). Short contacts between non-disordered BF_4^- and $[FeL_2]^{2+}$: B–F···π(pyrimidine): F1···Cg 3.013(5) Å, γ = 12.27°, B-F···Cg 120.7(5)°;C–H···F contacts: H25···F1 2.33 Å, H3···F2 2.48 Å, H15C···F3 2.41 Å, H8···F4 2.50 Å; C–H···N hydrogen bond: N1···H5C 2.66 Å.

3. X-RAY DIFFRACTION ANALYSIS OF POLYCRYSTALS

XPRD analysis of polycrystals was performed on Shimadzu XRD-7000 diffractometer (Cu-K_α radiation, Ni – filter, 5 – 60° 2θ range, 0.03° 2θ step, 5s per point). Most of the polycrystalline samples were slightly ground with hexane in an agate mortar, and the resulting suspension was deposited on the polished side of a standard quartz sample holder. A smooth thin layer was formed after drying. The samples $\mathbf{1}^{\mathbf{LS}} \cdot \mathbf{EtOH} \cdot \mathbf{H_2O}$ and $\mathbf{1}^{\mathbf{E/LS}} \cdot \boldsymbol{y}\mathbf{EtOH} \cdot \boldsymbol{z}\mathbf{H_2O}$ were slightly ground and fixed using a minimal amount of Vaseline.

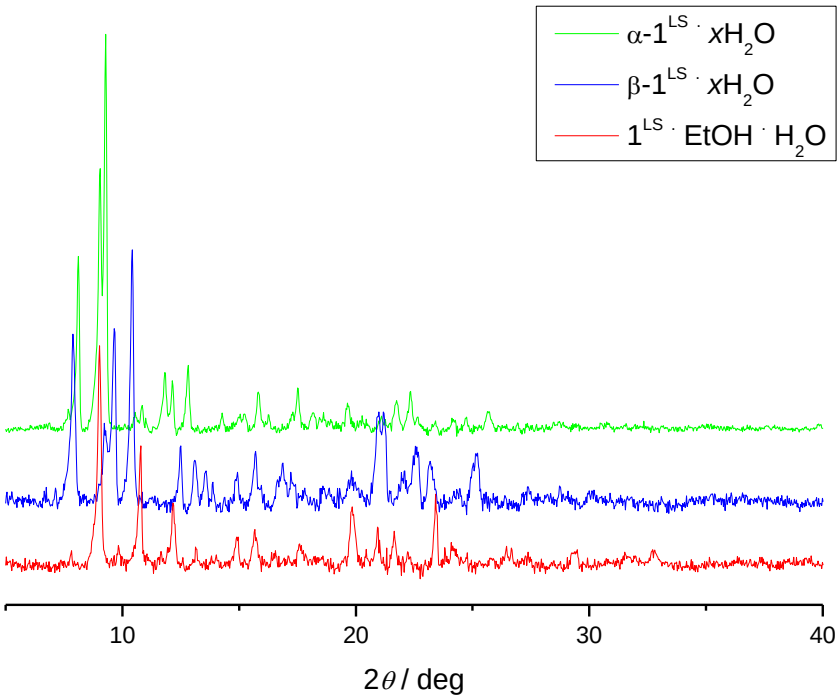

Figure S19. XRPD patterns of the parent phases **α-1^{LS} · *x*H_2O**, **β-1^{LS} · *x*H_2O** and **1^{LS} · EtOH · H_2O**.

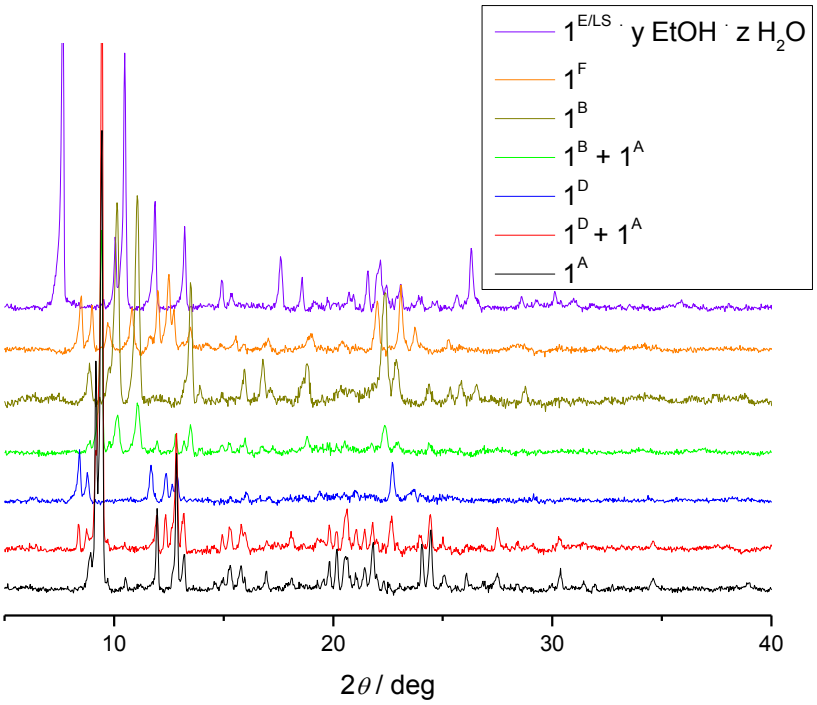

Figure S20. XRPD patterns of the phases **$1^{E/LS}$ · *y*EtOH · *z*H_2O**, **1^F**, **1^B**, **1^D**, **1^A** and the mixtures **1^B + 1^A** and **1^D + 1^A**.

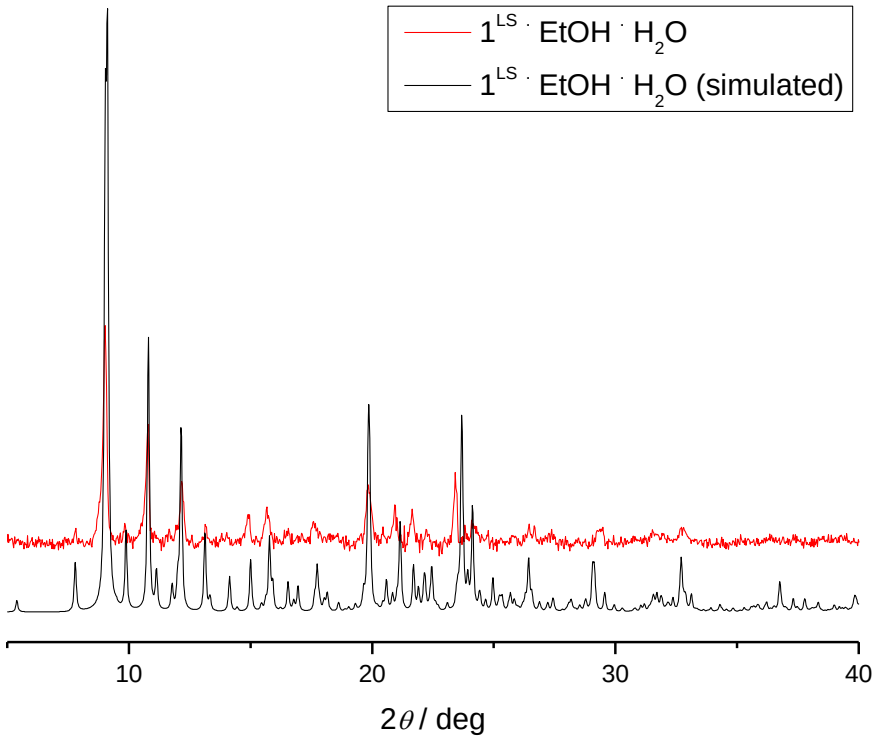

Figure S21. Comparison of XRPD pattern of the phase $\mathbf{1^{LS} \cdot EtOH \cdot H_2O}$ with simulated pattern.

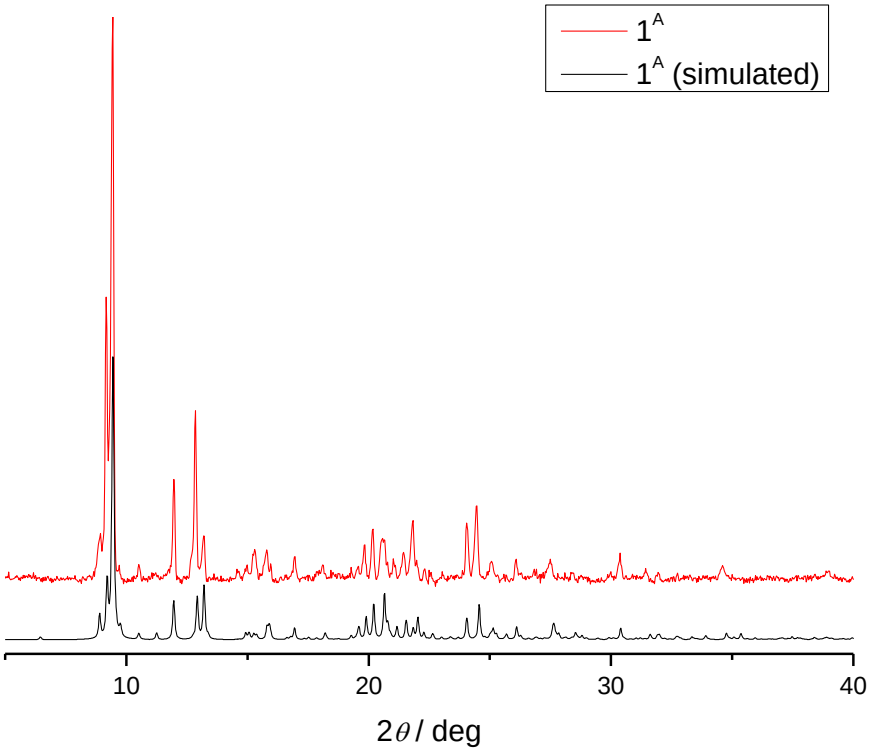

Figure S22. Comparison of XRPD pattern of the phase $\mathbf{1^{A/LS}}$ with simulated pattern.

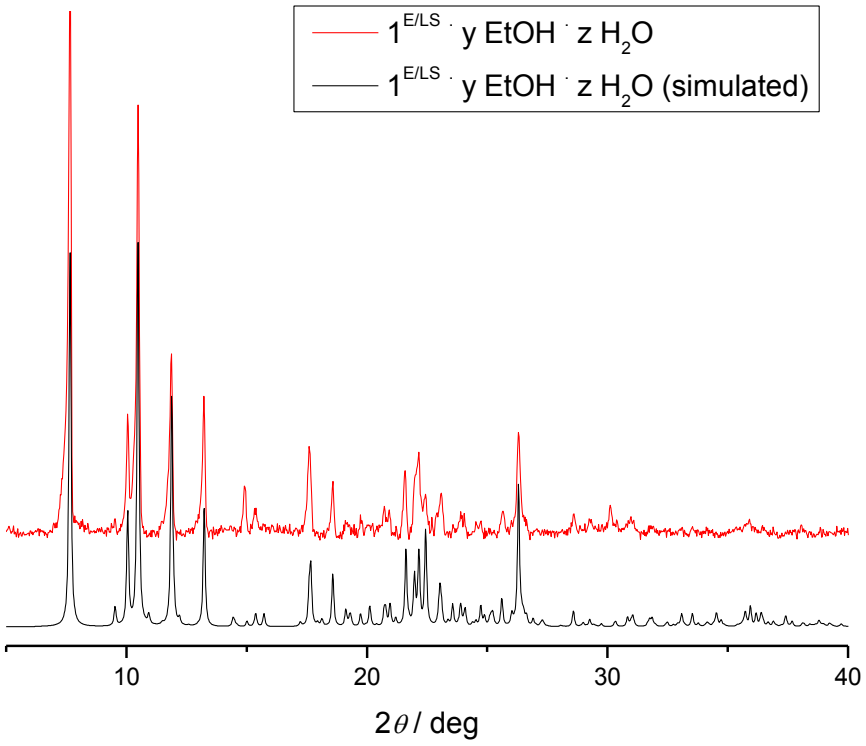

Figure S23. Comparison of XRPD pattern of the phase $\mathbf{1^{E/LS} \cdot \mathit{y}EtOH \cdot \mathit{z}H_2O}$ with simulated pattern.

4. DIFFERENTIAL SCANNING CALORIMETRY

Thermodynamic properties were studied using differential scanning calorimeter NETZSCH DSC 204 F1 Phoenix. DSC measurements of the samples were performed by heat flow measurement method at heating/cooling rate 6 K min^{-1} in 25 ml min^{-1} Ar flow. The baseline signal obtained by heating two empty crucibles was subtracted from the experimental results for the samples. The sensitivity calibration of the sample carrier sensors and temperature scale graduation included melting peak area measurements of six melting standard samples from calibration set 6.239.2–91.3 supplied by Netzsch. The transition temperatures were defined from the resulting heat flow as intersections of the peak onset with the corresponding baseline. Netzsch Proteus Analysis software was used to determine DSC peak area and transition temperatures and for further averaging the results of 3 experiments. Thermodynamic properties have been investigated in sealed aluminum crucibles. Differential scanning measurements were carried out over the temperature range 293 – 500 K at warming and cooling modes. Molar enthalpy of transition, ΔH, was calculated as the area of the DSC peak. The excess entropy of the transition was calculated by the formula $\Delta S = \Delta H/T$, which is valid for the first order phase transitions.

Cycle 1: 1st day. After the first cycle had been done the sample was allowed to stay at room temperature.
Cycles 2, 3: 22nd day
Cycles 4, 5: 23rd day
Cycles 6, 7: 26th day

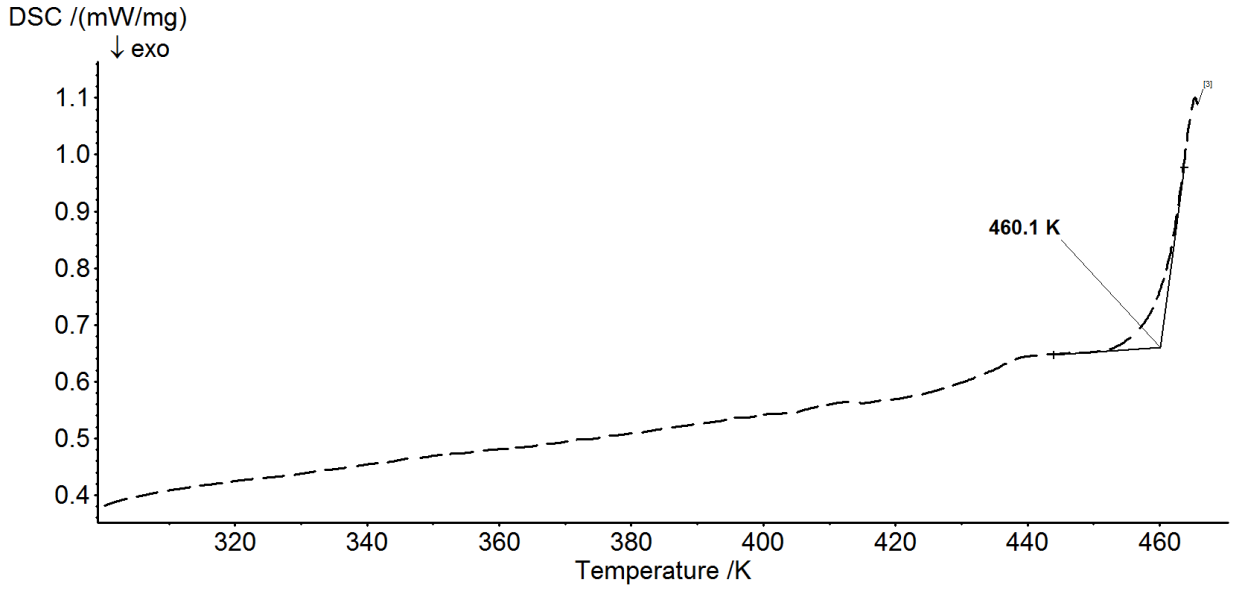

Figure S24. DSC curve for the first heating run.

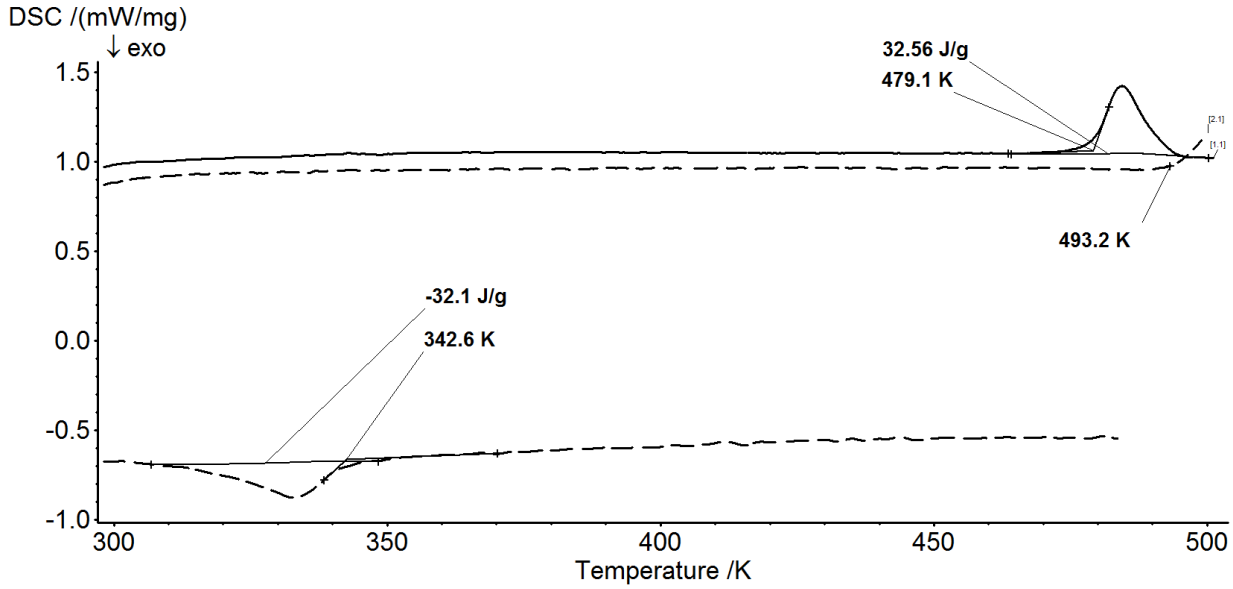

Figure S25. DSC curves for the transition $\mathbf{1}^{\mathbf{A/LS}} \leftrightarrow \mathbf{1}^{\mathbf{A/HS}}$ (2^{nd} (dashed line) and 3^{rd} (solid line) cycles).

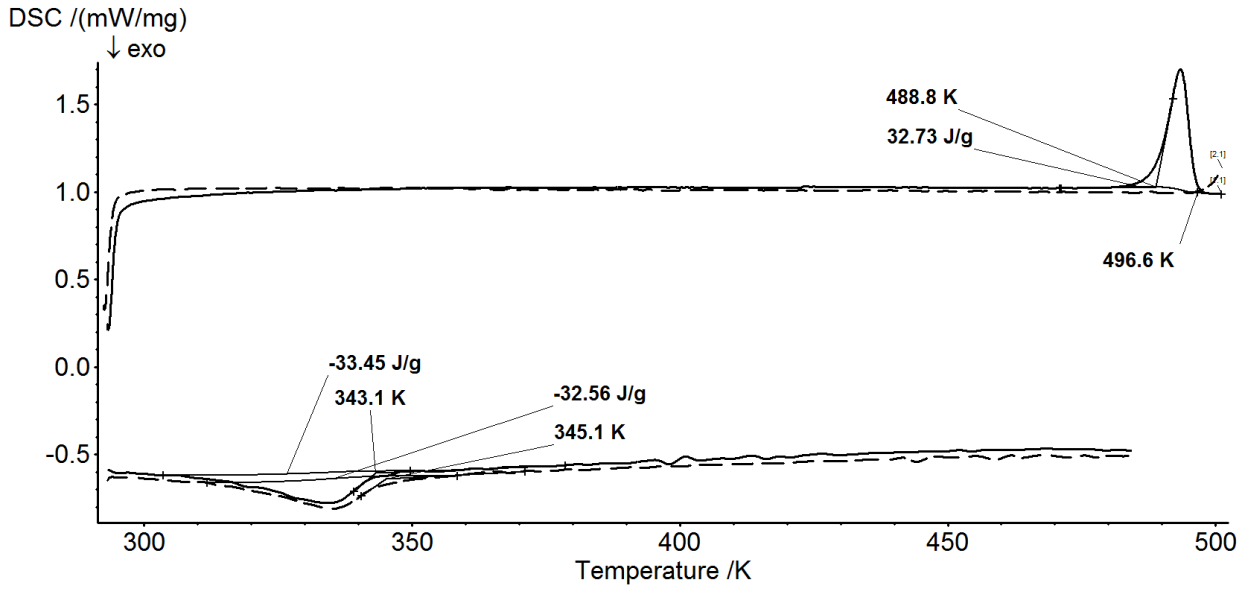

Figure S26. DSC curves for the transition $\mathbf{1}^{\mathbf{A/LS}} \leftrightarrow \mathbf{1}^{\mathbf{A/HS}}$ (4^{th} (dashed line) and 5^{th} (solid line) cycles).

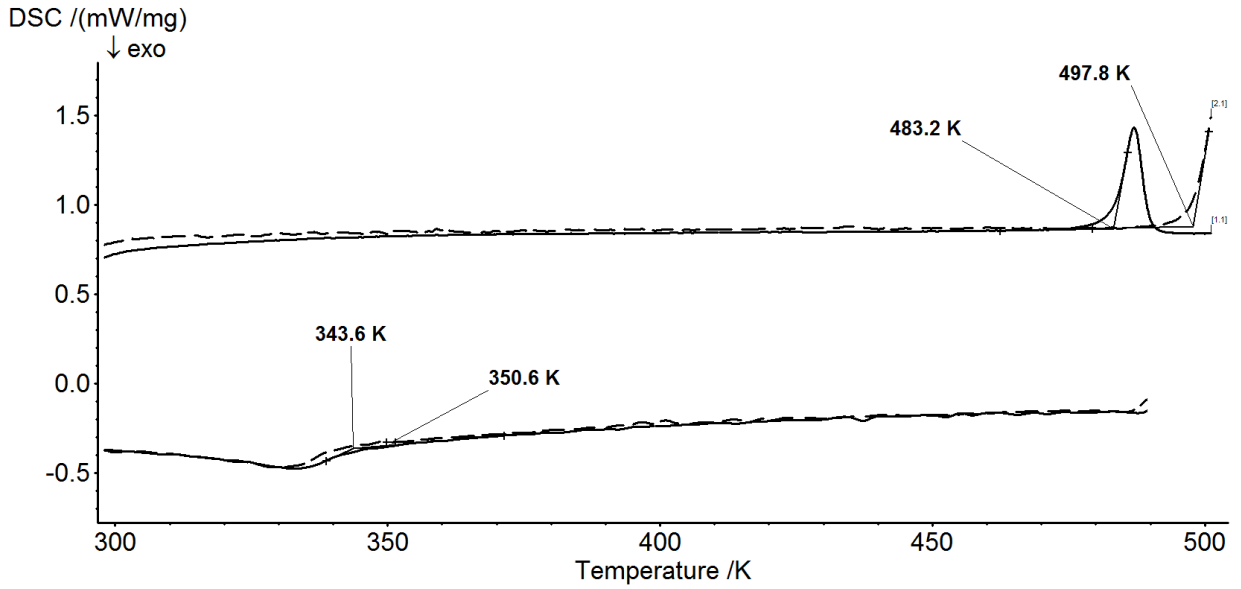

Figure S27. DSC curves for the transition $\mathbf{1}^{\mathbf{A/LS}} \leftrightarrow \mathbf{1}^{\mathbf{A/HS}}$ (6^{th} (dashed line) and 7^{th} (solid line) cycles).

5. IR SPECTROSCOPY

IR absorption spectra were recorded on a Scimitar FTS 2000 spectrometer.

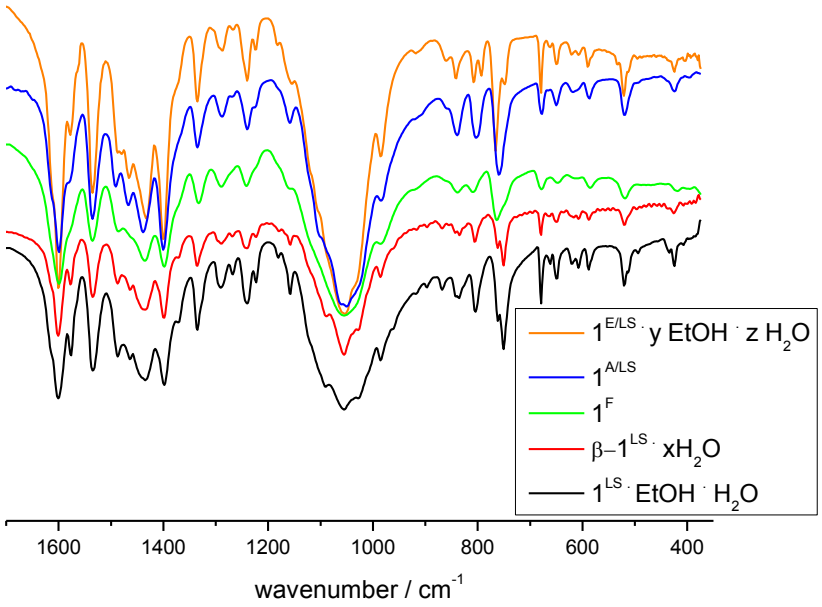

Figure S28. IR spectra of $\mathbf{1^{LS} \cdot EtOH \cdot H_2O}$, $\mathbf{\beta\text{-}1^{LS} \cdot \mathit{x}H_2O}$, $\mathbf{1^{A/LS}}$, $\mathbf{1^{E/LS} \cdot \mathit{y}EtOH \cdot \mathit{z}H_2O}$ and $\mathbf{1^{F}}$ (1700 – 350 cm^{-1}, KBr).

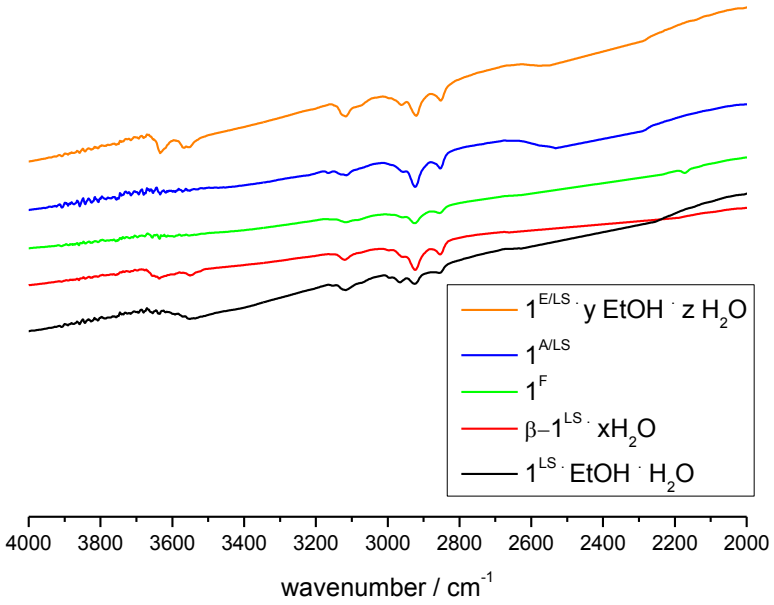

Figure S29. IR spectra of $\mathbf{1^{LS} \cdot EtOH \cdot H_2O}$, $\mathbf{\beta\text{-}1^{LS} \cdot \mathit{x}H_2O}$, $\mathbf{1^{A/LS}}$, $\mathbf{1^{E/LS} \cdot \mathit{y}EtOH \cdot \mathit{z}H_2O}$ and $\mathbf{1^{F}}$ (4000 – 2000 cm^{-1}, fluorinated oil). IR spectra of the phases $\mathbf{1^{LS} \cdot EtOH \cdot H_2O}$, $\mathbf{\beta\text{-}1^{LS} \cdot \mathit{x}H_2O}$ and $\mathbf{1^{E/LS} \cdot \mathit{y}EtOH \cdot \mathit{z}H_2O}$ contain ν(OH) bands of low intensity. This means that the phases contain outerspheric ethanol and water molecules.

6. THERMAL ANALYSIS

Simultaneous thermal analysis (STA) of $\mathbf{1^{LS} \cdot EtOH \cdot H_2O}$, $\mathbf{\beta\text{-}1^{LS} \cdot \mathit{x}H_2O}$, $\mathbf{1^{A/LS}}$, $\mathbf{1^{D}}$, $\mathbf{1^{E/LS} \cdot \mathit{y}EtOH \cdot \mathit{z}H_2O}$ and $\mathbf{1^{F}}$, including thermogravimetric (TG) and differential scanning calorimetry (DSC) measurements, was performed on NETZSCH instruments (NETZSCH TG 209 F1, NETZSCH STA 449F1, NETZSCH STA 409 PC/PG; open Al crucible, heating rate 10 K min^{-1}).

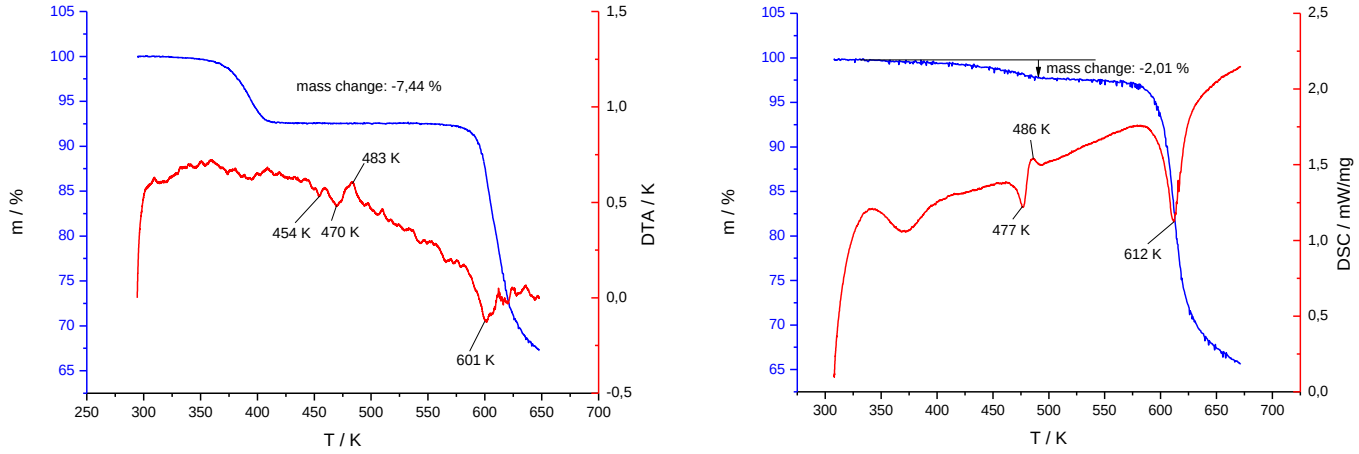

Figure 30. TG and DTA/DSC curves for the complex $\mathbf{1^{LS} \cdot EtOH \cdot H_2O}$ (**sample #1**, just after filtration, left) and $\mathbf{\beta\text{-}1^{LS} \cdot \mathit{x}H_2O}$ (**sample #1**, 10 days after filtration, right).

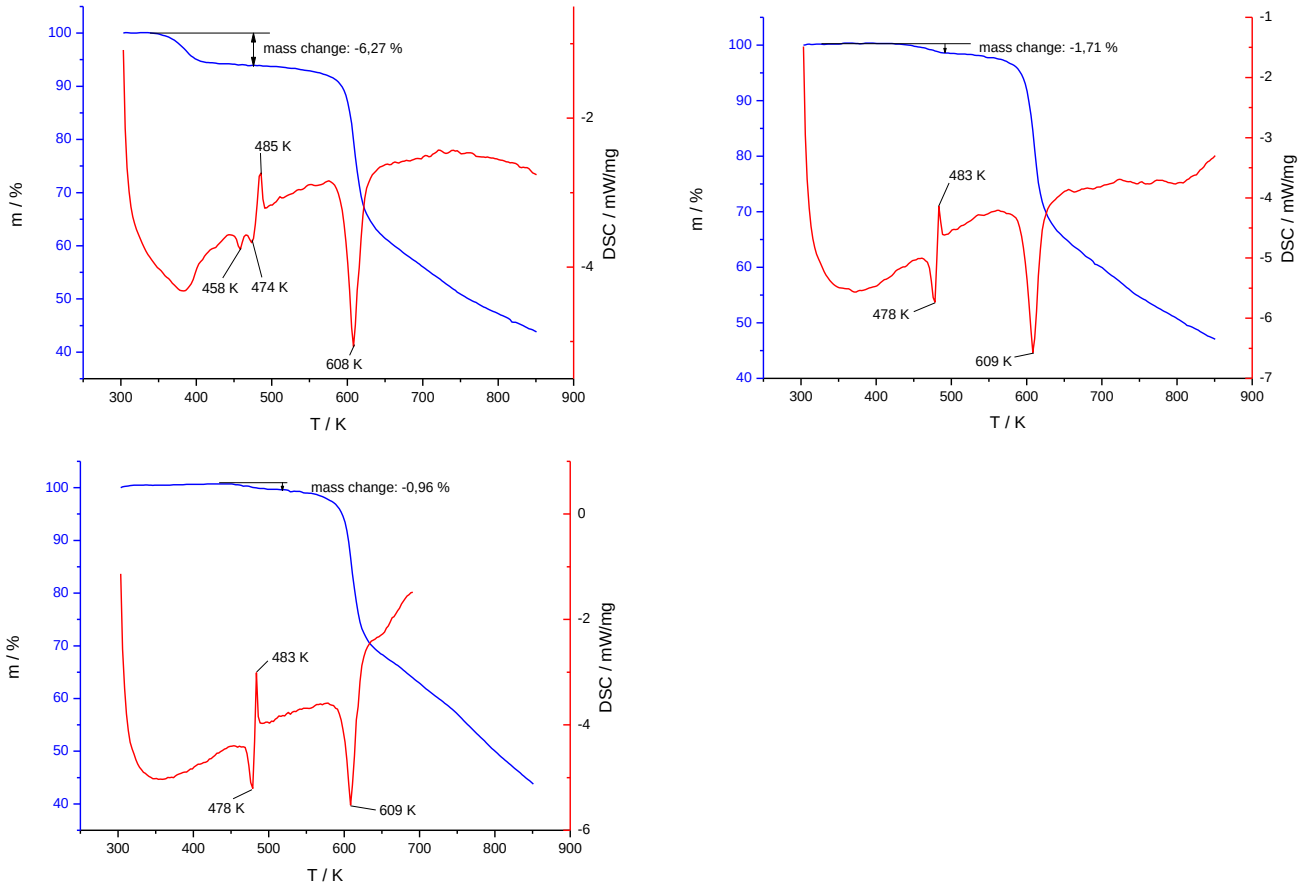

Figure S31. TG and DSC curves for the complex $\mathbf{1^{LS} \cdot EtOH \cdot H_2O}$ (**sample #2**, *ca*. 2 h after filtration, top, left), $\mathbf{\beta\text{-}1^{LS} \cdot \textit{x}H_2O}$ (**sample #2**, 20 days after filtration, top, right) and $\mathbf{\beta\text{-}1^{LS} \cdot \textit{x}H_2O}$ (**sample #2**, two months after filtration, bottom).

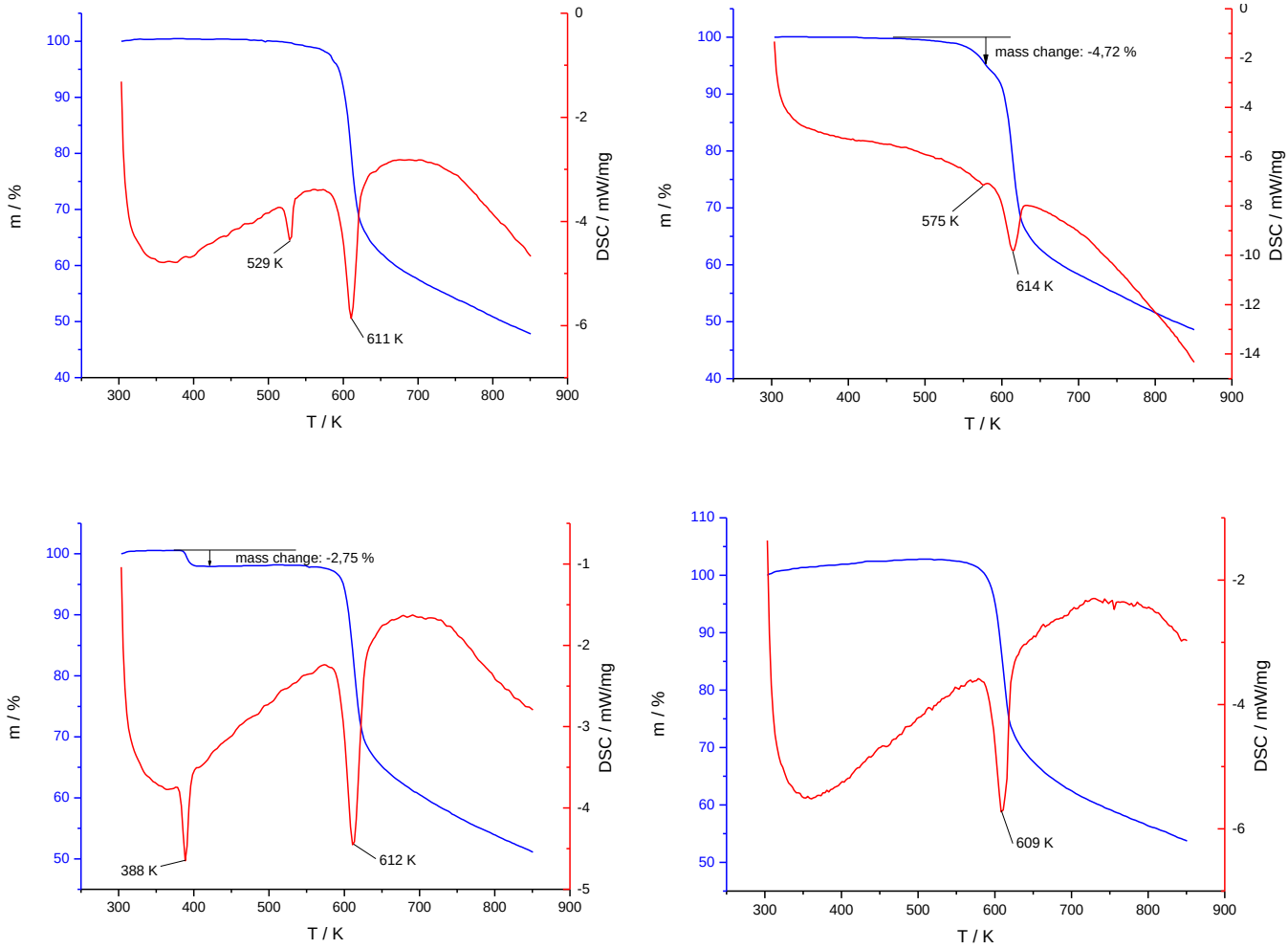

Figure S32. TG and DSC curves for the complex $\mathbf{1}^{\mathbf{A/LS}}$ (top, left), $\mathbf{1}^{\mathbf{D}}$ (top, right), $\mathbf{1}^{\mathbf{E/LS}}\cdot\boldsymbol{y}\mathbf{EtOH}\cdot\boldsymbol{z}\mathbf{H_2O}$ (bottom, left) and $\mathbf{1}^{\mathbf{F}}$ (bottom, right).

7. MAGNETIC DATA: EXPERIMENTS AND FITTING

Experimental details

The study of magnetic properties of the complexes was performed on a Faraday balance in the temperature range 80 – 500 K in the magnetic fields from 5.8 to 10.9 kOe. The measurements showed that magnetic susceptibility of the samples did not depend on the magnetic field strength proving the absence of ferromagnetic impurities. Further measurements of the magnetic susceptibility were performed in the field of 9.09 kOe. Magnetic measurements on the samples **19** and **20** were performed in open quartz ampoules under vacuum. All the other samples were placed into quartz ampoules and sealed. The molar magnetic susceptibility (χ_M) was calculated taking into account the diamagnetism of the atoms using the Pascal additive scheme and a correction for the sample holder was applied. Details on the parent phases are given below. The values of the *m*/*V* ratio are collected in Table S2.

Typically, heating/cooling rate in "dynamic" magnetic measurements was 0.9 K min^{-1}. Magnetic properties of the samples **5-1** and **12-1** were studied at rates 0.9, 0.4 and 0.25 K min^{-1}. To study SCO kinetics in "static" measurements, the samples were rapidly cooled or heated (at 4 K min^{-1}) to the temperature of annealing. Any deviation from this is stated below.

Fitting

Fitting of sigmoidal curves has been done according to the Johnson–Mehl–Avrami–Kolmogorov (JMAK) model using the equation

$$\gamma = 1 - \exp(-kt^n),$$

where γ is the fraction transformed at time t ($0 \leq \gamma \leq 1$), n is the Avrami exponent and k is the overall rate constant (s^{-n}). The fractions γ_{HS} and γ_{LS} were normalized using the equations

$$\gamma_{HS} = \frac{(\chi_M T)_t - (\chi_M T)_{min}}{(\chi_M T)_{max} - (\chi_M T)_{min}}$$

and

$$\gamma_{LS} = 1 - \frac{(\chi_M T)_t - (\chi_M T)_{min}}{(\chi_M T)_{max} - (\chi_M T)_{min}}$$

where $(\chi_M T)_t$ is the $\chi_M T$ value at time t, $(\chi_M T)_{min}$ is a minimal $\chi_M T$ value at a given temperature T and $(\chi_M T)_{max}$ is a maximal $\chi_M T$ value at a given temperature T.

Fitting of exponential curves has been done in the frame of bi- or tri-exponential approximation using the equations

$$\chi_M T = (\chi_M T)_1 e^{(-\frac{t}{\tau_1})} + (\chi_M T)_2 e^{(-\frac{t}{\tau_2})} + (\chi_M T)_0$$

and

$$\chi_M T = (\chi_M T)_1 e^{(-\frac{t}{\tau_1})} + (\chi_M T)_2 e^{(-\frac{t}{\tau_2})} + (\chi_M T)_3 e^{(-\frac{t}{\tau_3})} + (\chi_M T)_0$$

where $(\chi_M T)_i$ are the initial $\chi_M T$ values for each exponent and τ_i are lifetimes of each exponent.

Cooperative effect for the transition $1^{A/LS} \rightarrow 1^{A/HS}$

The Slichter-Drickamer model (SDM) describes an SCO system in terms of mean field theory as a regular solution of HS and LS molecules. It uses a phenomenological parameter of cooperative interaction, Γ, which reflects the tendency of SCO molecule in a certain spin state to be surrounded by SCO molecules of the same spin state (Γ>0). The SDM reproduces various forms of SCO curves as well as hysteresis effect. A first-order phase transition as well as a possibility for hysteretic bistable behavior are predicted when $\Gamma > 2RT_c$. The SDM uses the following equation for the HS molar fraction γ_{HS}:

$$\ln\left(\frac{1-\gamma_{HS}}{\gamma_{HS}}\right) = \frac{\Delta H + \Gamma(1-2\gamma_{HS})}{RT} - \frac{\Delta S}{R} \quad , \qquad (1)$$

where ΔH and ΔS are the enthalpy and entropy changes associated with spin transition.

We calculated the $\gamma_{HS}(T)$ values and the value of Γ as follows.

1) Magnetic contributions of HS and LS fractions were extracted from magnetic susceptibility data above and below the transition region.

2) The $\gamma_{HS}(T)$ values were calculated at different temperatures from magnetic data using the equation $\chi'_M = \gamma_{HS}\chi'_M(HS) + (1-\gamma_{HS})\chi'_M(LS)$, where $\chi'_M(HS)$ and $\chi'_M(LS)$ stand for magnetic contributions of HS and LS fractions at high and low temperature limits, respectively.

3) Parameter Γ was determined by the least squares method, by minimizing numerically the sum

$$\sum_T \left[\ln\left(\frac{1-\gamma_{HS}(T)}{\gamma_{HS}(T)}\right) - \frac{\Delta H + \Gamma(1-2\gamma_{HS}(T))}{RT} + \frac{\Delta S}{R} \right]^2 . \qquad (2)$$

The Sorai-Seki model (SSM) assumes that the crystal lattice consists of N non-interacting domains of equal size containing n molecules and that the spin transition in each domain occurs

simultaneously. The SSM does not describe the hysteresis effects. The equation to calculate model value of γ_{HS} can be written as

$$\gamma_{HS}^{mod} = \frac{1}{1+\exp\left(\frac{-n\Delta H}{R}\left(\frac{1}{T}-\frac{1}{T_{1/2}}\right)\right)}, \quad (3)$$

where $T_{1/2}$ is the temperature at which the number of domains in the HS and LS forms is equal. The parameter n was determined by minimizing the sum

$$\sum_{T}\left[\gamma_{HS}^{mod}(T)-\gamma_{HS}(T)\right]^2. \quad (4)$$

Sample 1

Parent phase $\mathbf{1^{LS} \cdot EtOH \cdot H_2O}$.

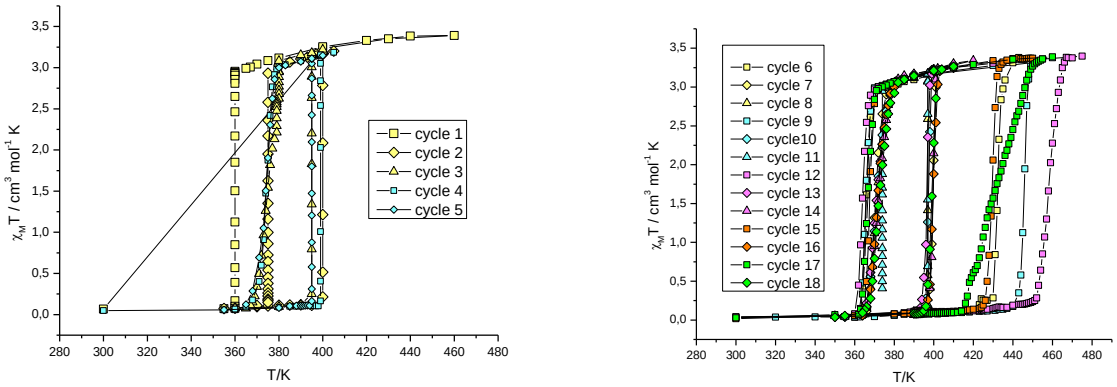

Figure S33. Sample **1**. Thermal cycles 1 – 5 (left) and 6 – 18 (right). Heating rate in the cycle 1 (300 – 400 K) was 10 K/min.

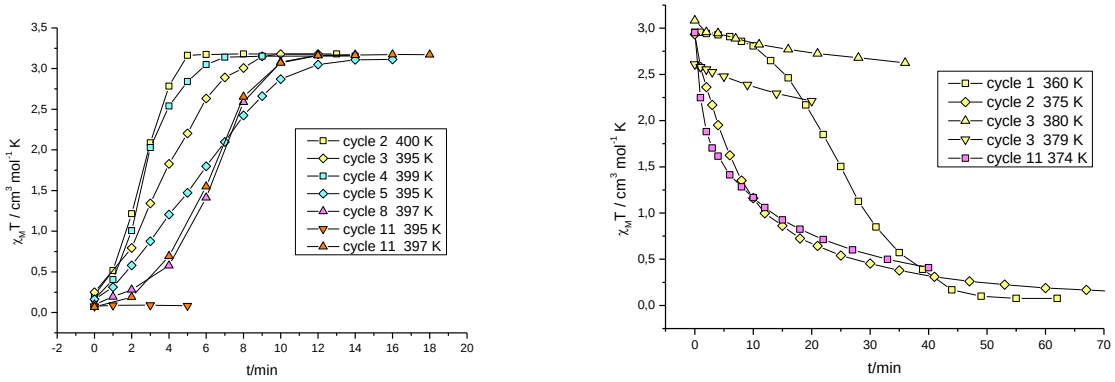

Figure S34. Sample **1**. Kinetic curves for the cycles 2 – 5, 8, 11 (LS → HS transformation, left) and 1 – 3 and 11 (HS → LS transformation, right).

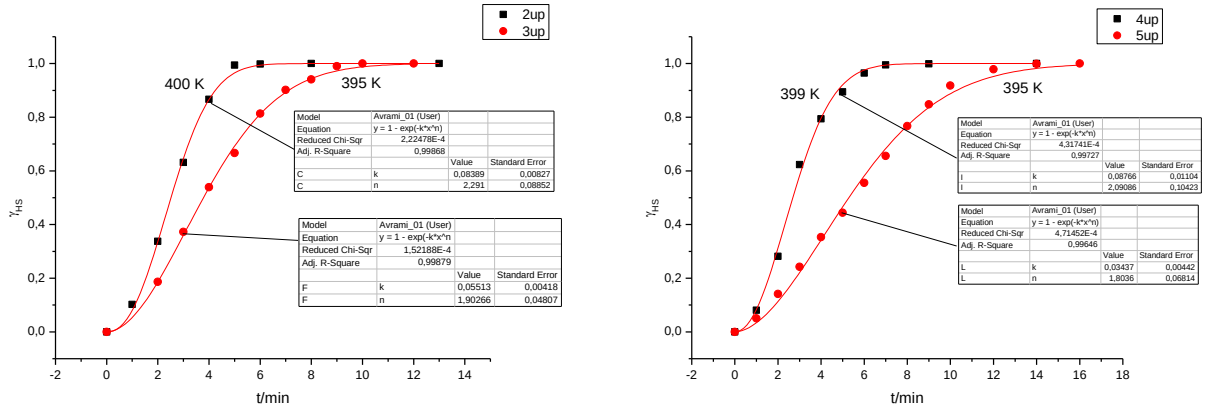

Figure S35. Fitting of kinetic curves for **1** using the JMAK model (LS → HS transformation; left: cycles 2 and 3, right: cycles 4 and 5).

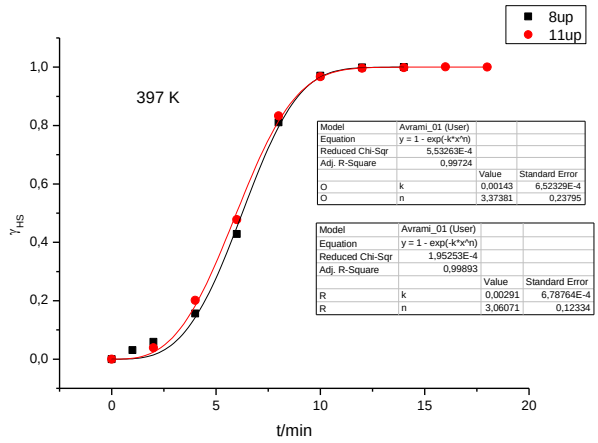

Figure S36. Fitting of kinetic curves for **1** using the JMAK model (LS → HS transformation; cycles 8 and 11).

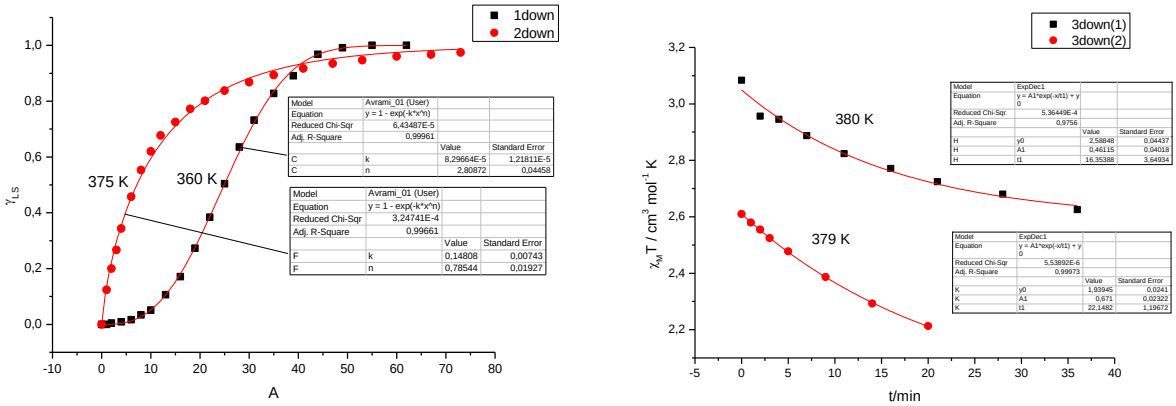

Figure S37. Fitting of kinetic curves for **1** using the JMAK model (right: cycles 1 and 2, HS → LS transformation) and the monoexponential law (left: cycle 3, LS → HS transformation).

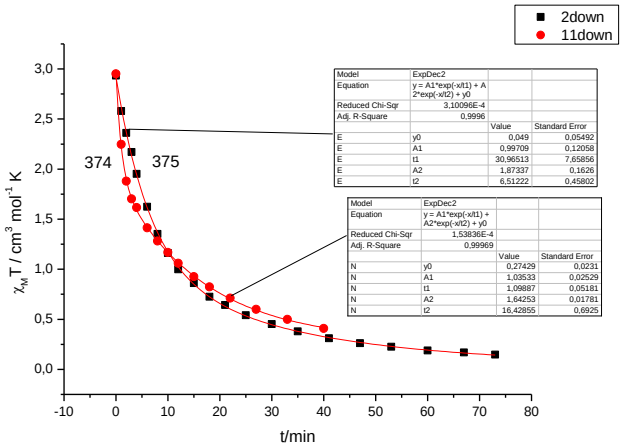

Figure S38. Fitting of kinetic curves for **1** in the bi-exponential approximation (cycles 2 and 11, LS → HS transformation).

Samples 2, 2-1, 2-2 and 2-3

Sample 2
Cycles 1 – 3. Parent phase $\mathbf{1}^{\mathbf{LS}} \cdot \mathbf{EtOH} \cdot \mathbf{H_2O}$.

Sample 2-1
Cycles 4 – 6. Parent phase $\mathbf{1}^{\mathbf{A/LS}}$. This sample was taken from the experiment **2**, placed in a new ampoule, dried in the ambient air for 3 days and sealed.

Sample 2-2
Cycles 7 – 11. Parent phases: a mixture of $\mathbf{1}^{\mathbf{A/LS}}$ and $\mathbf{1}^{\mathbf{B/LS}}$. This sample was exposed to water vapor for 48 h. This was followed by the increase in the mass of the sample by 1.9 % and by a drop in the magnetic moment. This sample was sealed and subjected to thermal cycling.

Sample 2-3
Cycles 12 - 14. Parent phase $\mathbf{1}^{\mathbf{A/LS}}$. This sample of the phase $\mathbf{1}^{\mathbf{A/LS}}$ was taken from the experiment **2-2**, exposed to water vapor for 1 h (no change in the mass was observed) and sealed.

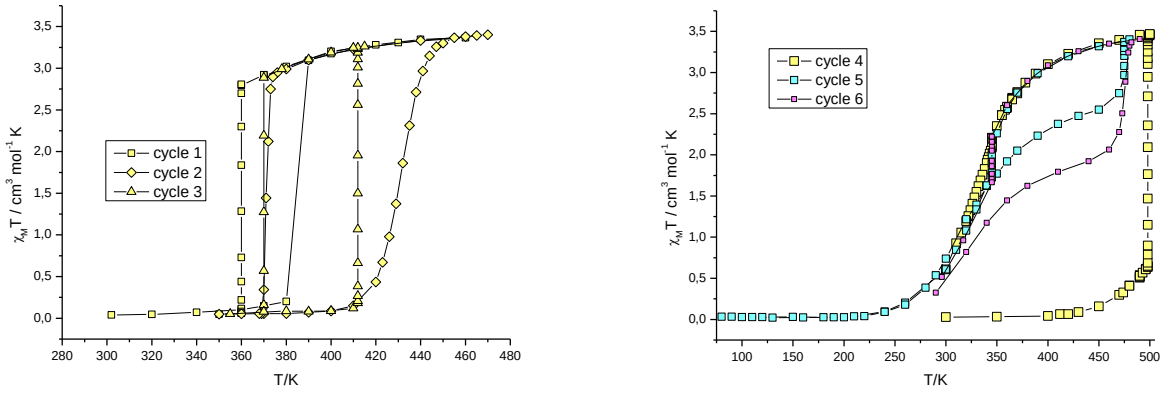

Figure S39. Left: sample **2**, thermal cycles 1 – 3. Right: sample **2-1** thermal cycles 4 – 6.

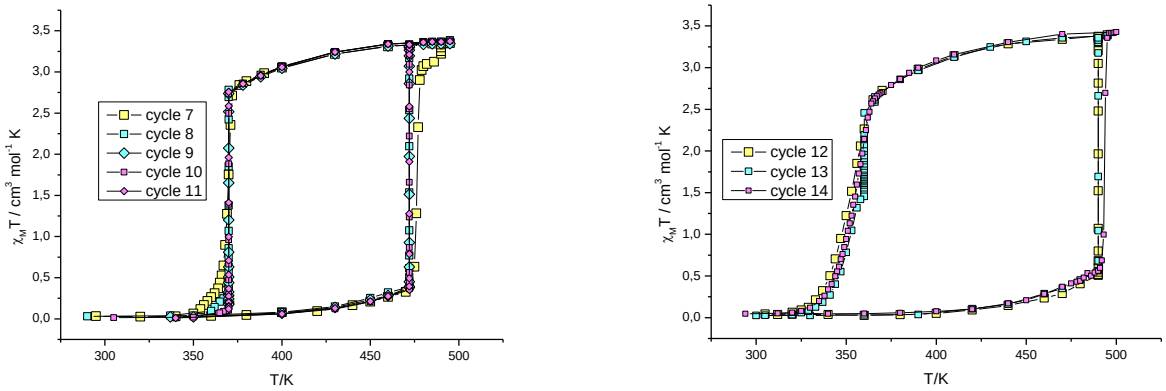

Figure S40. Left: sample **2-2**, thermal cycles 7 – 11. Right: sample **2-3**, thermal cycles 12 – 14.

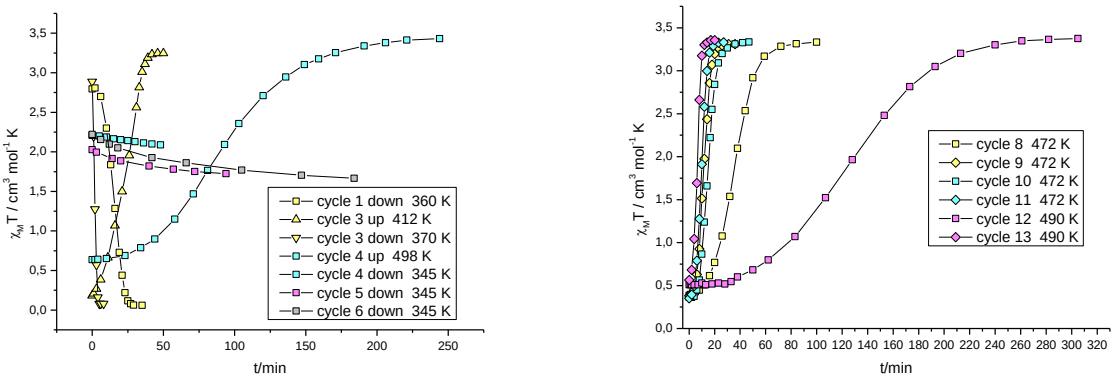

Figure S41. Left: samples **2, 2-1** and **2-2**. Kinetic curves for the cycles 1, 3 – 6 (LS → HS and HS → LS transformations). Right: sample **2-3**. Kinetic curves for the cycles 8 – 13 (LS → HS transformation).

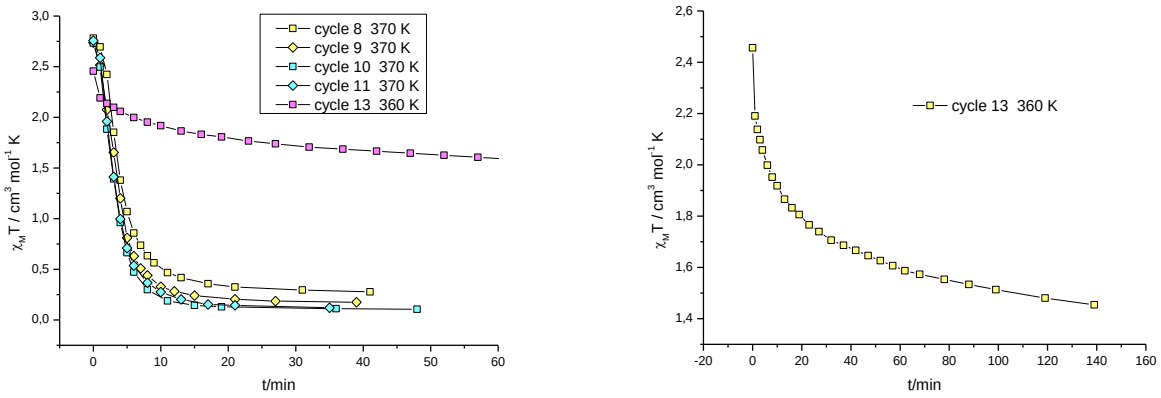

Figure S42. Samples **2-2** and **2-3**. Kinetic curves for the cycles 8 – 11 and 13 (HS → LS transformation).

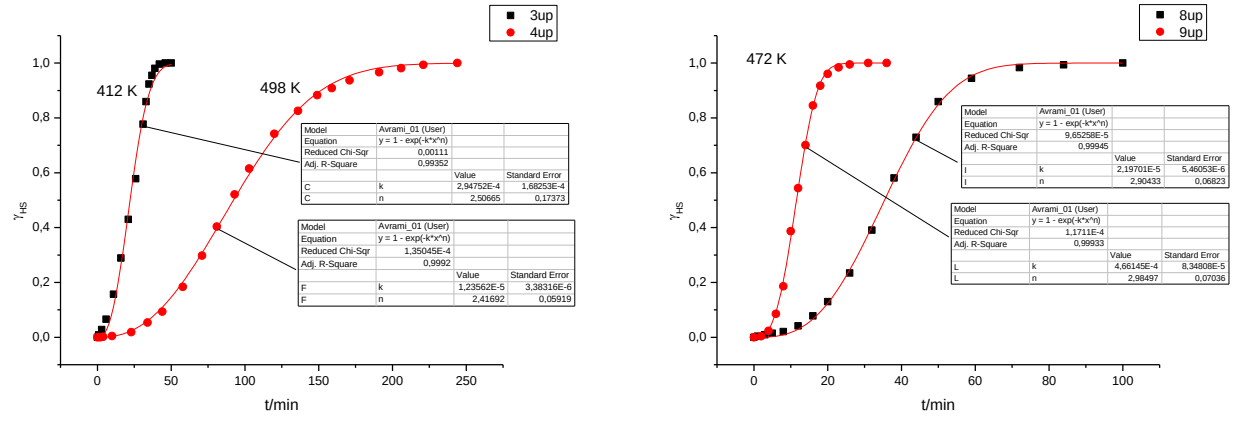

Figure S43. Fitting of kinetic curves for **2**, **2-1** and **2-2** using the JMAK model (LS → HS transformation; left: cycles 3 and 4; right: cycles 8 – 9).

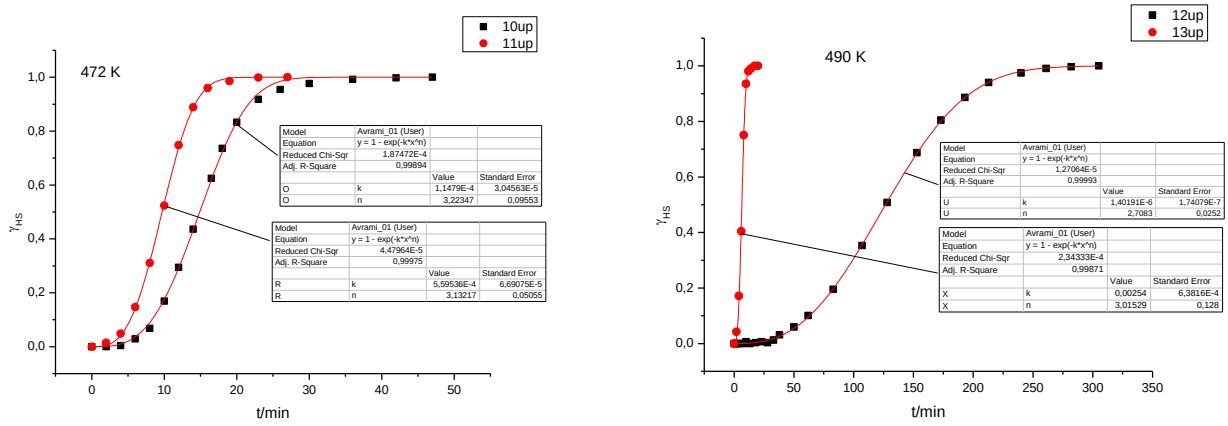

Figure S44. Fitting of kinetic curves for **2-2** and **2-3** using the JMAK model (LS → HS transformation; left: cycles 10 and 11; right: cycles 12 and 13).

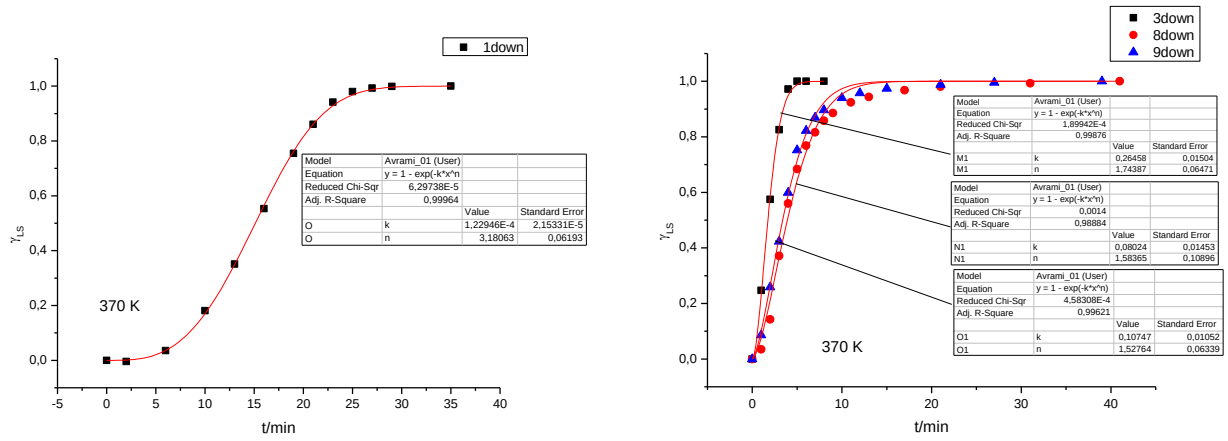

Figure S45. Fitting of kinetic curves for **2** and **2-2** using the JMAK model (HS → LS transformation; left: cycle 1; right: cycles 3, 8 and 9).

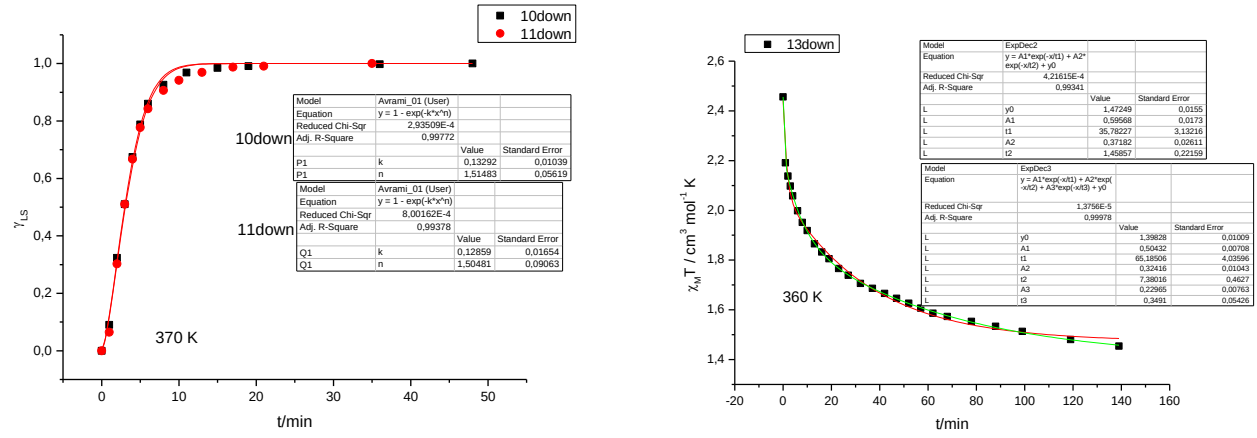

Figure S46. Left: fitting of kinetic curves for **2-2** using the JMAK model (HS → LS transformation; cycles 10 and 11). Right: fitting of a kinetic curve for **2-3** in bi- and tri-exponential approximations (HS → LS transformation; cycle 13).

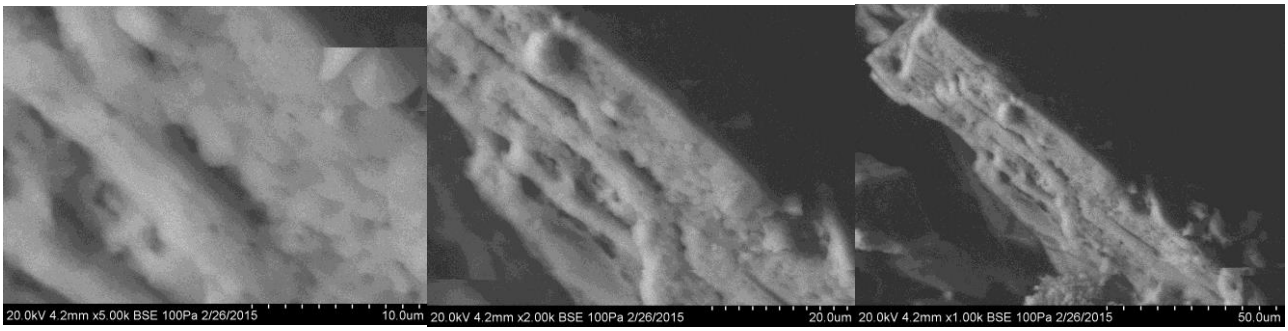

Figure S47. SEM images of the sample **2-3** after thermal cycling.

Sample 2-4

Parent phase $\mathbf{1}^{\mathbf{A/LS}}$. This sample of the phase $\mathbf{1}^{\mathbf{A/LS}}$ was taken from the experiment **2-2**, vigorously ground with pestle and mortar, exposed to water vapor for 1 h (no change in the mass was observed) and sealed.

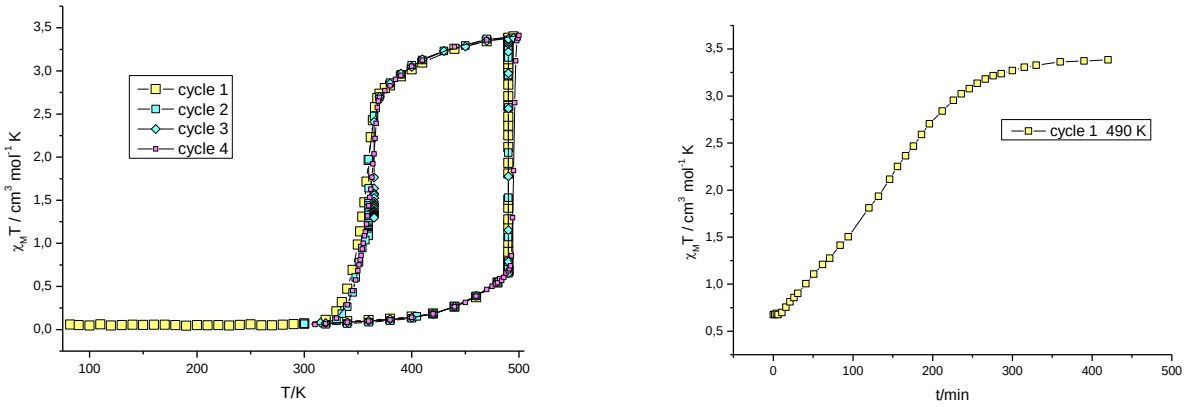

Figure S48. Sample **2-4**. Thermal cycles 1 – 4 (left) and a kinetic curve for the cycle 1 (LS → HS, right).

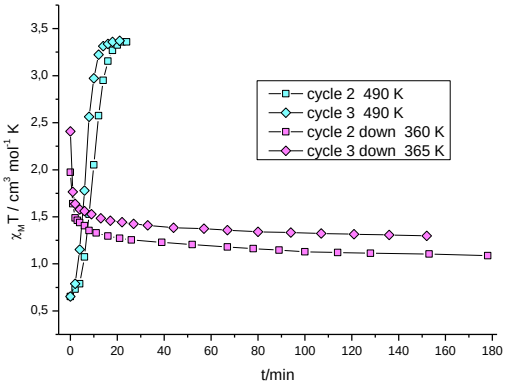

Figure S49. Sample **2-4**. Kinetic curves for the cycles 2 and 3 (LS → HS and HS → LS transformations).

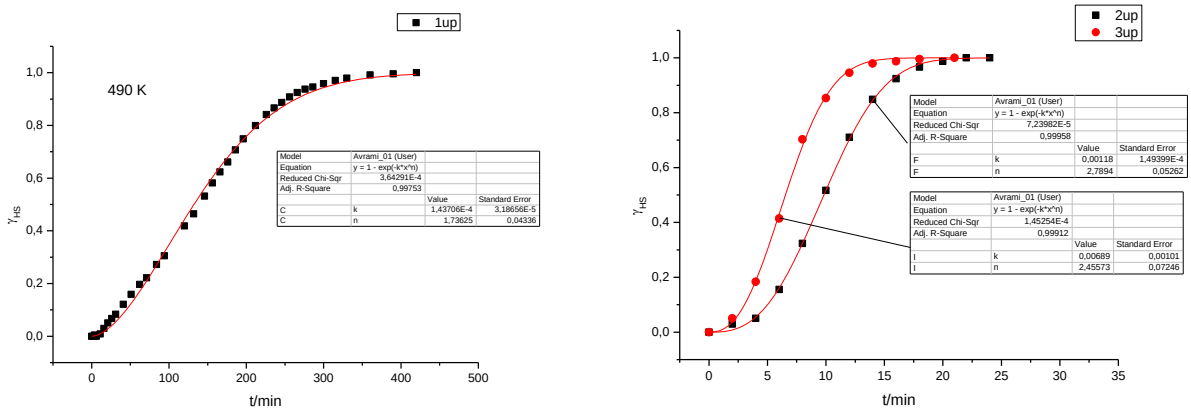

Figure S50. Fitting of kinetic curves for **2-4** using the JMAK model (LS → HS; left: cycle 1; right: cycles 2 and 3).

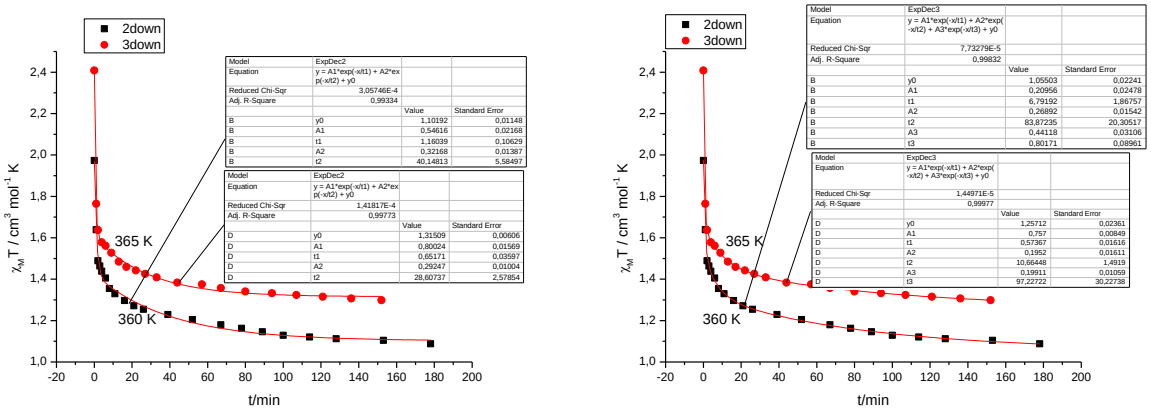

Figure S51. Fitting of kinetic curves for **2-4** (HS → LS; cycles 2 and 3) in bi- and tri-exponential approximations.

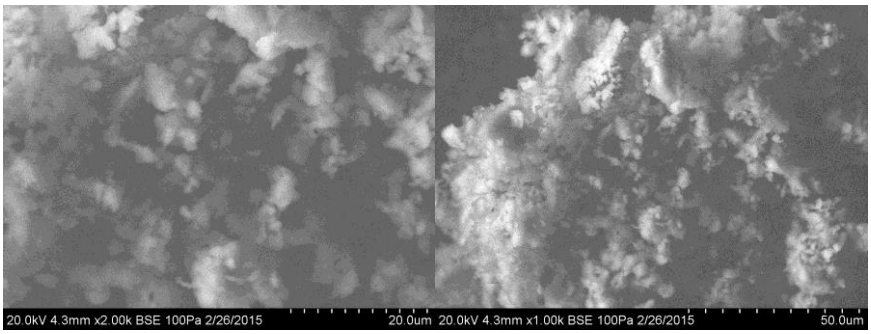

Figure S52. SEM images of the sample **2-4** after thermal cycling.

Sample 3

Parent phase $\mathbf{1^{LS} \cdot EtOH \cdot H_2O}$.

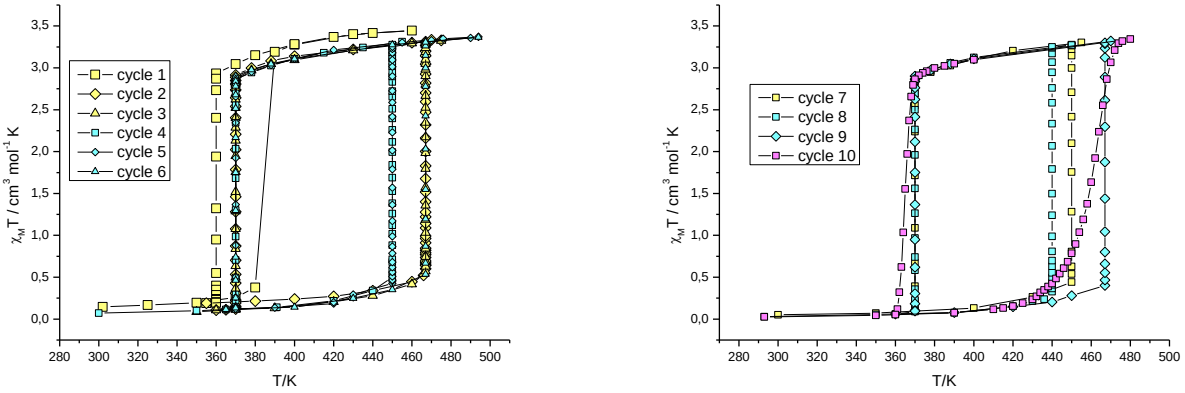

Figure S53. Sample **3**. Thermal cycles 1 – 6 (left) and 7 – 10 (right). Cycles 2, 3, 6 and 9: heating rate 6 K min^{-1}.

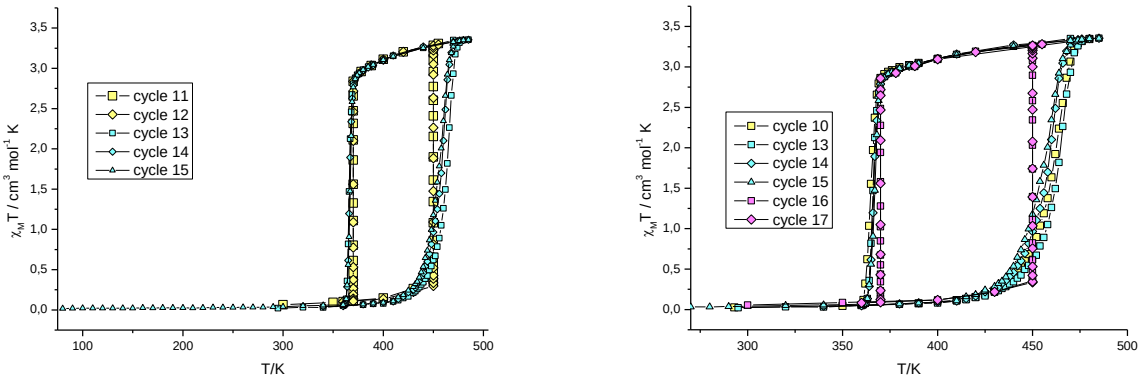

Figure S54. Sample **3**. Thermal cycles 11 – 15 (left) and 10, 13 – 17 (right).

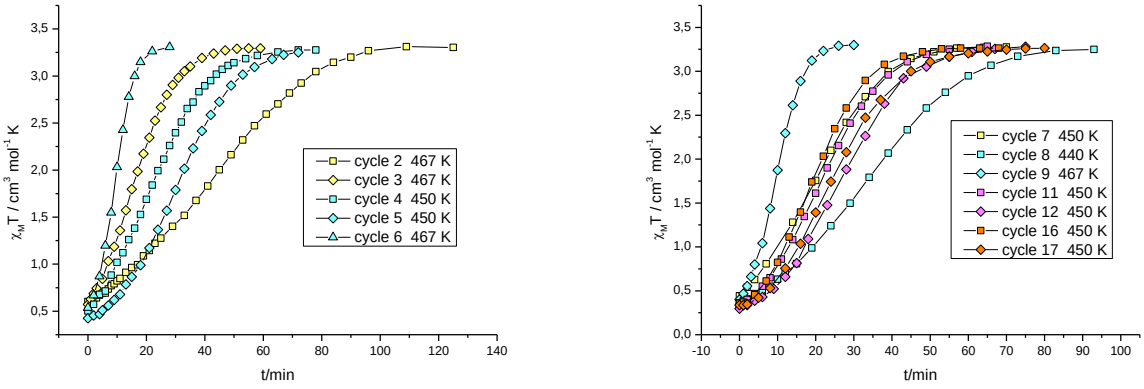

Figure S55. Sample **3**. LS → HS transformation. Kinetic curves for the cycles 2 – 6 (left) and 7 – 9, 11, 12, 16 and 17 (right).

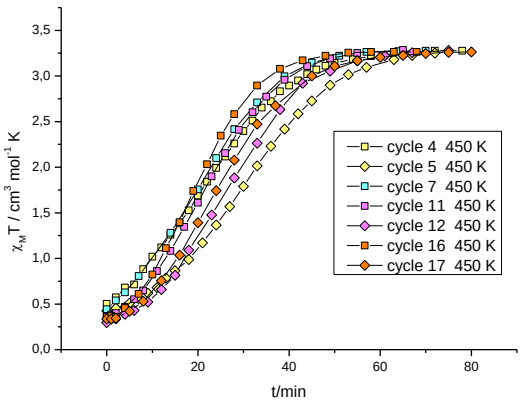

Figure S56. Sample **3**. Kinetic curves for LS → HS transformation at 450 K.

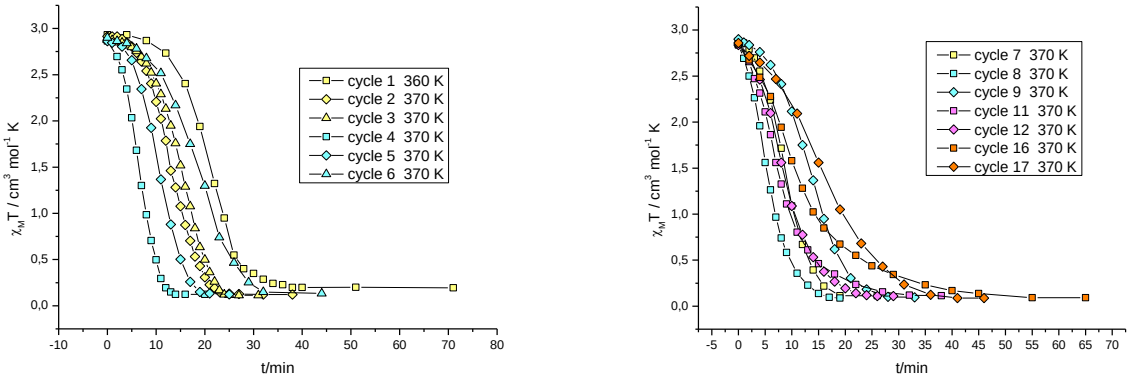

Figure S57. Sample **3**. HS → LS transformation. Kinetic curves for the cycles 1 – 6 (left) and 7 – 9, 11, 12, 16 and 17 (right).

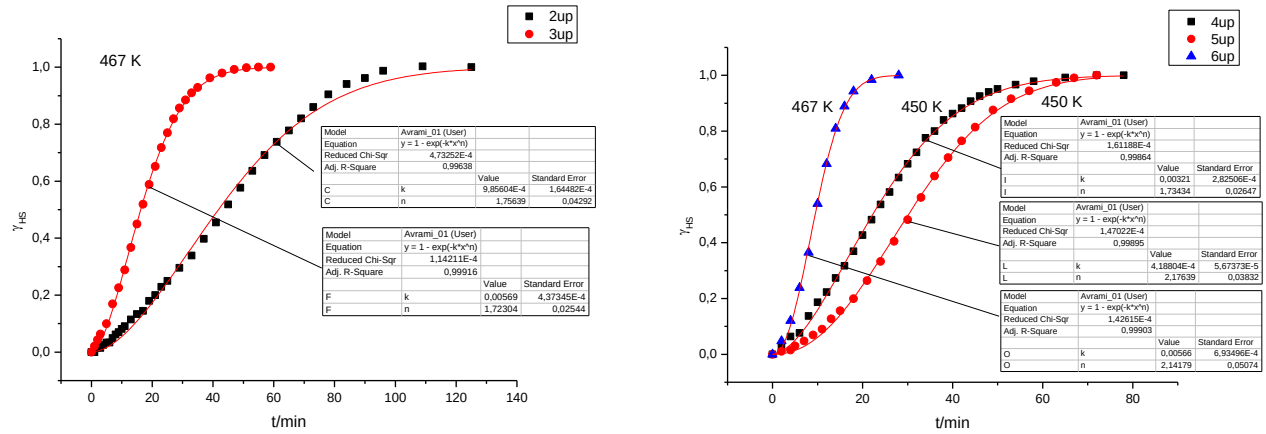

Figure S58. Fitting of kinetic curves for **3** using the JMAK model (LS → HS transformation; left: cycles 2 and 3; right: cycles 4 – 6).

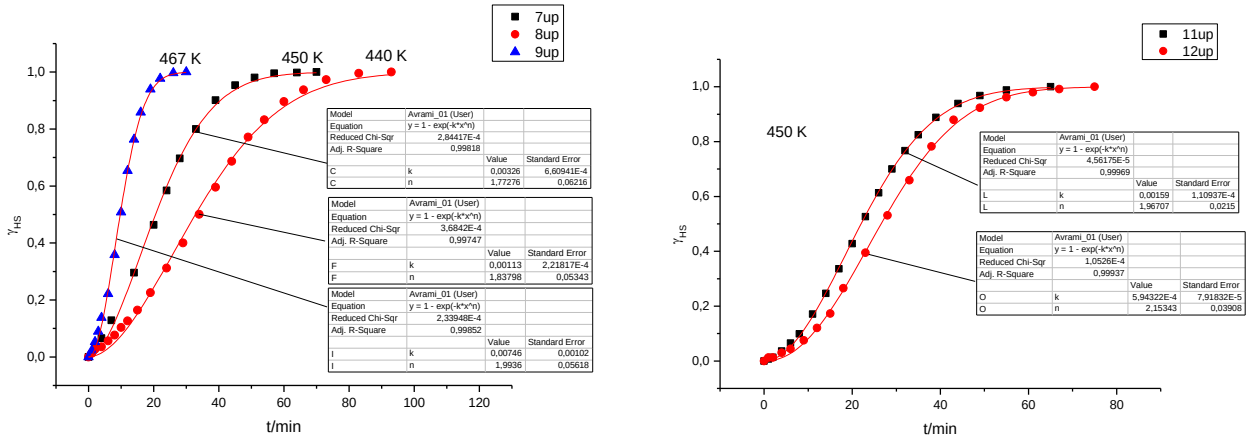

Figure S59. Fitting of kinetic curves for **3** using the JMAK model (LS → HS transformation; left: cycles 7 – 9; right: cycles 11 and 12).

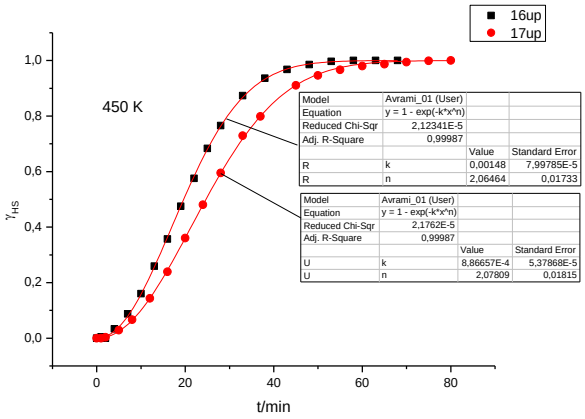

Figure S60. Fitting of kinetic curves for **3** using the JMAK model (LS → HS transformation; cycles 16 and 17).

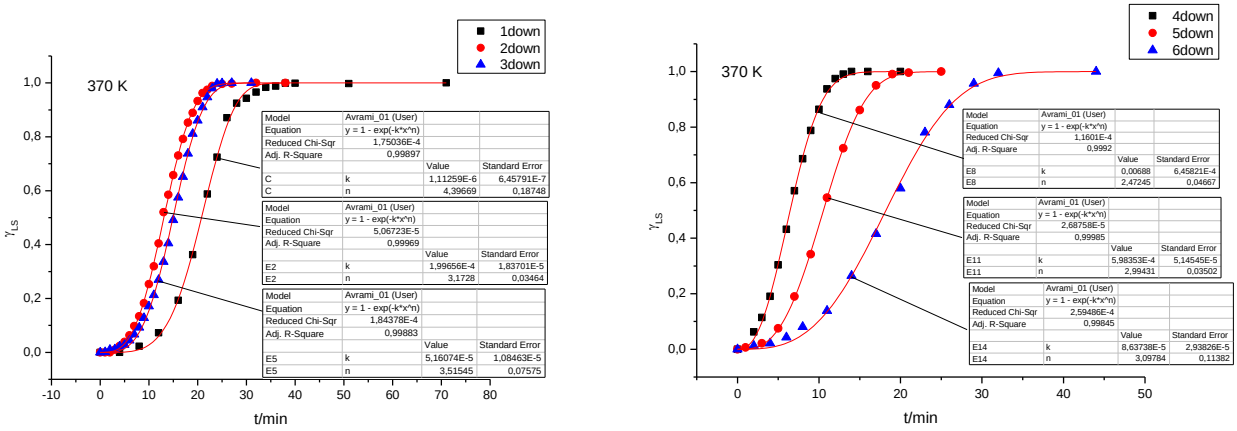

Figure S61. Fitting of kinetic curves for **3** using the JMAK model (HS → LS transformation left: cycles 1 – 3; right: cycles 4 – 6).

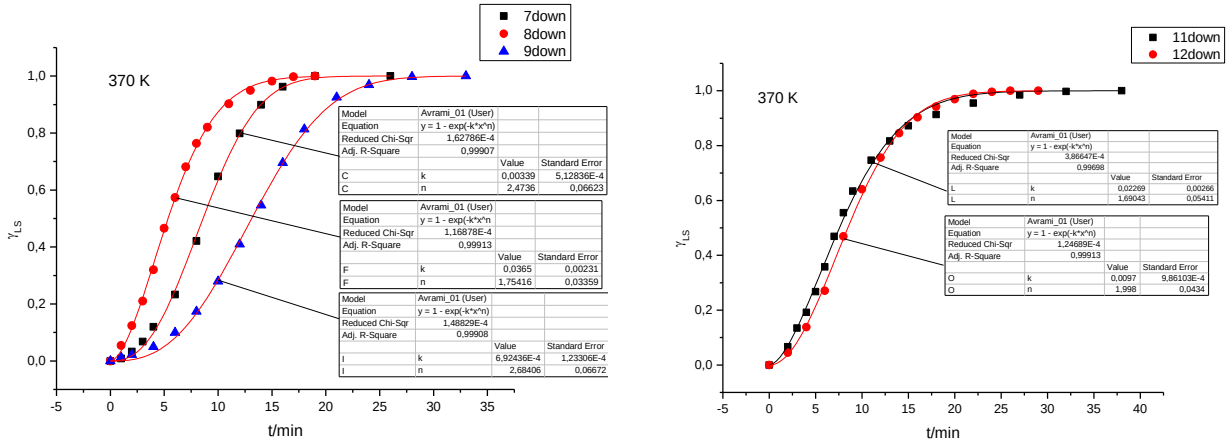

Figure S62. Fitting of kinetic curves for **3** using the JMAK model (HS → LS transformation; left: cycles 7 – 9; right: cycles 11 – 12).

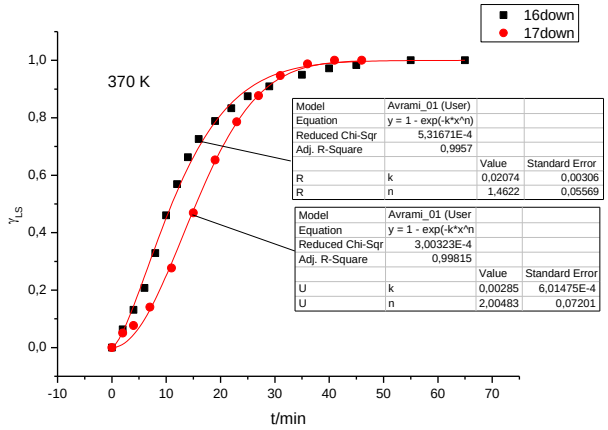

Figure S63. Fitting of kinetic curves for **3** using the JMAK model (HS → LS transformation; cycles 16 and 17).

Sample 4

Parent phase **β-1^{LS} · *x*H_2O**.

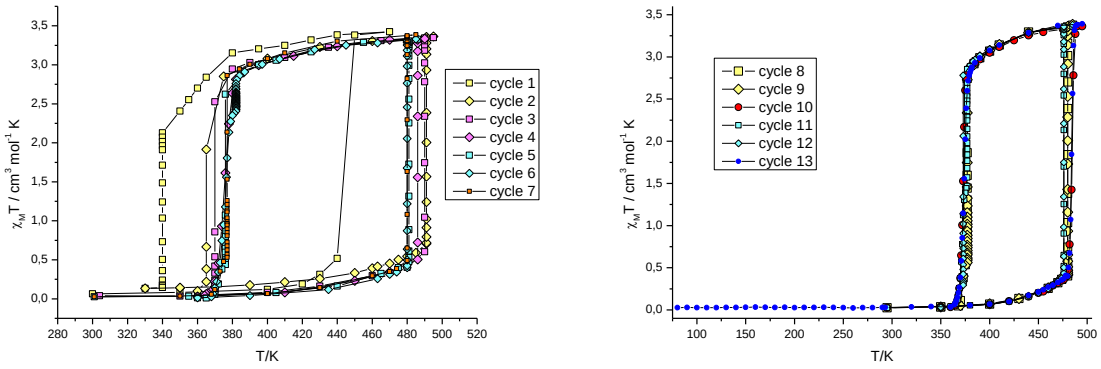

Figure S64. Sample **4**. Thermal cycles 1 – 7 (left) and 8 – 13 (right).

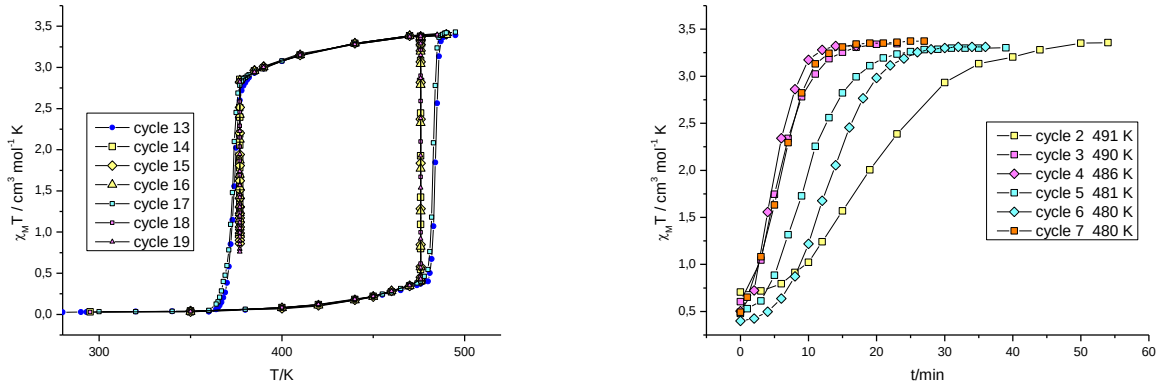

Figure S65. Sample **4**. Thermal cycles 13 – 19 (left) and kinetic curves for the cycles 2 – 7 (LS → HS; right).

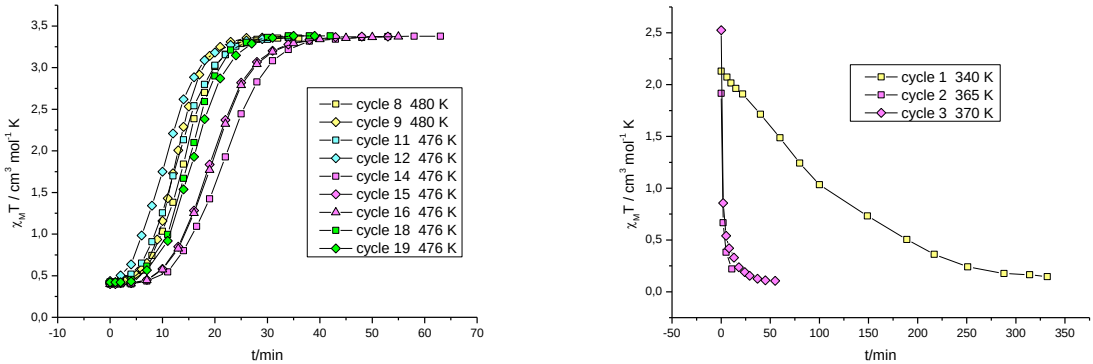

Figure S66. Sample **4**. Kinetic curves for the cycles 8, 9, 11, 12, 14 – 16, 18 and 19 (LS → HS; left) and for the cycles 1 – 3 (HS → LS; right).

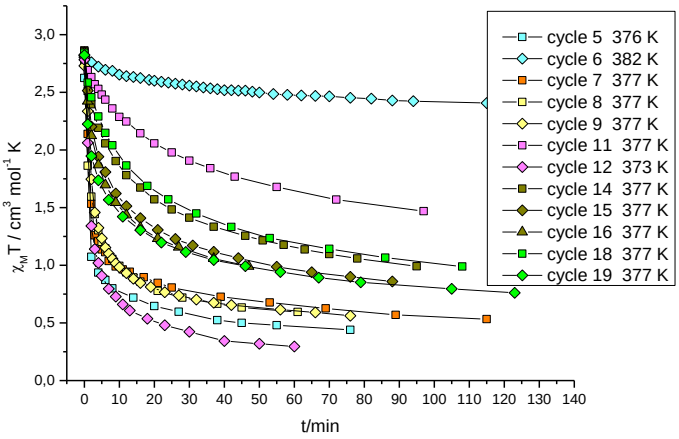

Figure S68. Sample **4**. Kinetic curves for the cycles 5 – 9, 11, 12, 14 – 16, 18 and 19 (HS → LS).

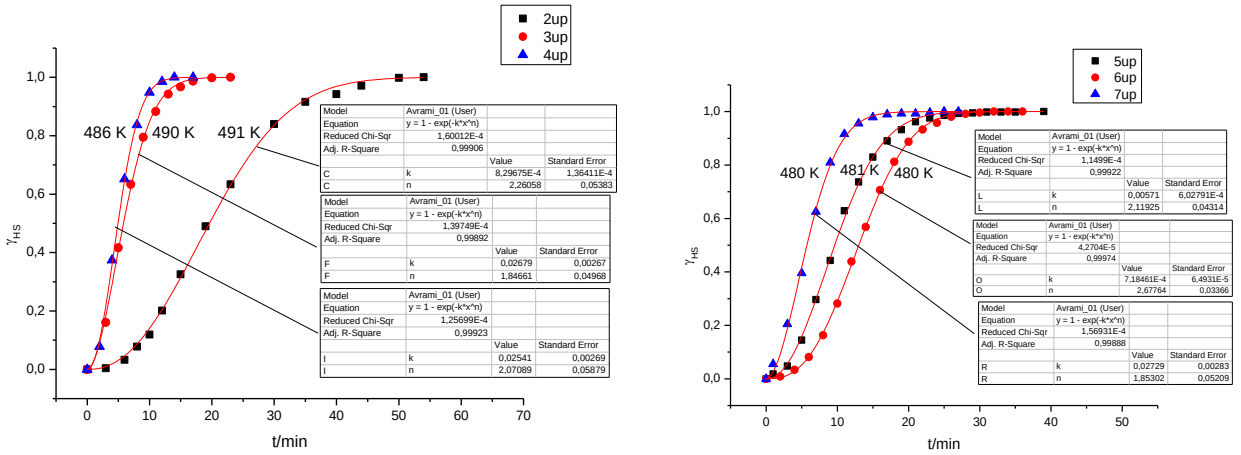

Figure S69. Fitting of kinetic curves for **4** using the JMAK model (LS → HS; left: cycles 2 – 4; right: cycles 5 and 7).

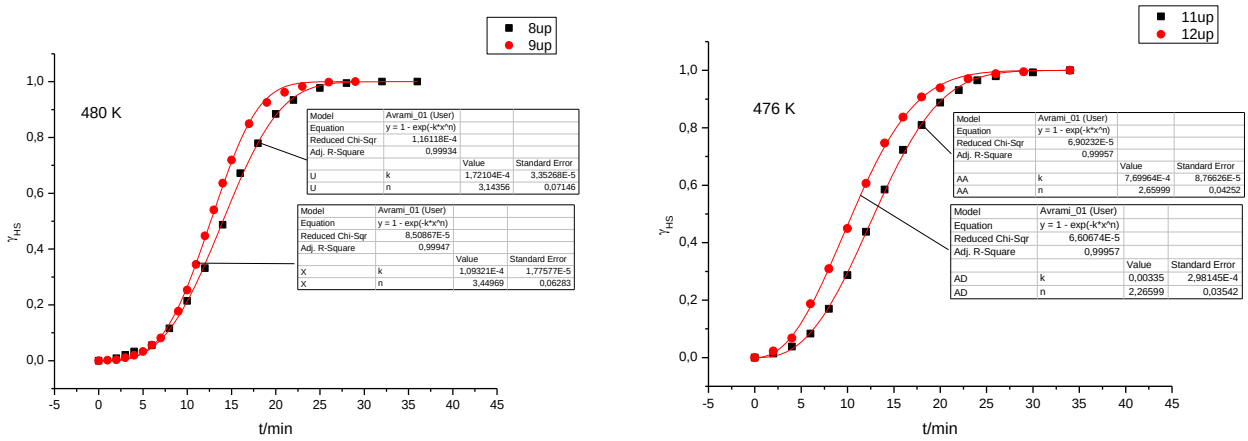

Figure S70. Fitting of kinetic curves for **4** using the JMAK model (LS → HS; left: cycles 8 and 9; right: cycles 11 and 12).

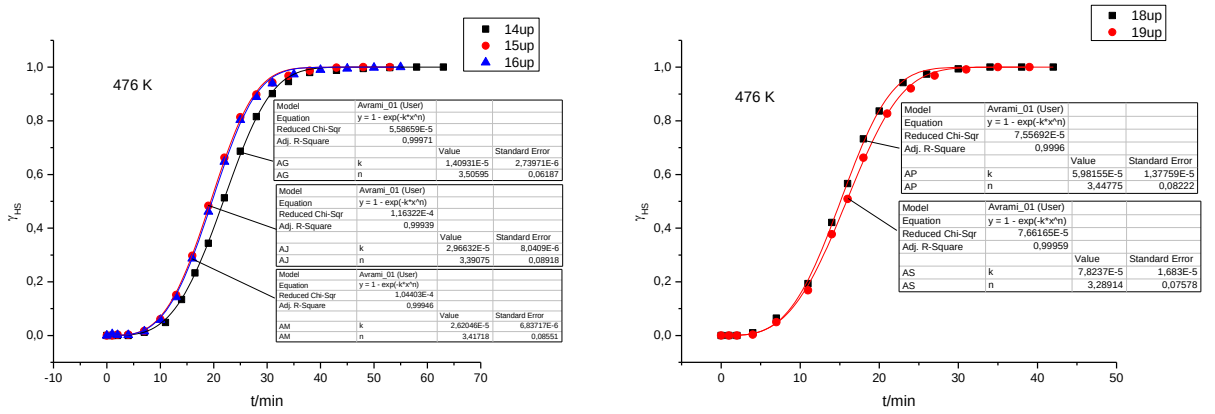

Figure S71. Fitting of kinetic curves for **4** using the JMAK model (LS → HS; left: cycles 14 – 16; right: cycles 18 and 19).

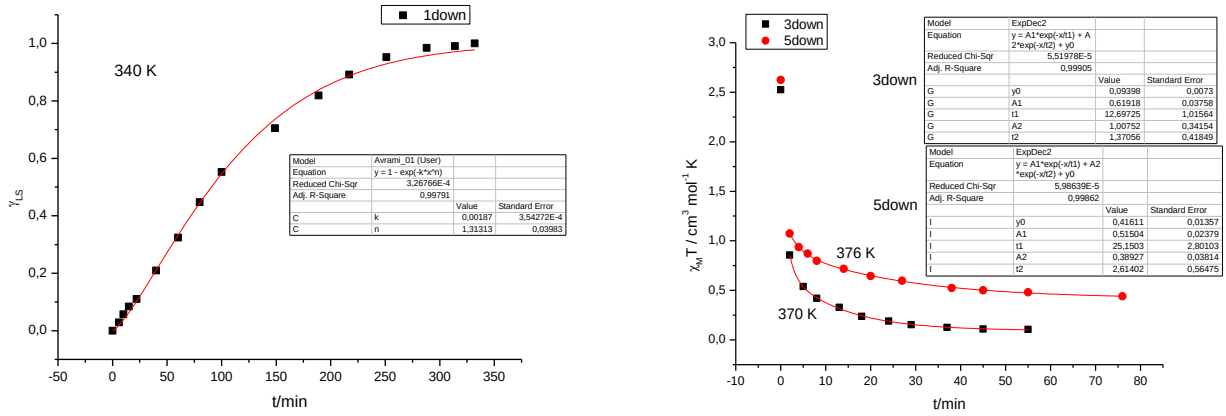

Figure S72. Fitting of kinetic curves for **4** using the JMAK model (left: cycle 1, HS → LS) and bi-exponential approximation (right: cycles 3 and 5, HS → LS).

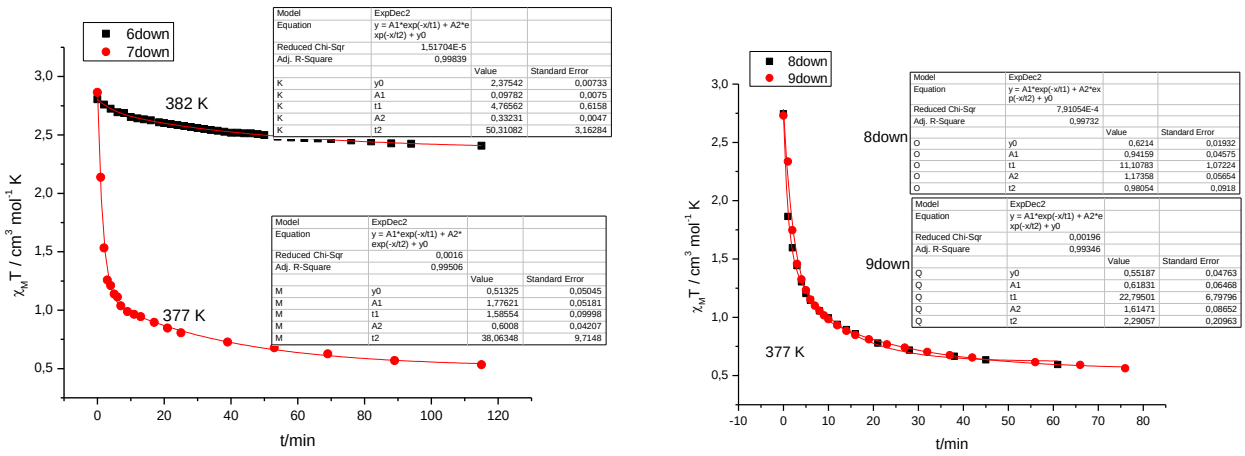

Figure S73. Fitting of kinetic curves for **4** in bi-exponential approximation (HS → LS; right: cycles 6 and 7; left: cycles 8 and 9).

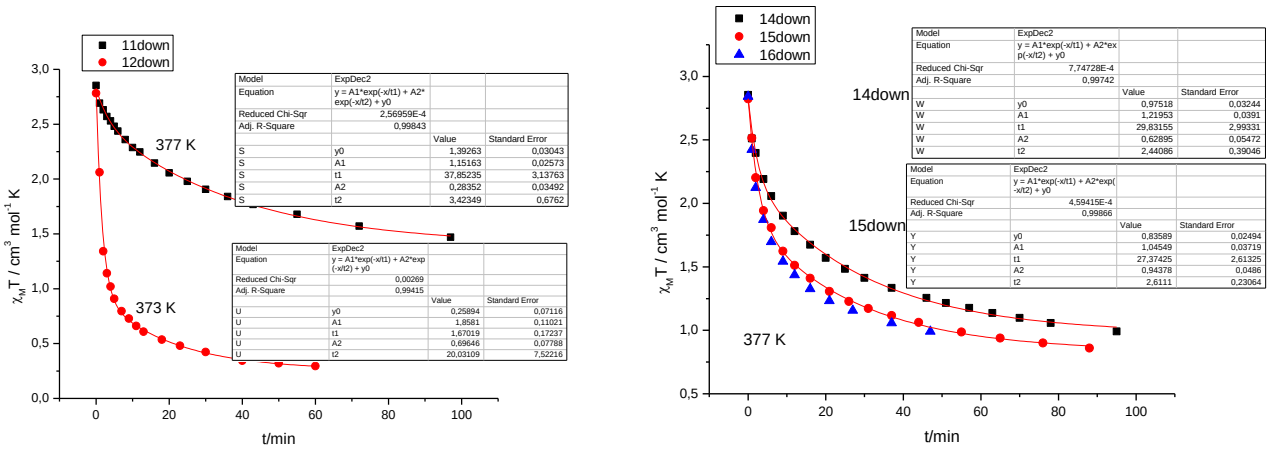

Figure S74. Fitting of kinetic curves for **4** in bi-exponential approximation (HS → LS; right: cycles 11 and 12; left: cycles 14 – 16).

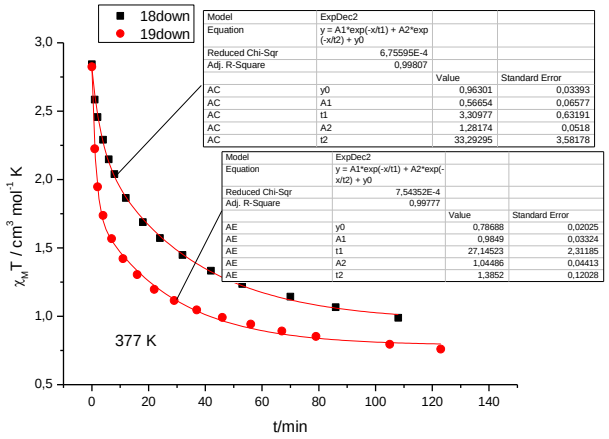

Figure S75. Fitting of kinetic curves for **4** in bi-exponential approximation (cycles 18 and 19, HS → LS).

Elemental analysis of the sample after thermal cycling (%), calcd for $C_{30}H_{30}N_{10}B_2F_8Fe$ (760.10): C 47.4, H 4.0, N 18.4; found C 47.2, H 4.1, N 18.4.

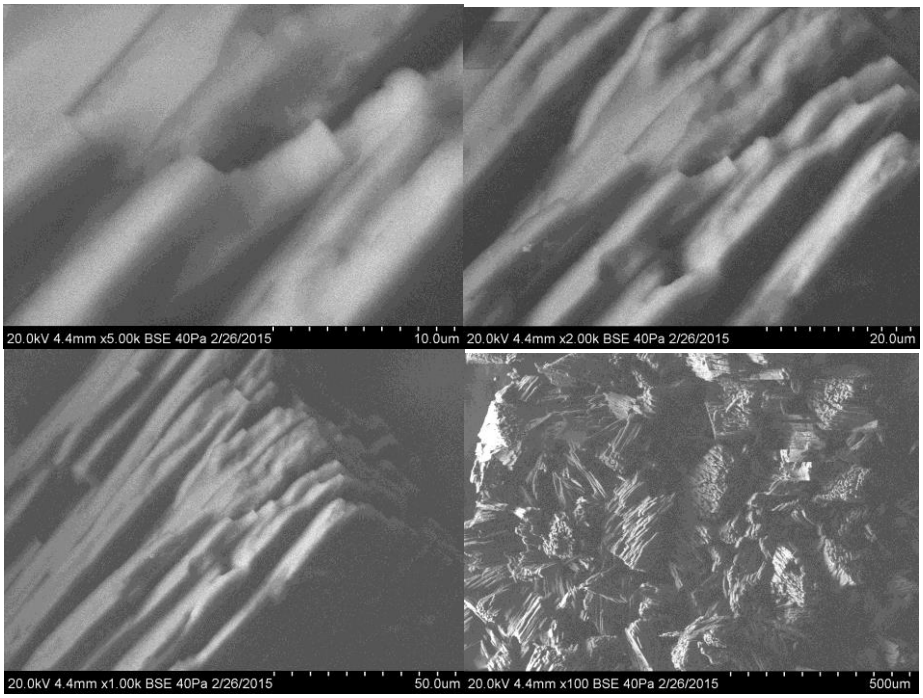

Figure S76. SEM images of the sample **4** after thermal cycling.

Samples 5 and 5-1

Sample 5

Cycles 1 and 2. Parent phase **β-1^{LS}·*x*H$_2$O**. The SCO regime in the cycles 1 and 2 is typical for the phase **1^{D}**.

Sample 5-1

Cycles 3 – 12. After the cycles 1 and 2 had been done the sample was taken off the ampoule, exposed to water vapor for 48 h (the value of $\chi_M T$ dropped to *ca*. 0.1 cm^3 mol^{-1} K; no change in the mass was detected) followed by ampoule sealing.

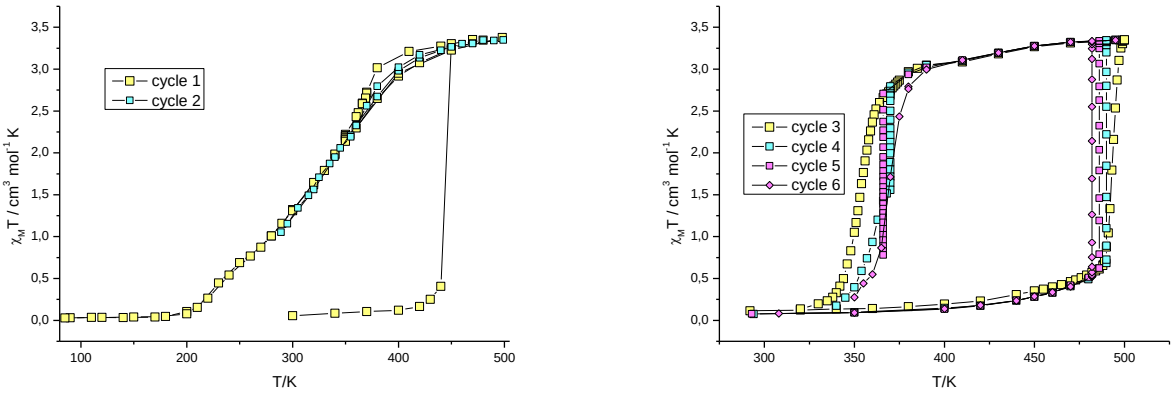

Figure S77. Left: sample **5**. Thermal cycles 1 and 2. Right: sample **5-1**. Thermal cycles 3 – 6.

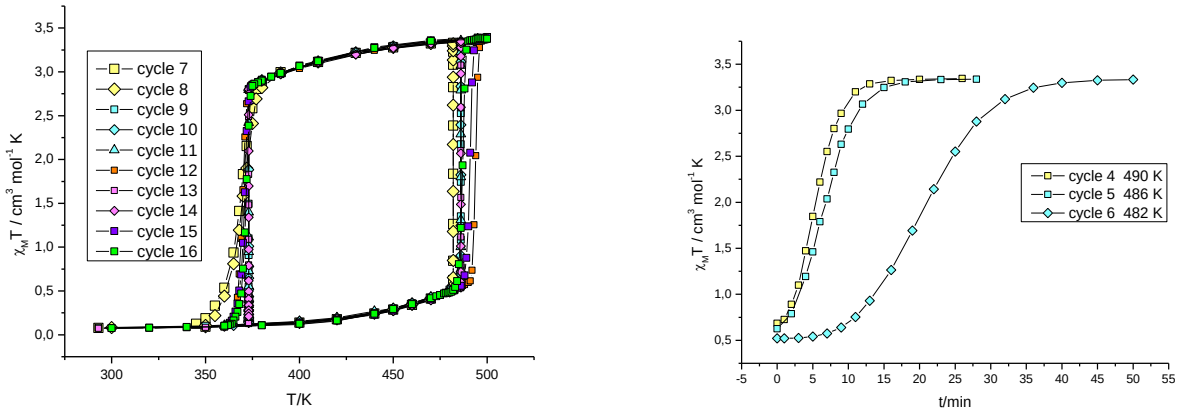

Figure S78. Sample **5-1**. Thermal cycles 8 –16 (left; cycle 12, 0.9 K min^{-1}; cycle 15, 0.4 K min^{-1}; cycle 16, 0.25 K min^{-1}) and kinetic curves for the cycles 4 – 6 (LS → HS transformation, right).

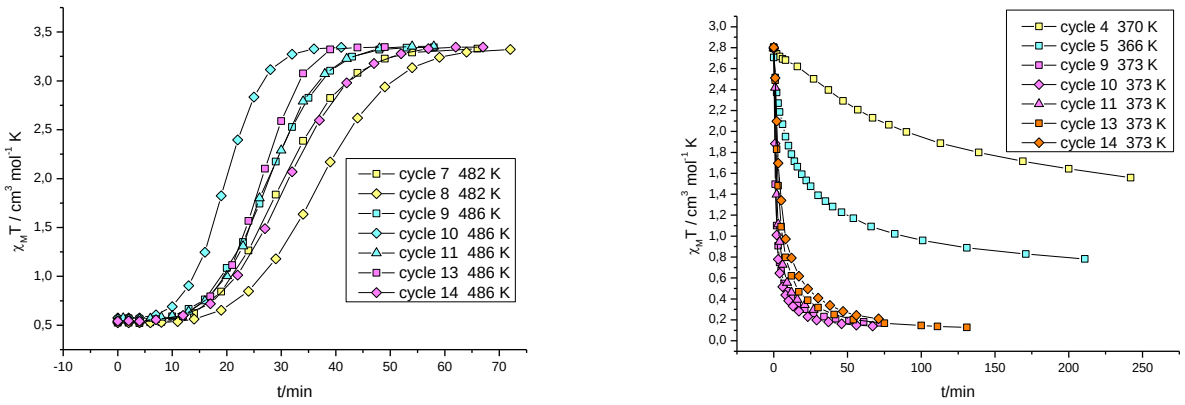

Figure S79. Sample **5-1**. Kinetic curves for the cycles 7 – 11, 13, 14 (LS → HS transformation, left) and 4, 5, 9 – 11, 13 and 14 (HS → LS transformation, left).

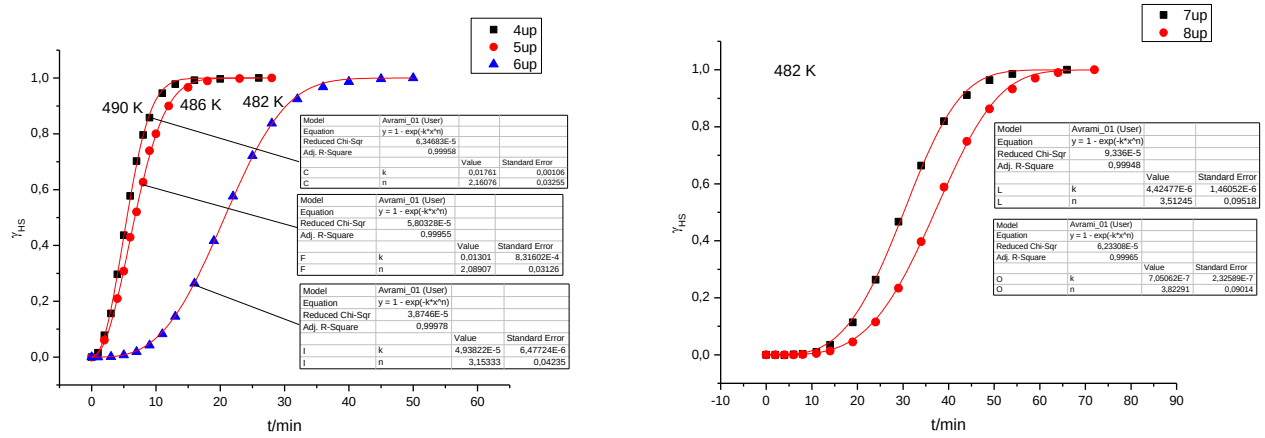

Figure S80. Fitting of kinetic curves for **5-1** using the JMAK model (LS → HS; left: cycles 4 – 6; right: cycles 7 and 8).

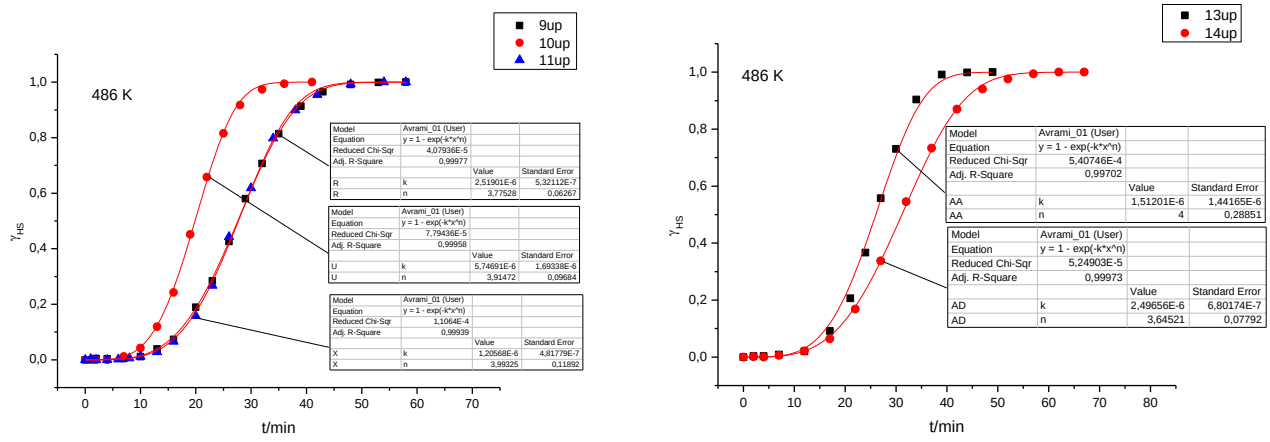

Figure S81. Fitting of kinetic curves for **5-1** using the JMAK model (LS → HS; left: cycles 9 – 11; right: cycles 13 and 14).

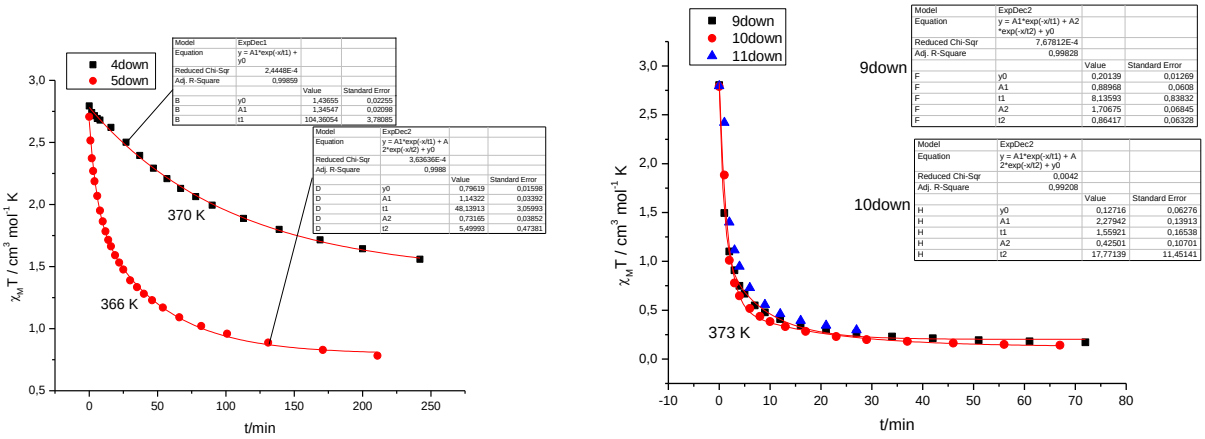

Figure S82. Fitting of kinetic curves for **5-1** in mono- and bi-exponential approximations (HS → LS; left: cycles 4 and 5; right: cycles 9 and 10).

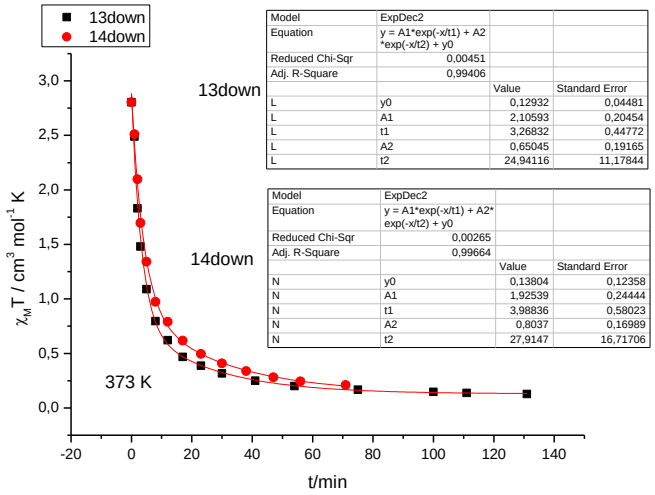

Figure S83. Fitting of kinetic curves for **5-1** in bi-exponential approximation (HS → LS; cycles 13 and 14).

Sample 6

Parent phase **β-1^{LS} · *x*H_2O**. The phase was exposed to water and ethanol vapors for 48 h (mass increase: 4.6 %).

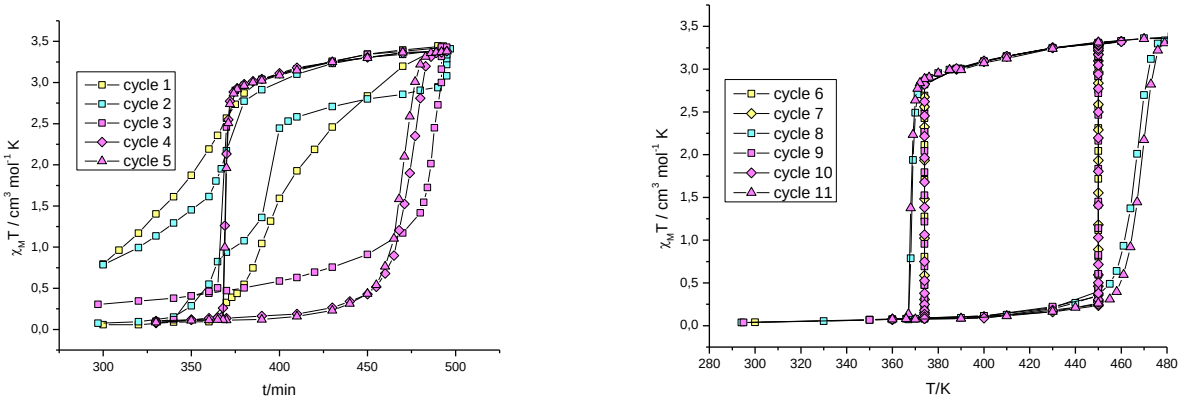

Figure S84. Sample **6**. Thermal cycles 1 –5 (left) and 6 – 11 (right).

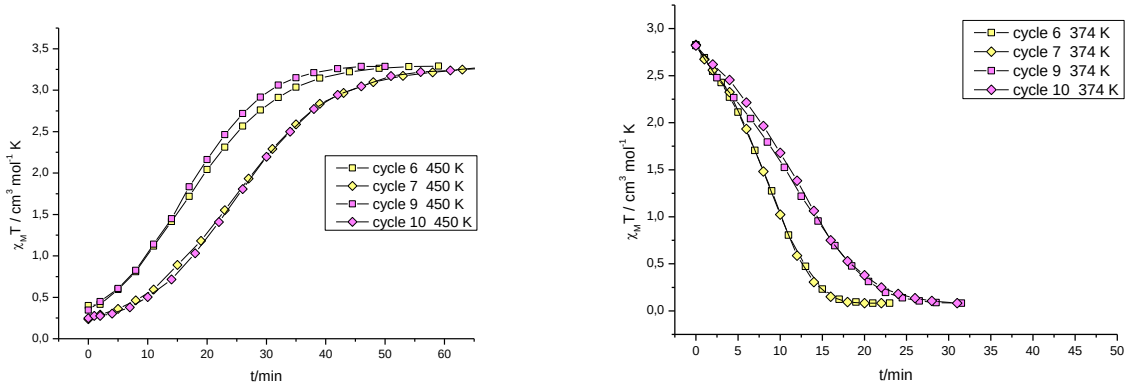

Figure S85. Sample **6**. Kinetic curves for the cycles 6, 7, 9, 10 (left: LS → HS transformation, right: HS → LS transformation).

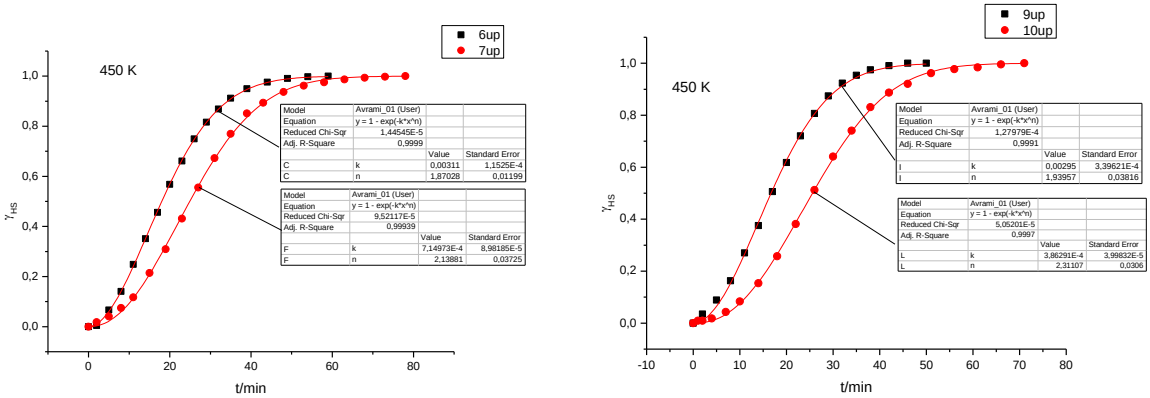

Figure S86. Fitting of kinetic curves for **6** using the JMAK model (LS → HS; left: cycles 6 and 7; right: cycles 9 and 10).

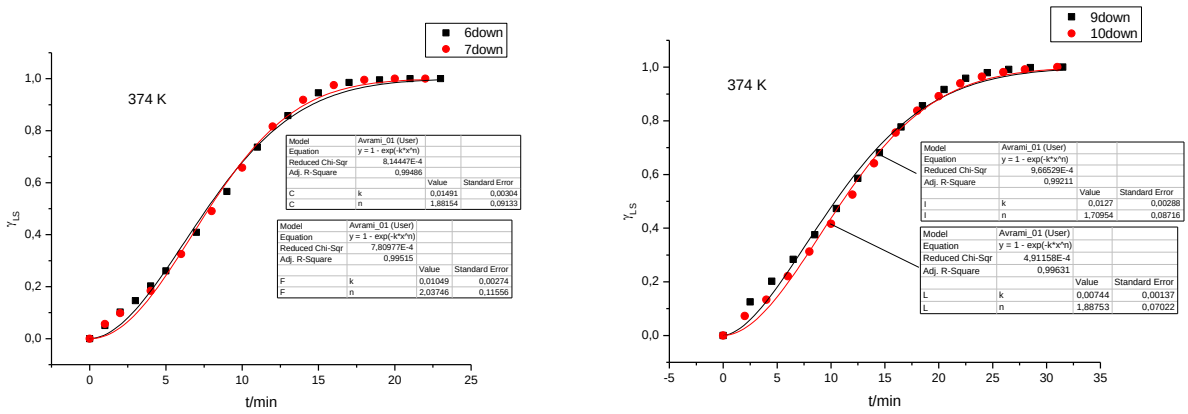

Figure S87. Fitting of kinetic curves for **6** using the JMAK model (HS → LS; left: cycles 6 and 7; right: cycles 9 and 10).

Sample 7

Parent phase $\mathbf{1^{LS} \cdot EtOH \cdot H_2O}$.

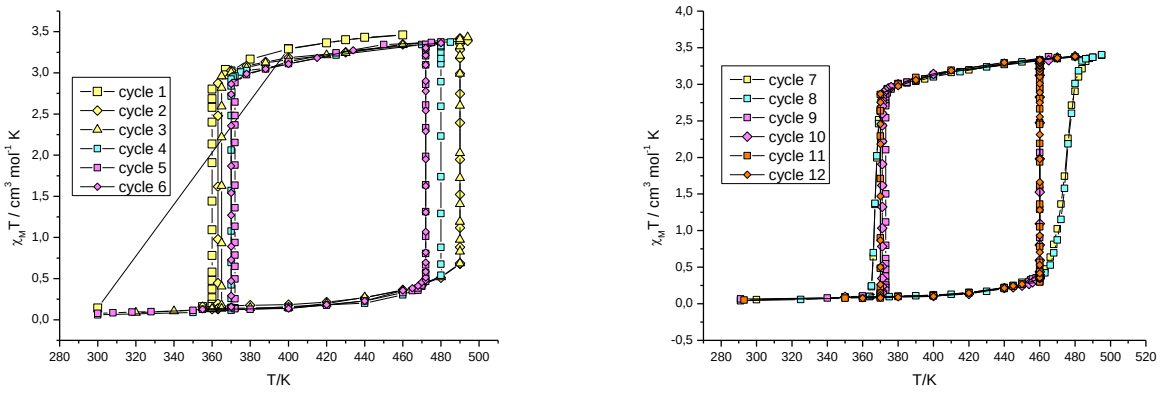

Figure S88. Sample **7**. Thermal cycles 1 – 6 (left) and 7 – 12 (right). Cycle 1: heating rate 10 K/min (300 – 400 K). Cycles 2, 3, 4, 11, 12: heating rate 6 K/min. Cycles 5, 6, 9, 10: heating rate 2 K min^{-1}.

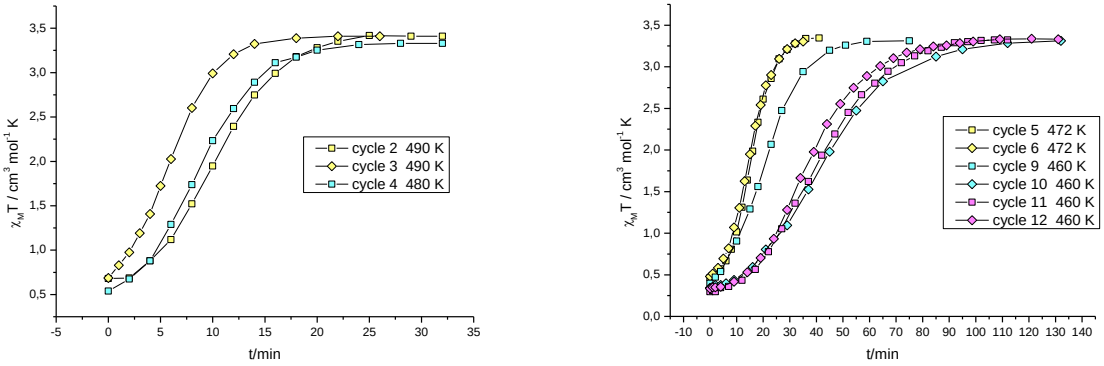

Figure S89. Sample **7**. LS → HS transformation. Kinetic curves for the cycles 2 – 4 (left) and 5, 6, 9 – 12 (right).

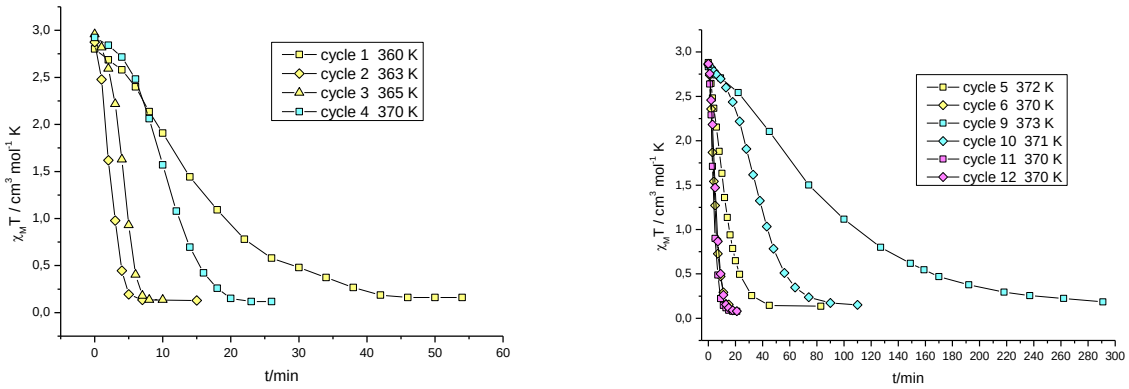

Figure S90. Sample **7**. HS → LS transformation. Kinetic curves for the cycles 1 – 4 (left) and 5, 6, 9 – 12 (right).

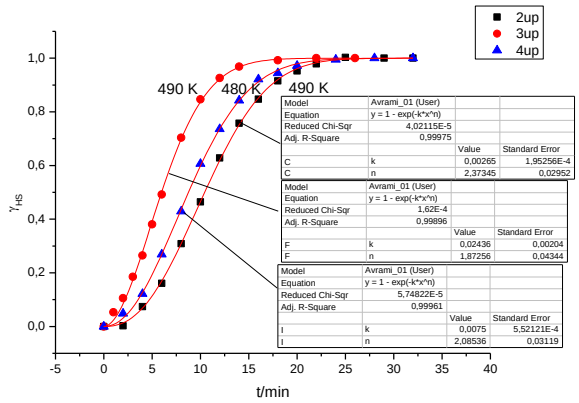

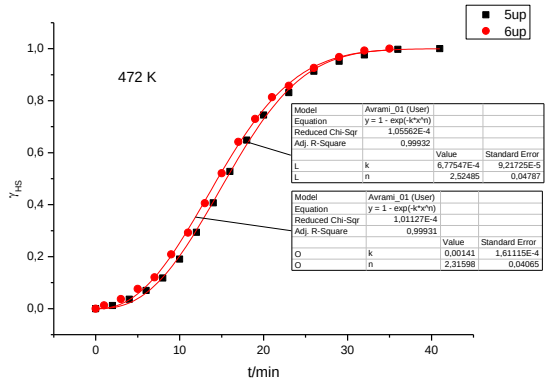

Figure S91. Fitting of kinetic curves for **7** using the JMAK model (LS → HS; left: cycles 2 – 4; right: cycles 5 and 6).

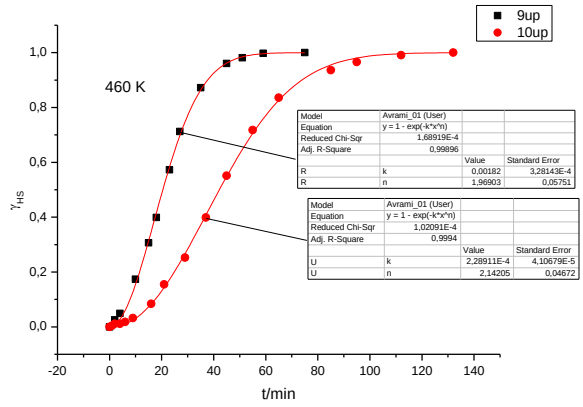

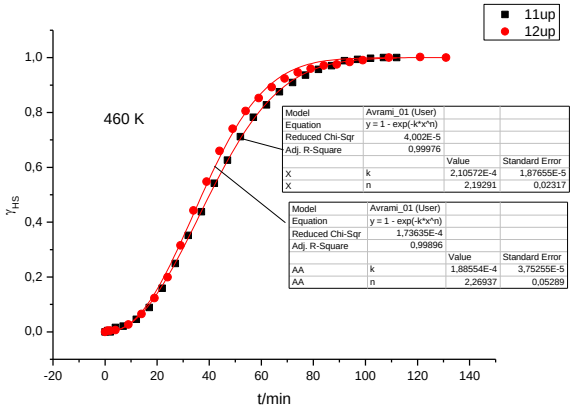

Figure S92. Fitting of kinetic curves for **7** using the JMAK model (LS → HS; left: cycles 9 and 10; right: cycles 11 and 12).

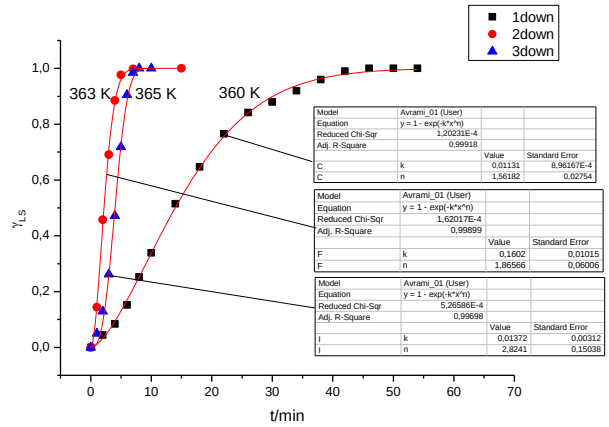

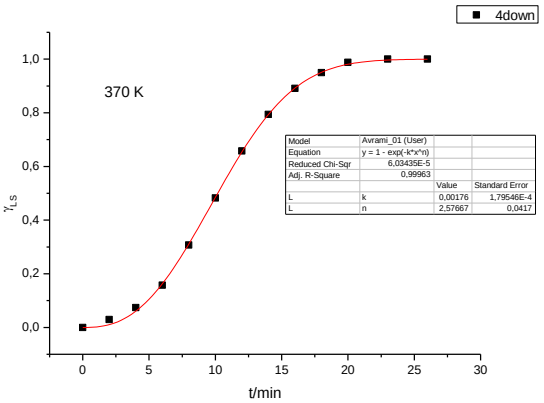

Figure S93. Fitting of kinetic curves for **7** using the JMAK model (HS → LS; left: cycles 1 – 3; right: cycle 4).

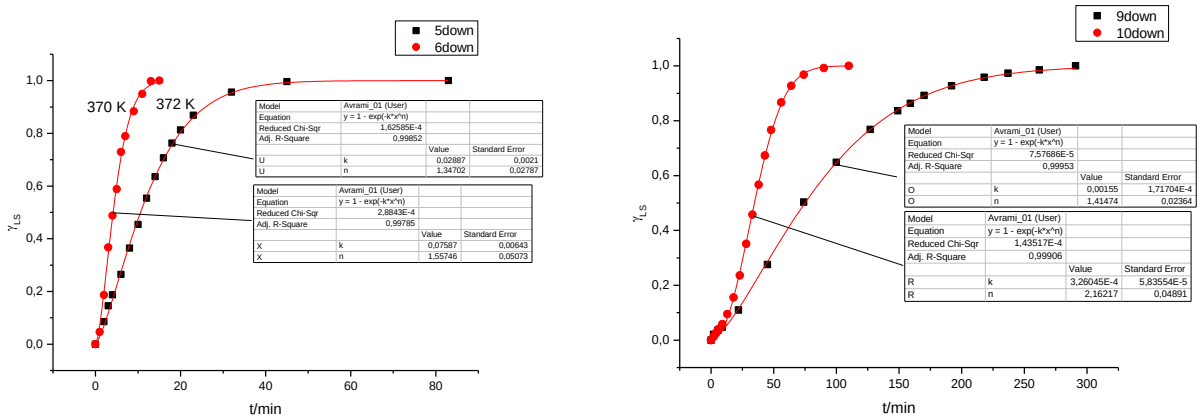

Figure S94. Fitting of kinetic curves for **7** using the JMAK model (HS → LS; left: cycles 5 and 6; right: cycles 9 and 10).

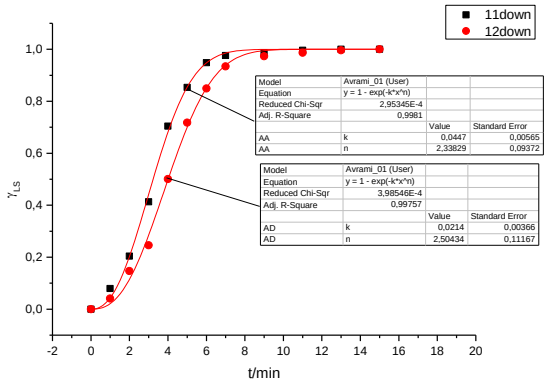

Figure S95. Fitting of kinetic curves for **7** using the JMAK model (HS → LS; cycles 11 and 12).

Sample 8

Parent phase $\mathbf{1^{LS} \cdot EtOH \cdot H_2O}$.

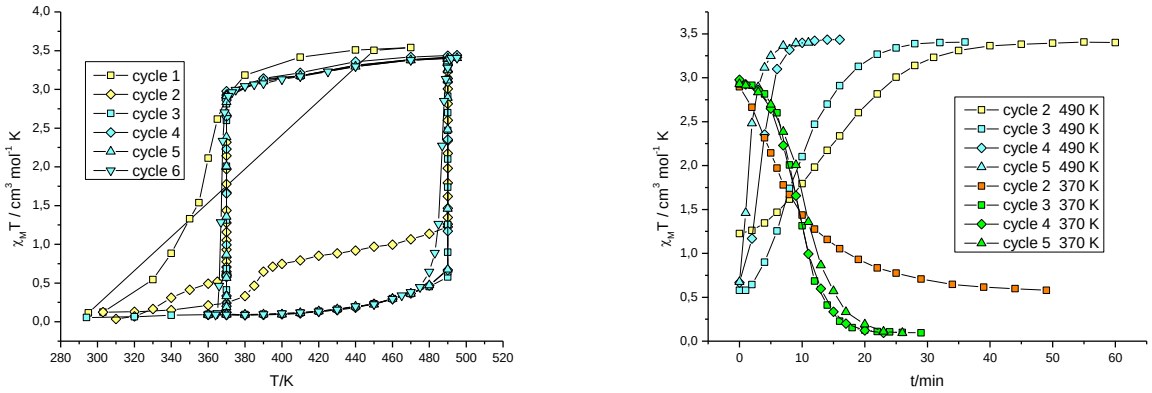

Figure S96. Sample **8**. Thermal cycles 1 – 6 (left) and kinetic curves for the cycles 2 – 5 (right). Heating rate in the cycle 1 was 10 K/min (300 – 450 K).

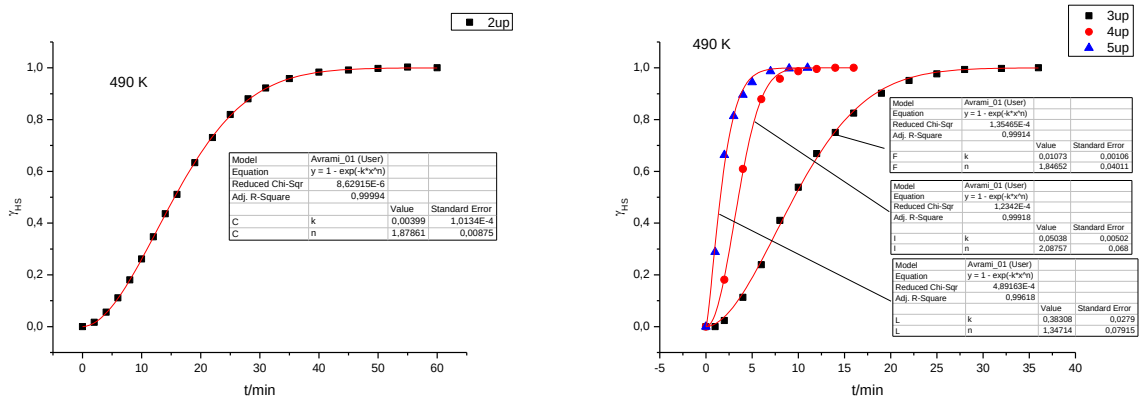

Figure S97. Fitting of kinetic curves for **8** using the JMAK model (LS → HS; left: cycle 2; right: cycles 3 – 5).

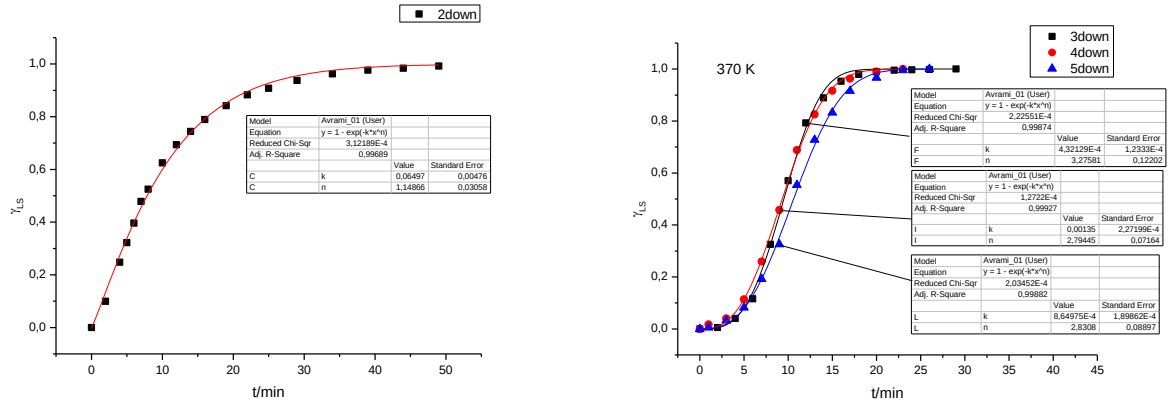

Figure S98. Fitting of kinetic curves for **8** using the JMAK model (HS → LS; left: cycle 2; right: cycles 3 – 5).

Sample 9

Parent phase **β-1^{LS} · *x*H_2O**.

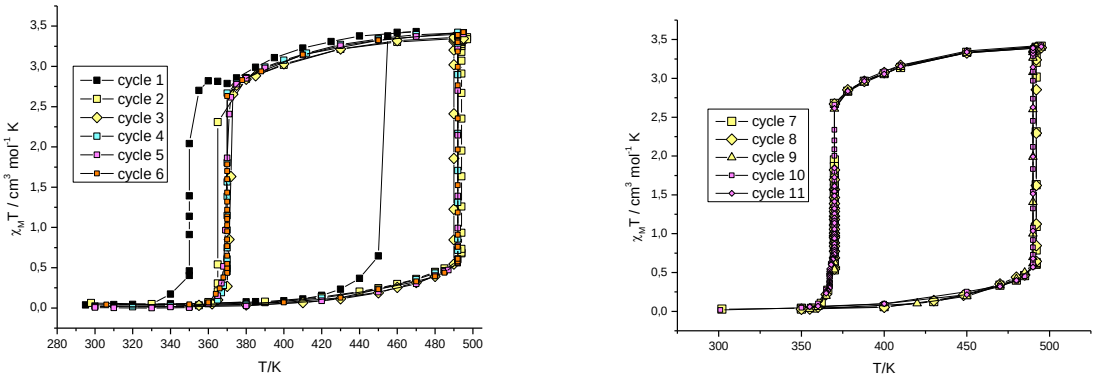

Figure S99. Sample **9**. Thermal cycles 1 – 6 (left) and 7 – 11 (right).

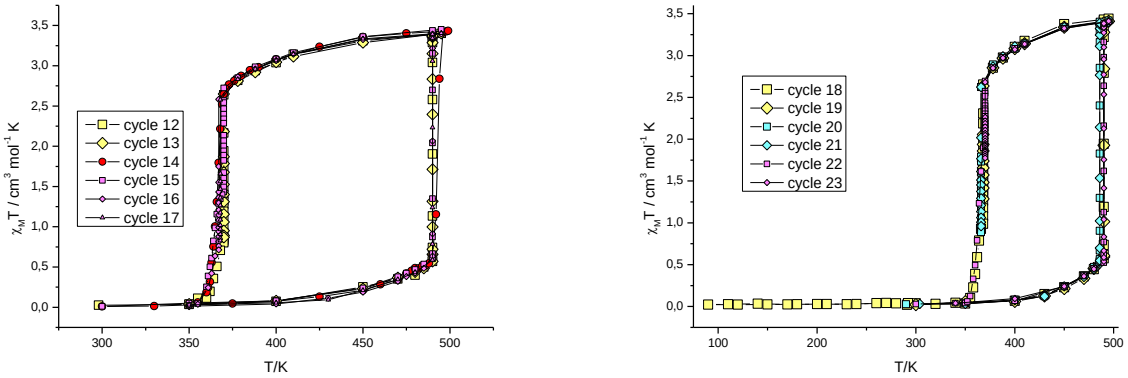

Figure S100. Sample **9**. Thermal cycles 12 – 17 (left) and 18 – 23 (right)

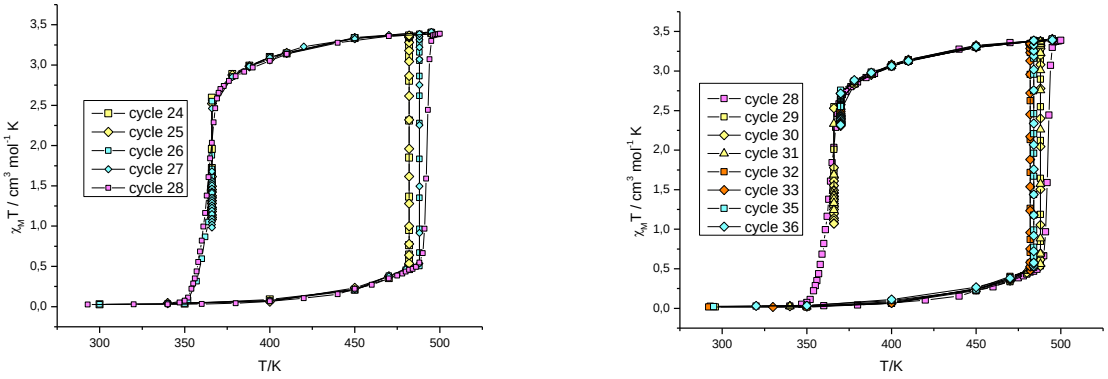

Figure S101. Sample **9**. Thermal cycles 24 – 28 (left) and 28 – 36 (right).

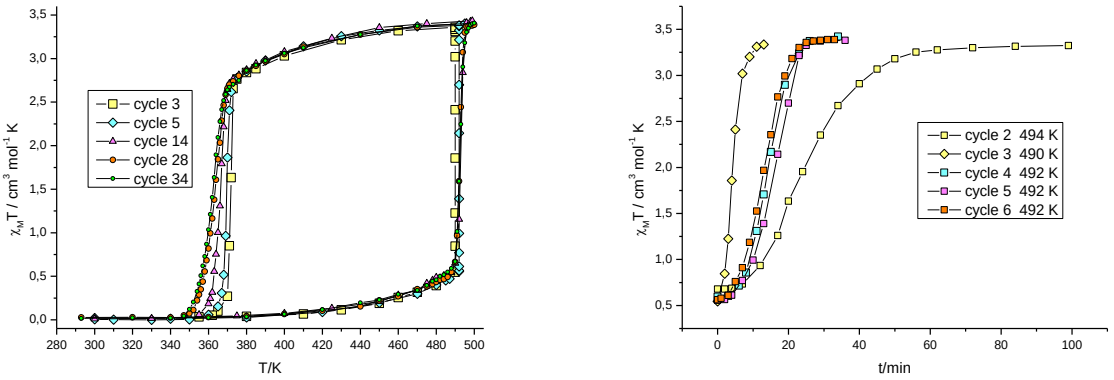

Figure S102. Sample **9**. Thermal cycles 3, 5, 14, 28 and 34 (left) and kinetic curves for the cycles 2 – 6 (right, LS → HS).

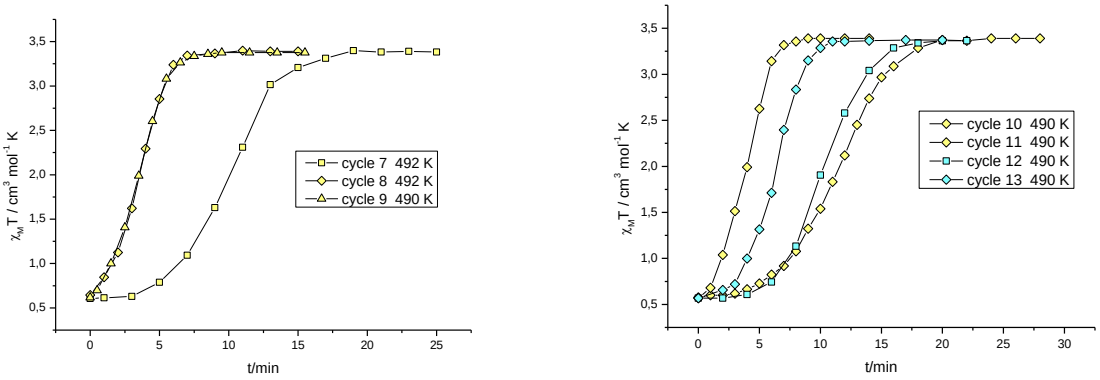

Figure S103. Sample **9**. Kinetic curves for the cycles 7 – 9 (LS → HS; right) and 10 – 13 (LS → HS; left).

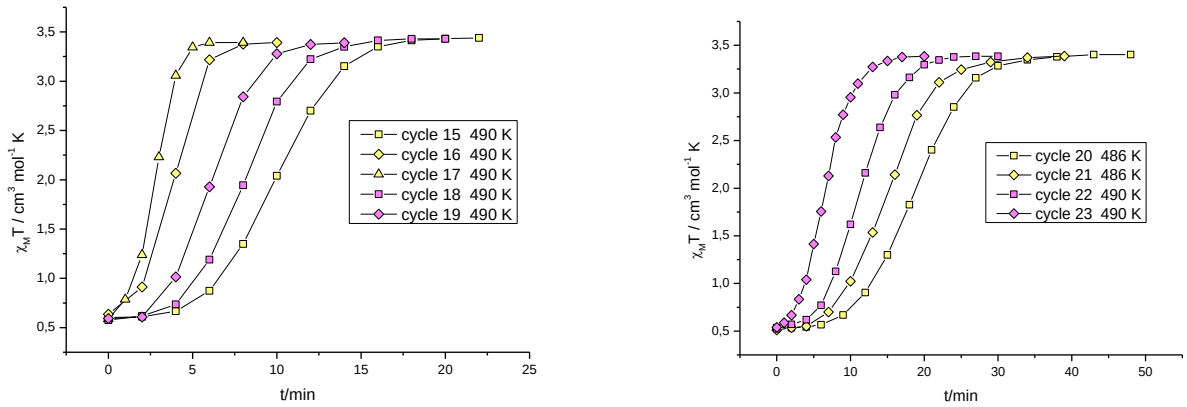

Figure S104. Sample **9**. Kinetic curves for the cycles 15 – 19 (LS → HS; right) and 20 – 23 (LS → HS; left).

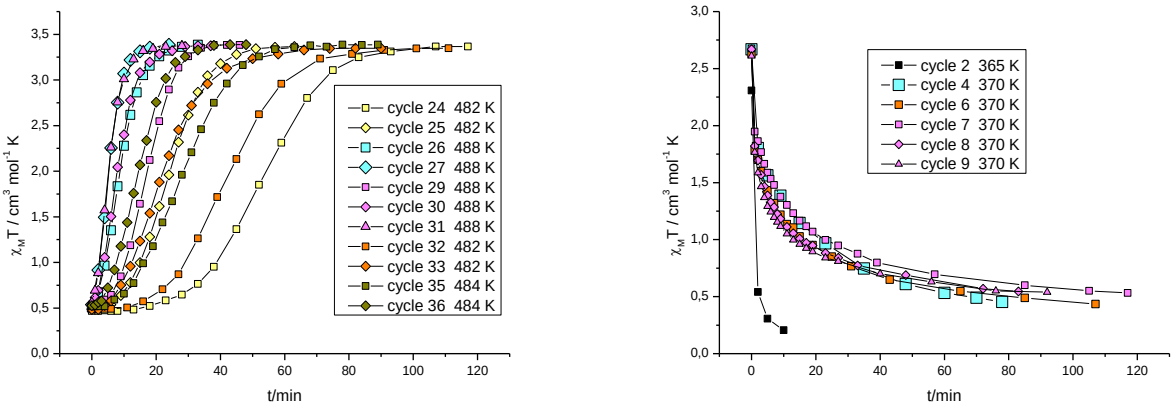

Figure S105. Sample **9**. Kinetic curves for the cycles 24 – 27, 29 – 33, 35 and 36 (LS → HS; left) and 2, 4, 6 – 9 (HS → LS; right).

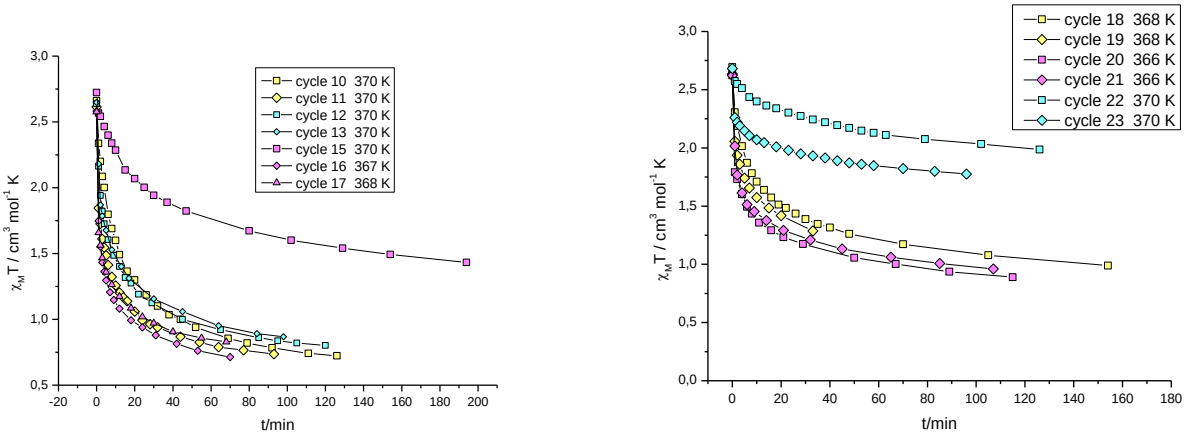

Figure S106. Sample **9**. Kinetic curves for the cycles 10 – 13 and 15 – 16 (HS → LS; left) and 18 – 23 (HS → LS; right).

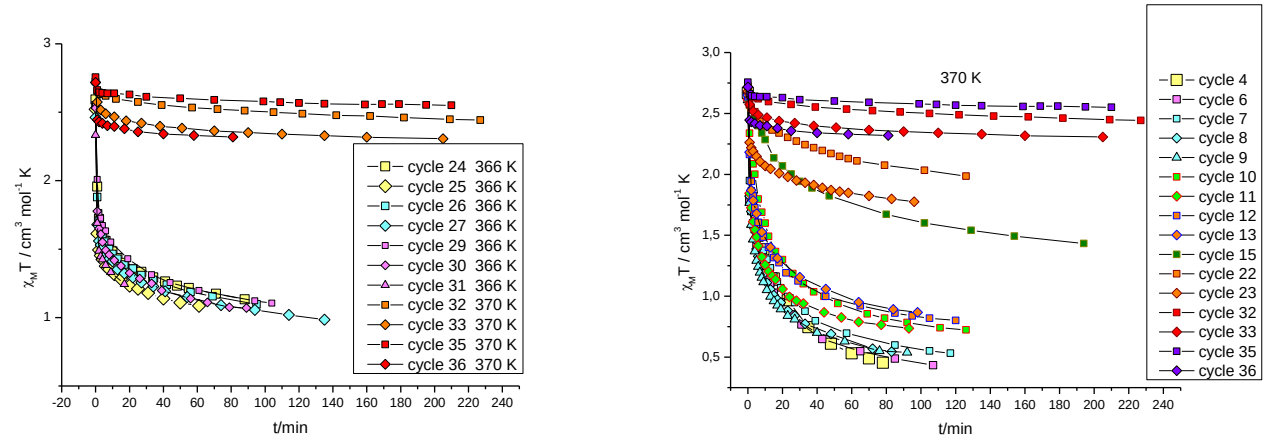

Figure S107. Sample **9**. Kinetic curves for the cycles 24 – 27, 29 – 33, 35 and 36 (HS → LS; left) and all kinetic curves at 370 K (HS → LS; right).

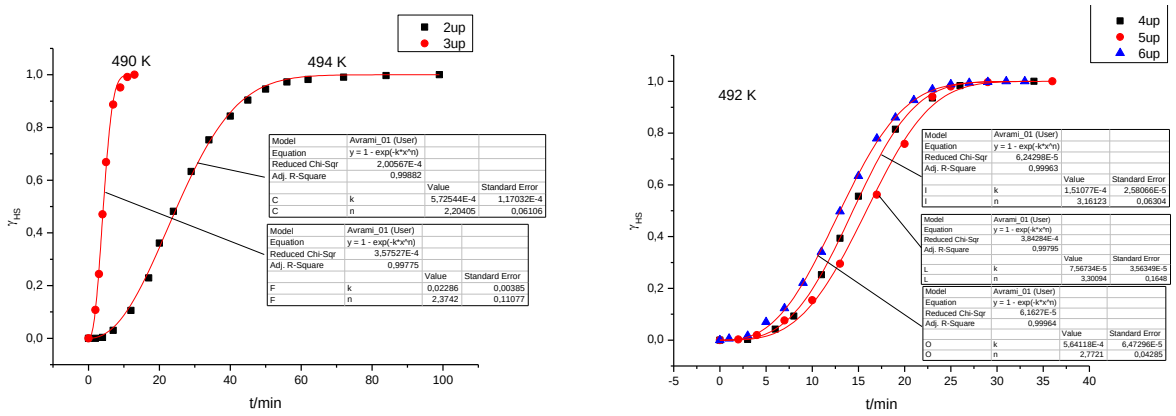

Figure S108. Fitting of kinetic curves for **9** using the JMAK model (LS → HS; left: cycles 2 and 3; right: cycles 4 - 6).

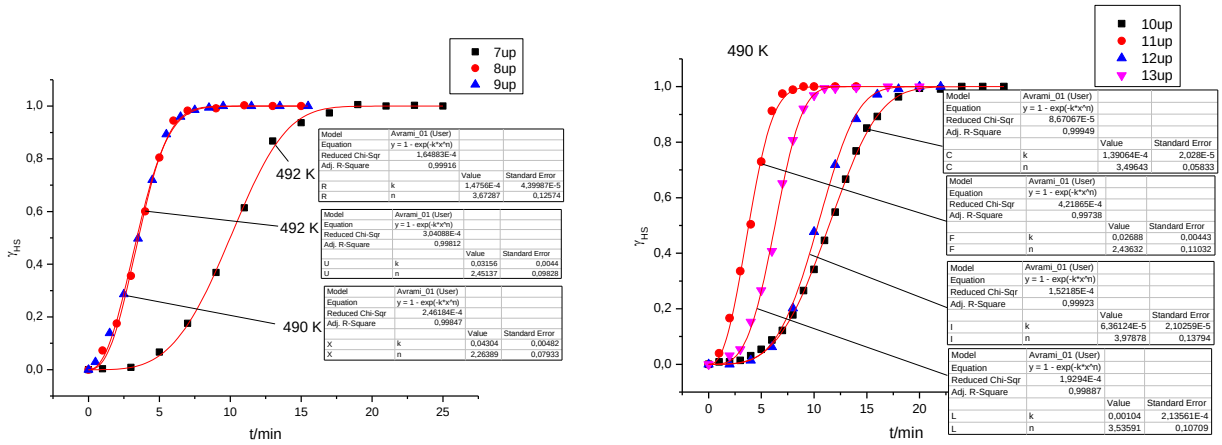

Figure S109. Fitting of kinetic curves for **9** using the JMAK model (LS → HS; left: cycles 7 - 9; right: cycles 10 – 13).

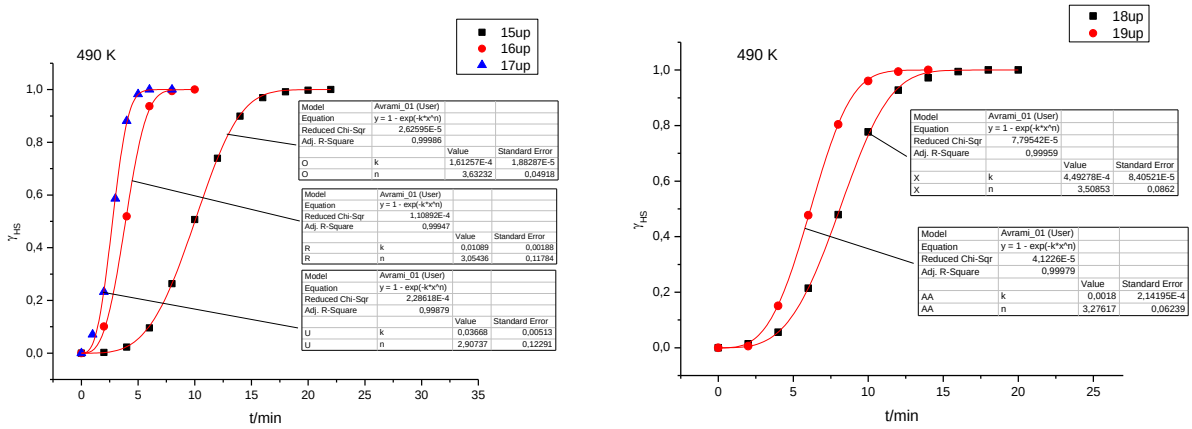

Figure S110. Fitting of kinetic curves for **9** using the JMAK model (LS → HS; left: cycles 15 - 17; right: cycles 18 and 19).

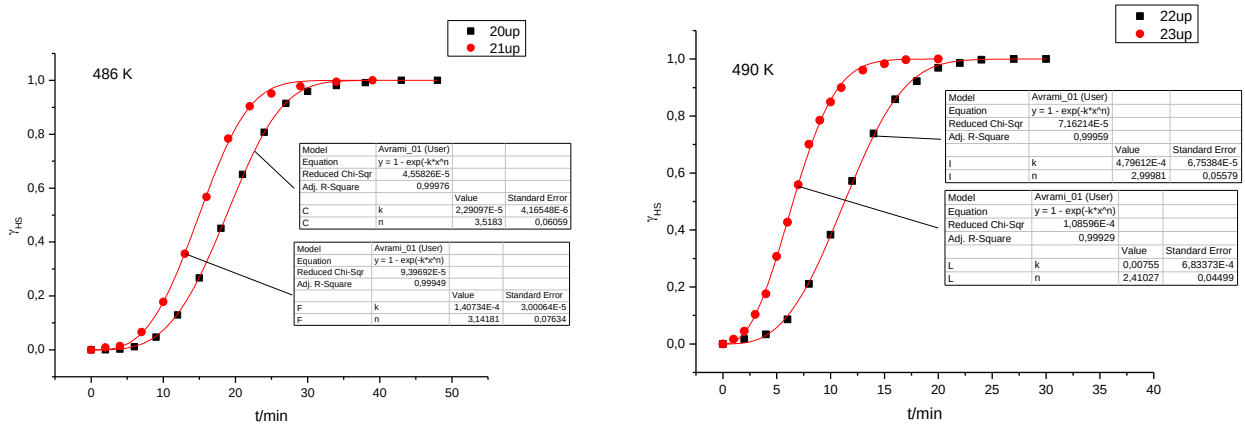

Figure S111. Fitting of kinetic curves for **9** using the JMAK model (LS → HS; left: cycles 20 and 21; right: cycles 22 and 23).

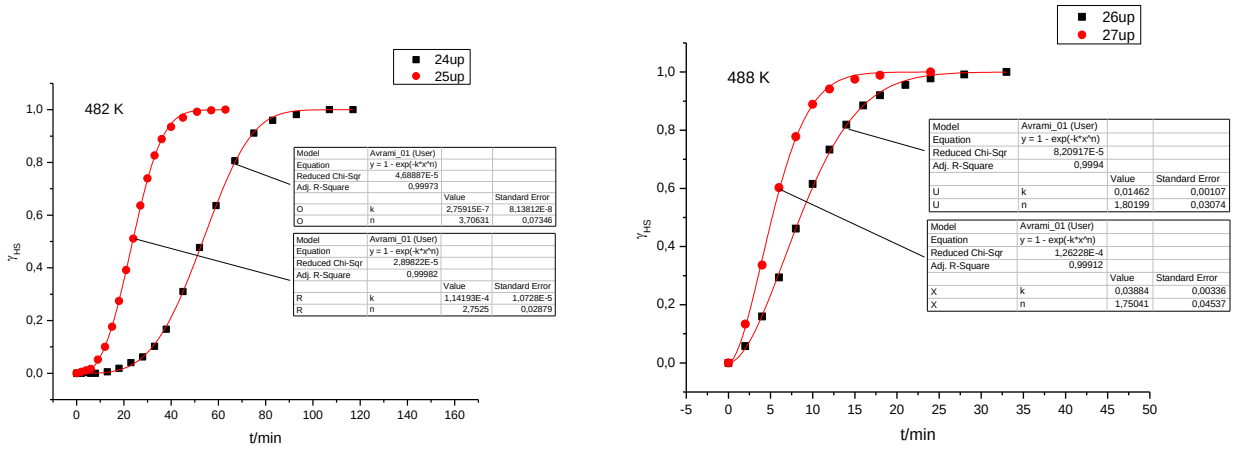

Figure S112. Fitting of kinetic curves for **9** using the JMAK model (LS → HS; left: cycles 24 and 25; right: cycles 26 and 27).

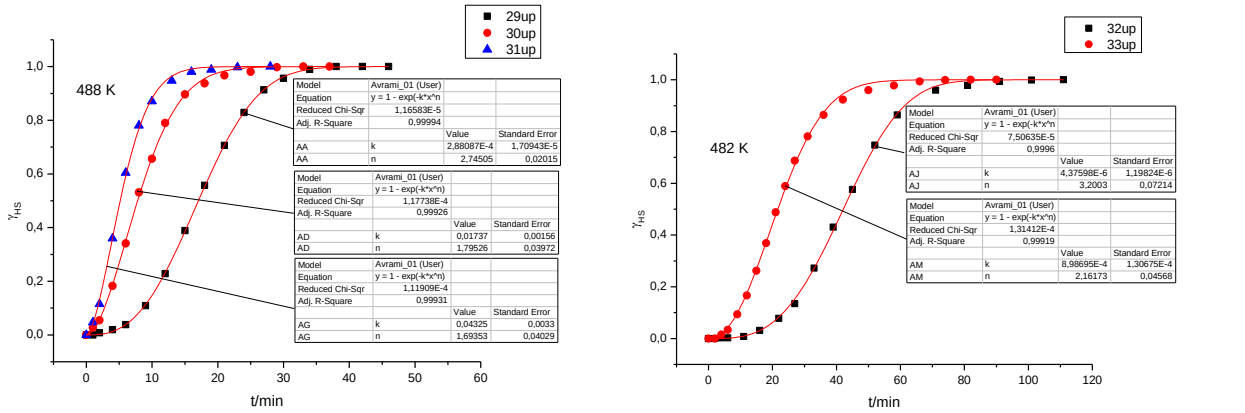

Figure S113. Fitting of kinetic curves for **9** using the JMAK model (LS → HS; left: cycles 29 – 31; right: cycles 32 and 33).

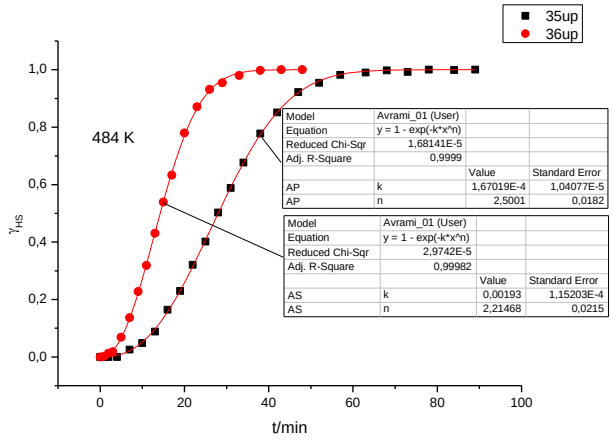

Figure S114. Fitting of kinetic curves for **9** using the JMAK model (LS → HS; cycles 35 and 36).

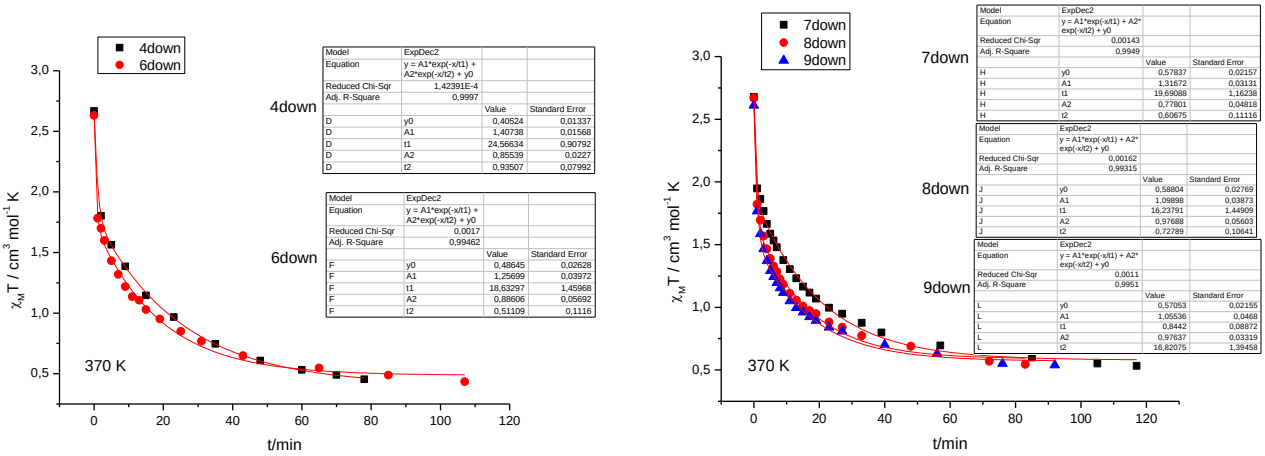

Figure S115. Fitting of kinetic curves for **9** in bi-exponential approximations (HS → LS; left: cycles 4 and 6; right: cycles 7 – 9).

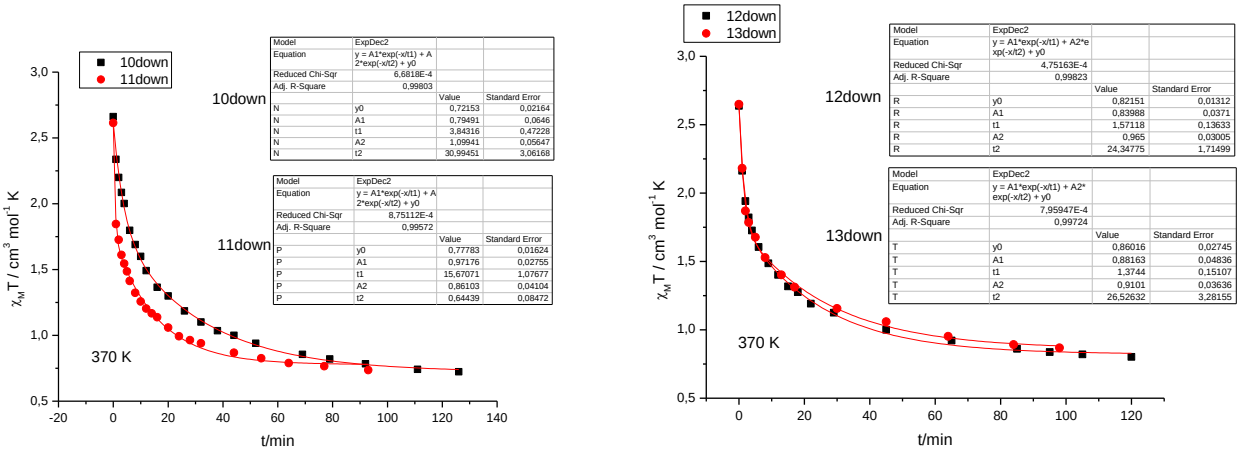

Figure S116. Fitting of kinetic curves for **9** in bi-exponential approximations (HS → LS; left: cycles 10 and 11; right: cycles 12 and 13).

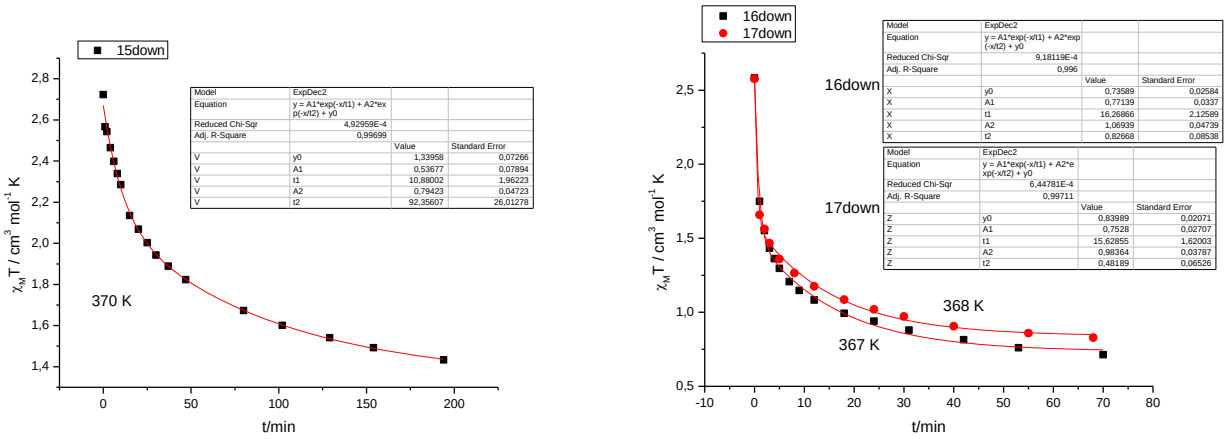

Figure S117. Fitting of kinetic curves for **9** in bi-exponential approximations (HS → LS; left: cycle 15; right: cycles 16 and 17).

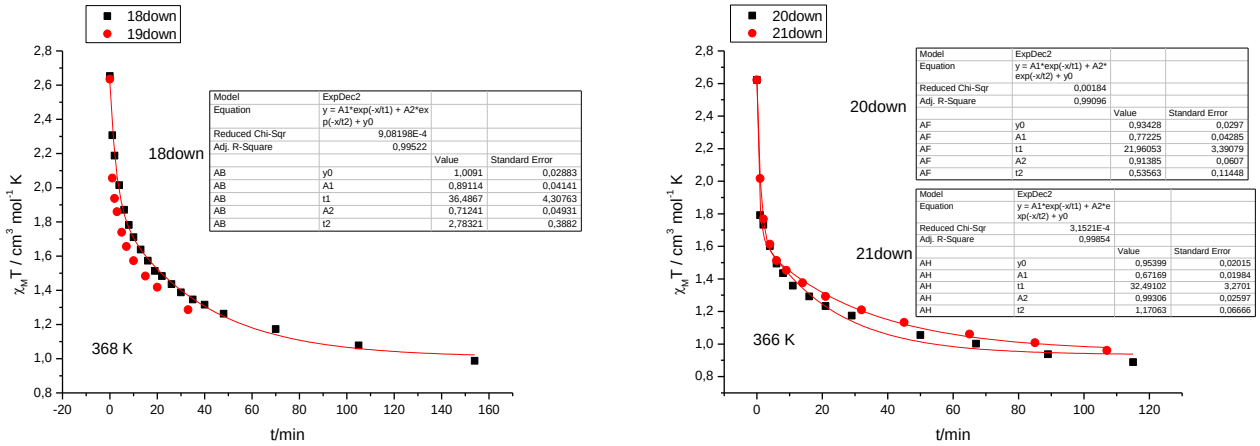

Figure S118. Fitting of kinetic curves for **9** in bi-exponential approximations (HS → LS; left: cycle 18; right: cycles 20 and 21).

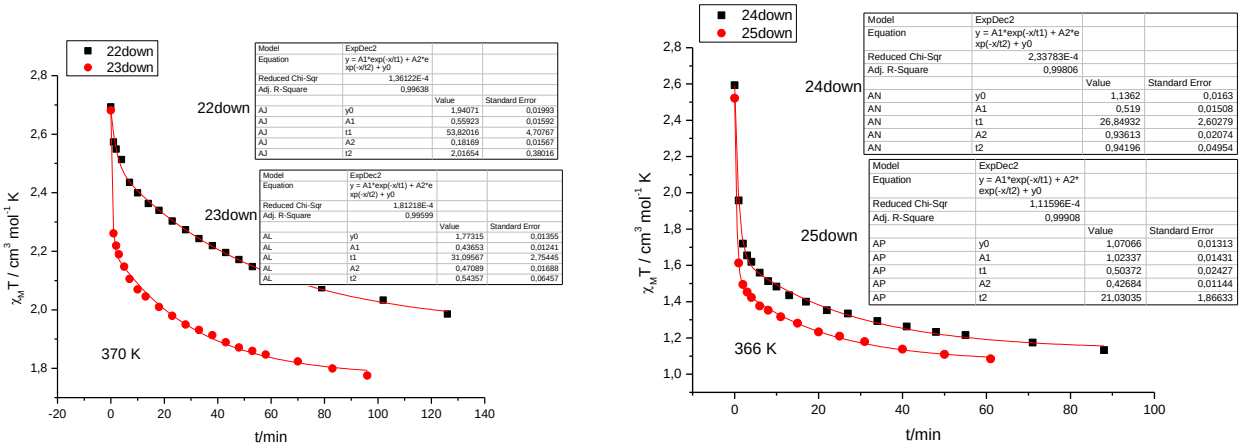

Figure S119. Fitting of kinetic curves for **9** in bi-exponential approximations (HS → LS; left: cycles 22 and 23; right: cycles 24 and 25).

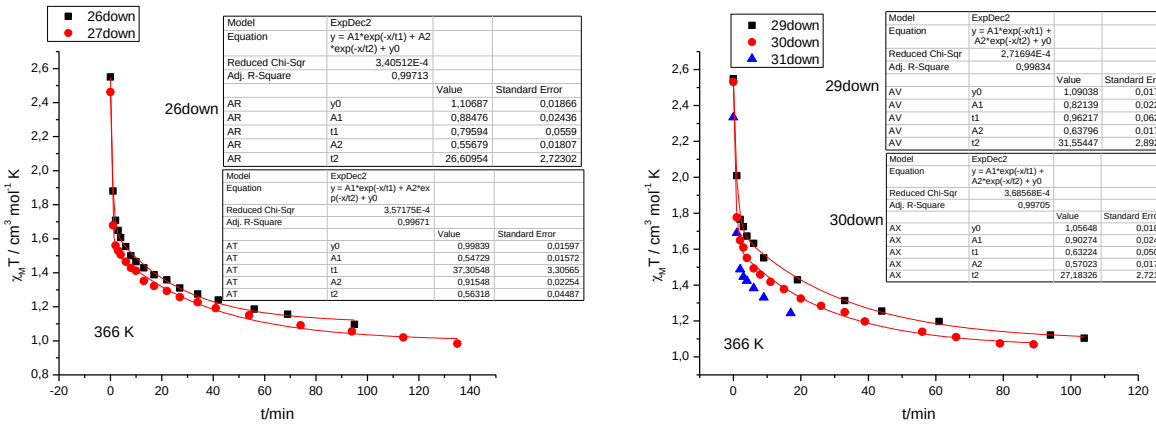

Figure S120. Fitting of kinetic curves for **9** in bi-exponential approximations (HS → LS; left: cycles 26 and 27; right: cycles 29 and 30).

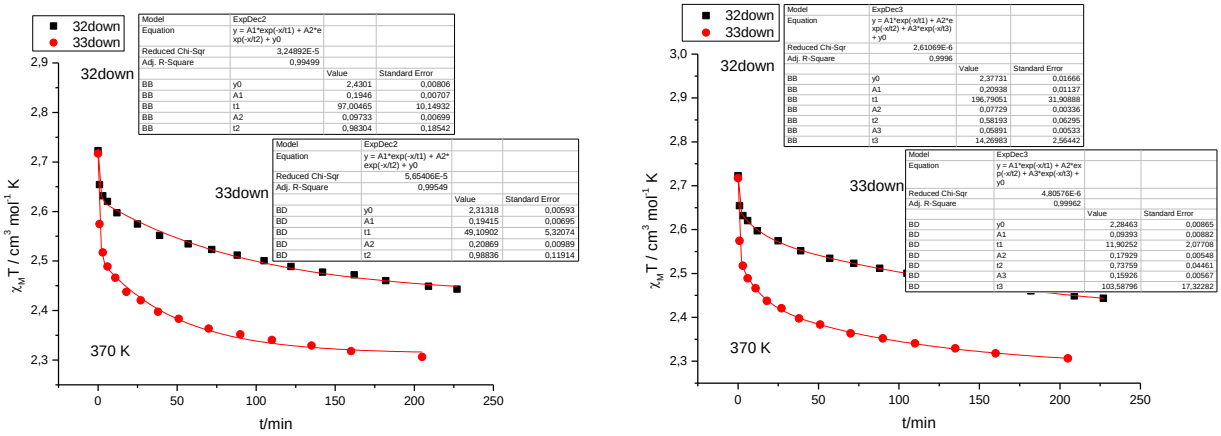

Figure S121. Fitting of kinetic curves for **9** in bi- and tri-exponential approximations (HS → LS; cycles 32 and 33; left: bi-exponential fitting, right: tri-exponential fitting).

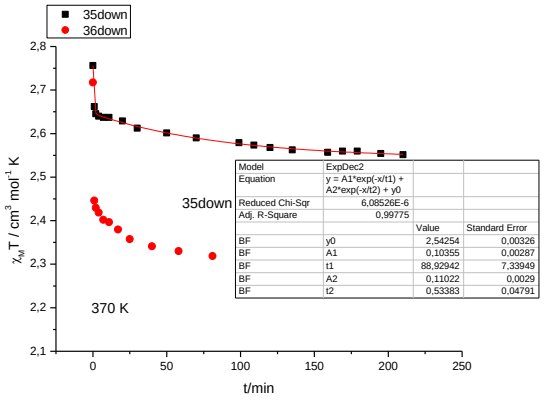

Figure S122. Fitting of a kinetic curve for **9** in bi-exponential approximations (HS → LS; cycle 35).

Samples 10 and 10-1

Sample 10

Cycles 1 – 3. Parent phase $\mathbf{1^{LS} \cdot EtOH \cdot H_2O}$. Crystals of the phase $\mathbf{1^{LS} \cdot EtOH \cdot H_2O}$ were exposed to ethanol vapor overnight and sealed. SCO regime typical for the phase $\mathbf{1^{E/LS} \cdot \textit{y}EtOH \cdot \textit{z}H_2O}$ was observed in the cycles 1 – 3. X-ray powder pattern of the sample agrees with the pattern obtained for the sample **21** (see below).

Sample 10-1

Cycles 4 – 10. Main part of the sample **10** (the phase $\mathbf{1^{E/LS} \cdot \textit{y}EtOH \cdot \textit{z}H_2O}$) was placed in a new ampoule and exposed to water vapor for 2 days. The mass of the sample slightly decreased (2.1 %) and the ampoule was sealed.

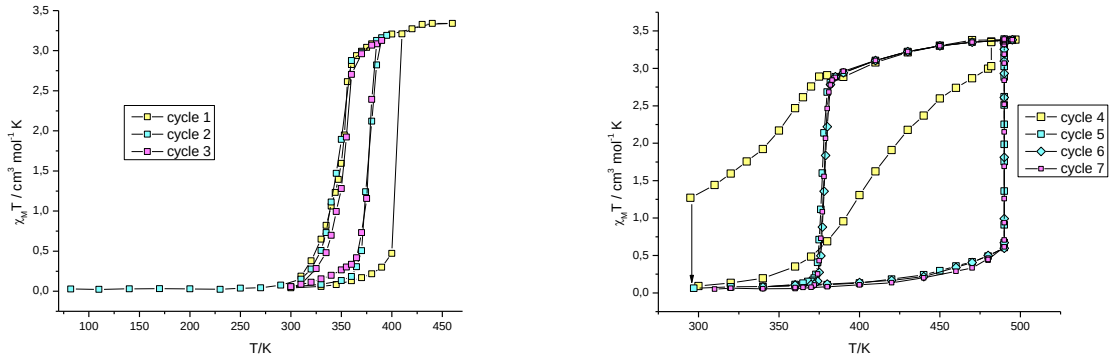

Figure S123. Left: sample **10**. Thermal cycles 1 – 3. Right: sample **10-1.** Thermal cycles 4 – 7.

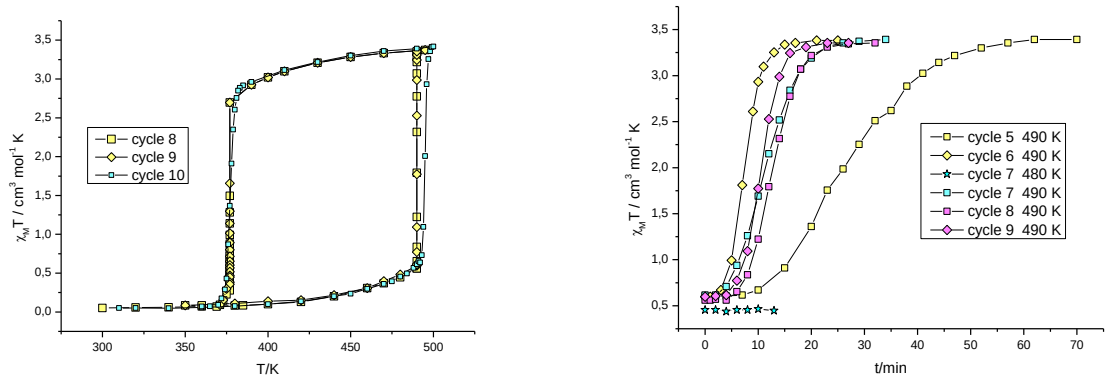

Figure S124. Left: sample **10-1**. Thermal cycles 8 – 10. Right: sample **10-1**. Kinetic curves for the cycles 5 – 9 (LS → HS).

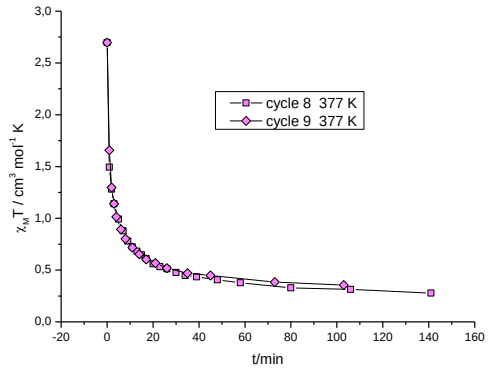

Figure S125. Sample **10-1**. Kinetic curves for the cycles 8 and 9 (LS → HS transformation).

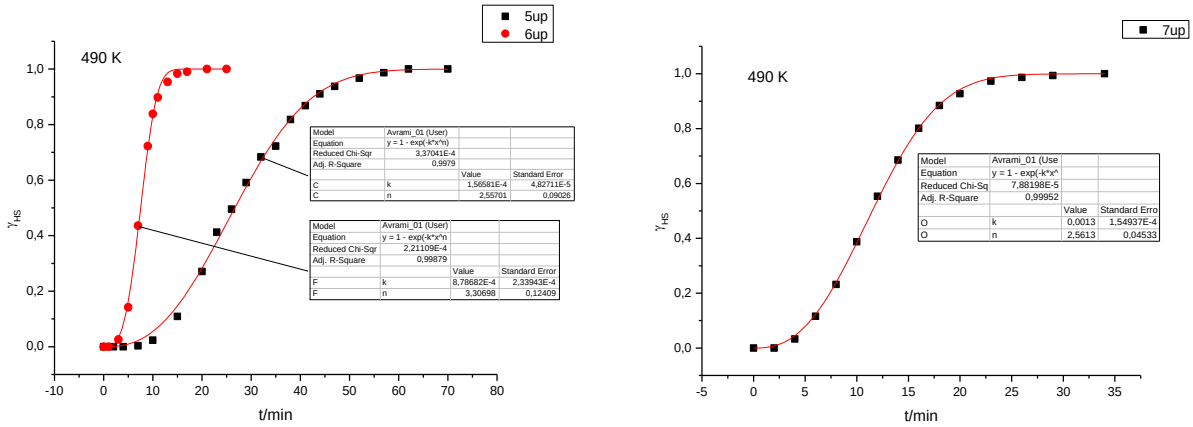

Figure S126. Fitting of kinetic curves for **10-1** using the JMAK model (LS → HS; left: cycles 5 and 6; right: cycle 7).

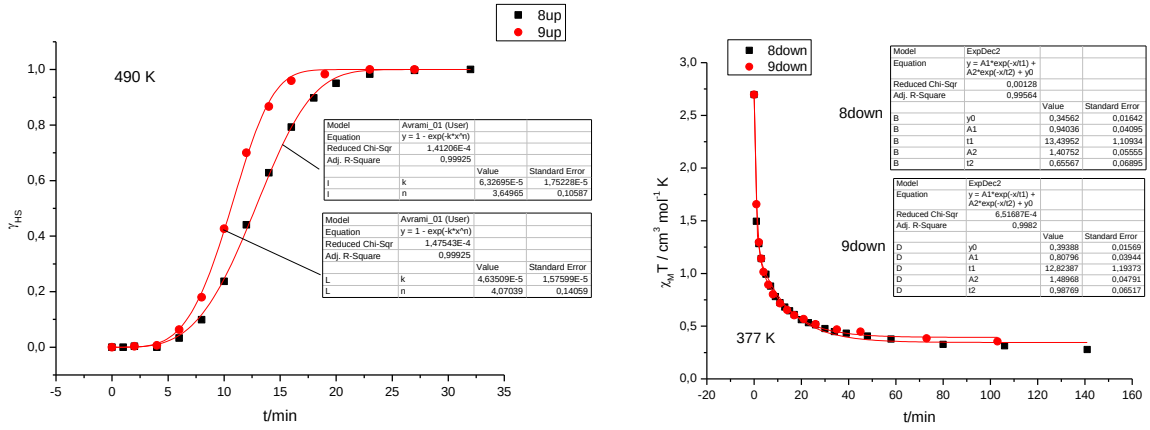

Figure S127. Fitting of kinetic curves for **10-1** using the JMAK model (left: cycles 8 and 9, LS → HS transformation) and bi-exponential approximation (right: cycles 8 and 9, HS → LS transformation).

Sample 11

Parent phase $\mathbf{1^{LS} \cdot EtOH \cdot H_2O}$.

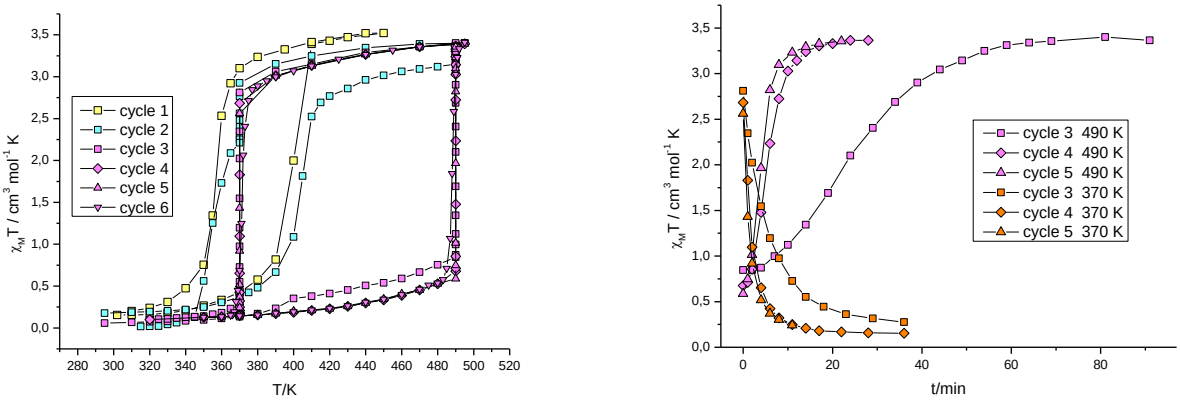

Figure S128. Sample **11**. Thermal cycles 1 – 6 (left) and kinetic curves for the cycles 3 – 5 (LS → HS and HS → LS transformations, right).

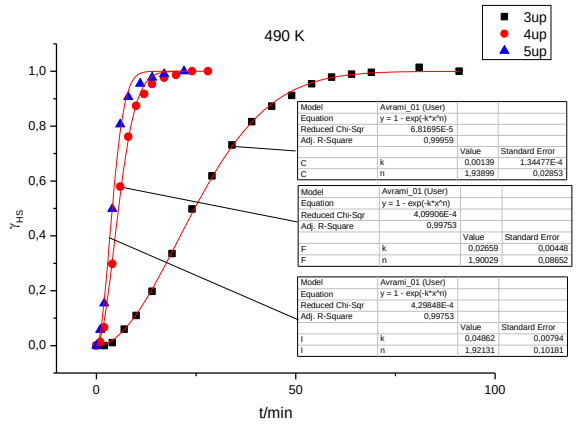

Figure S129. Fitting of kinetic curves for **11** using the JMAK model (LS → HS; cycles 3 – 5).

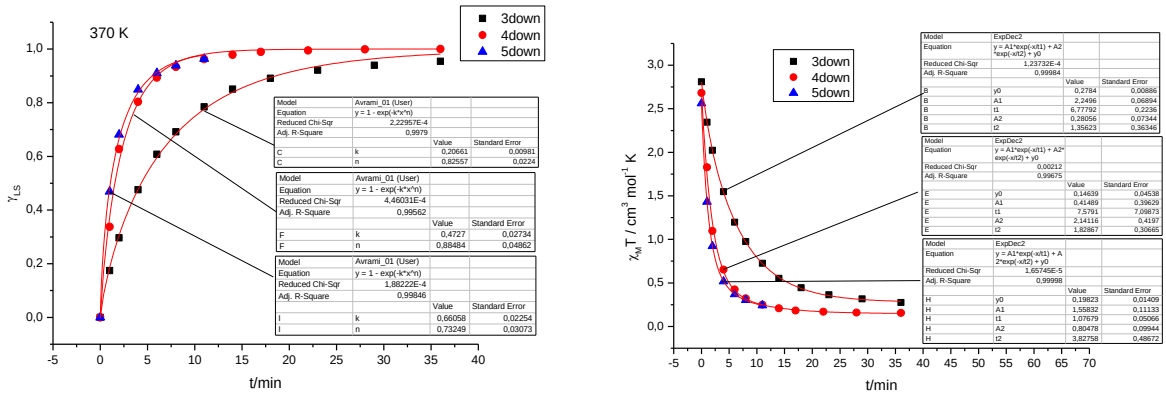

Figure S130. Fitting of kinetic curves for **11** using the JMAK model (left: cycles 3 – 5) and biexponential approximation; right: cycles 3 – 5). The JMAK model gives very small and non-typical values of $n < 1$.

Samples 12 and 12-1

Sample 12

Cycle 1. Parent phase **β-1**$^{\mathbf{LS}}\cdot x\mathbf{H_2O}$.

Sample 12-1

Cycles 2 – 18. After the first cycle had been done the sample **12** was allowed to stand at room temperature in a sealed ampoule. X-ray powder diffraction pattern of the sample was recorded after *ca*. 9 months. The sample appeared to be the phase **1**$^{\mathbf{A/LS}}$. It was placed in a new quartz ampoule, exposed to ethanol vapor for 1 h and sealed.

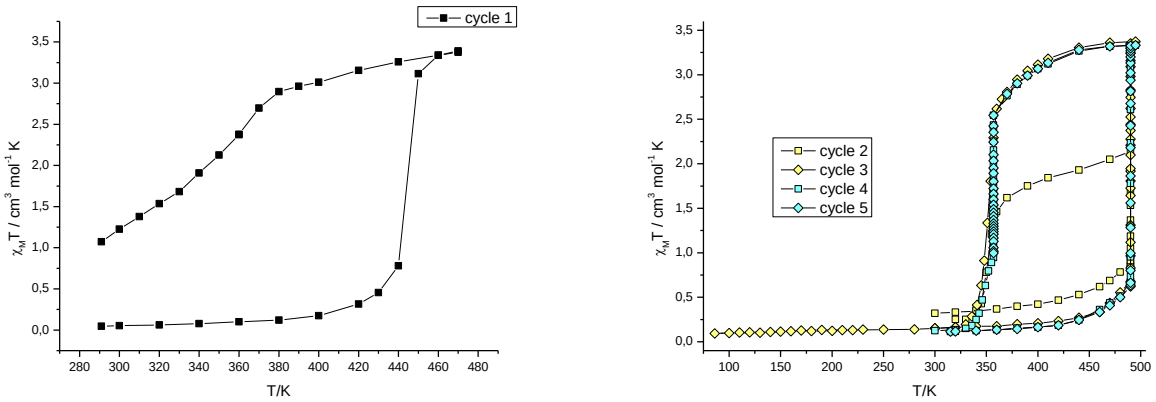

Figure S131. Thermal cycle 1 (left) and cycles 2 – 5 (right) for the samples **12** and **12-1**.

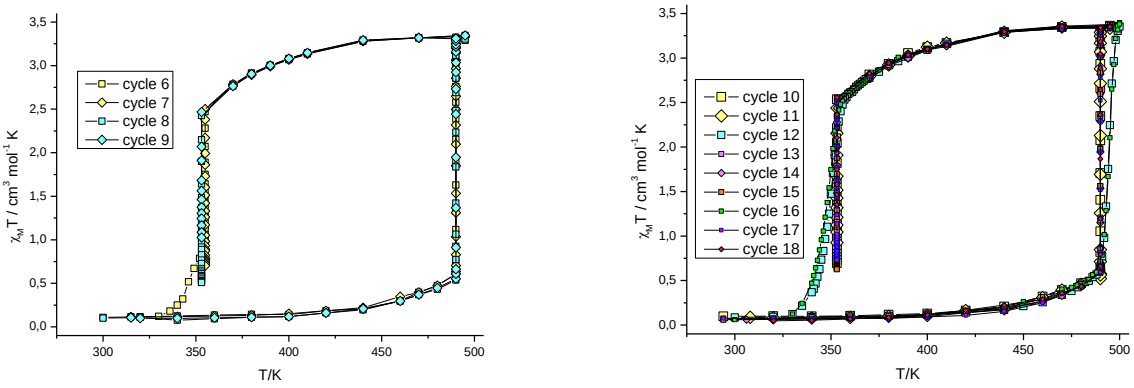

Figure S132. Sample **12-1**. Thermal cycles 6 – 9 (left) and 10 – 18 (right).

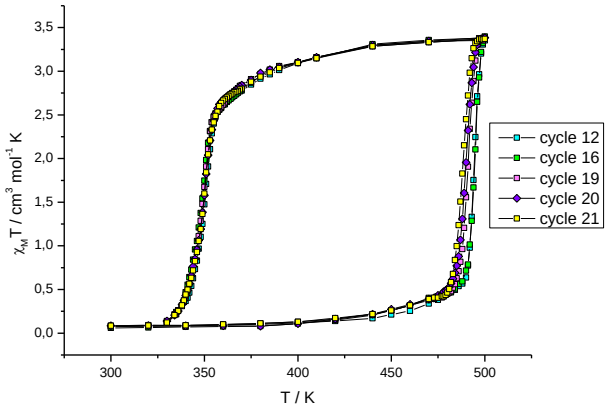

Figure S133. Sample **12-1**. Thermal cycles at heating/cooling rate of 0.9 K min^{-1} (cycles 12 and 16), 0.4 K min^{-1} (cycles 19 and 20) and 0.25 K min^{-1} (cycle 21).

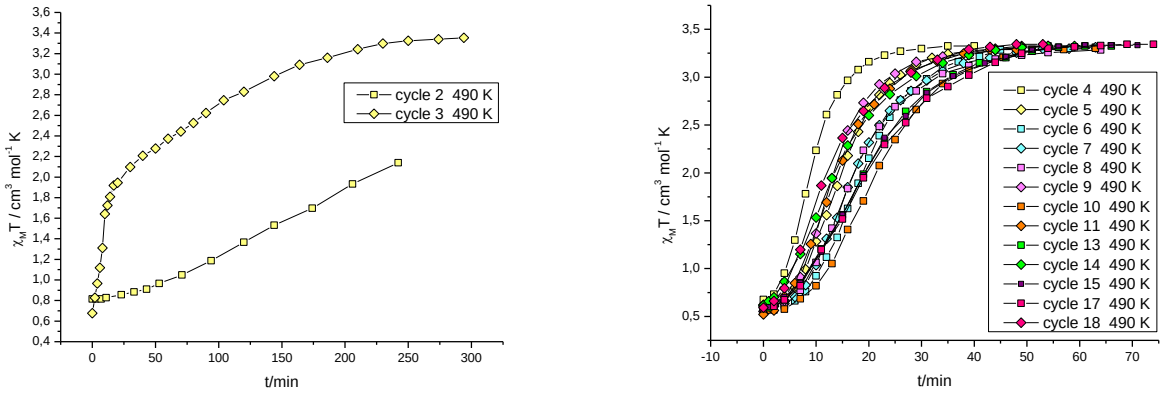

Figure S134. Sample **12-1**. Kinetic curves (LS → HS; left: cycles 2 and 3; right: cycles 4 – 18).

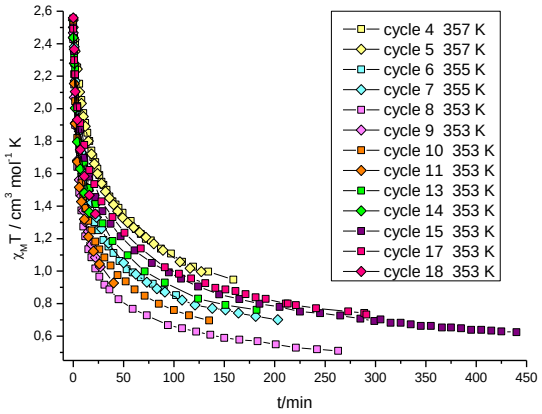

Figure S135. Sample **12-1**. Kinetic curves (HS → LS; cycles 4 – 10, 11, 13 – 15, 17, 18).

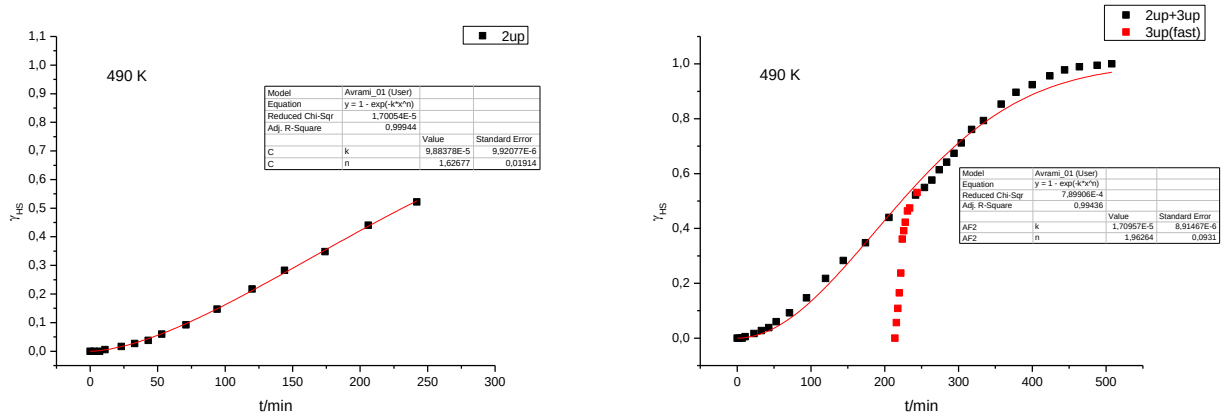

Figure S136. Fitting of kinetic curves for **12-1** using the JMAK model (LS → HS; cycles 2, 3 and fitting of the "combined" slow branch of the cycles 2 and 3, points of the fast branch of the cycle 3 (red squares) were not taken into the fitting).

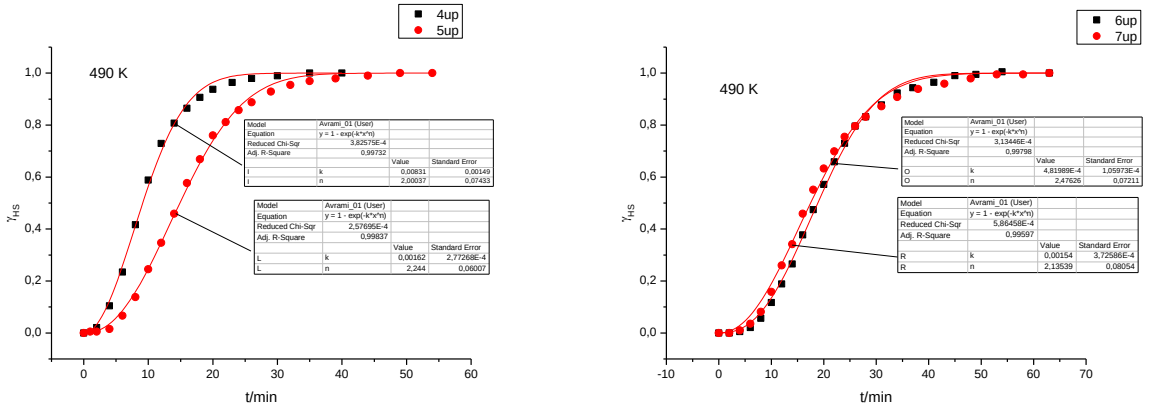

Figure S137. Fitting of kinetic curves for **12-1** using the JMAK model (LS → HS; left: cycles 4, 5; right: cycles 6, 7).

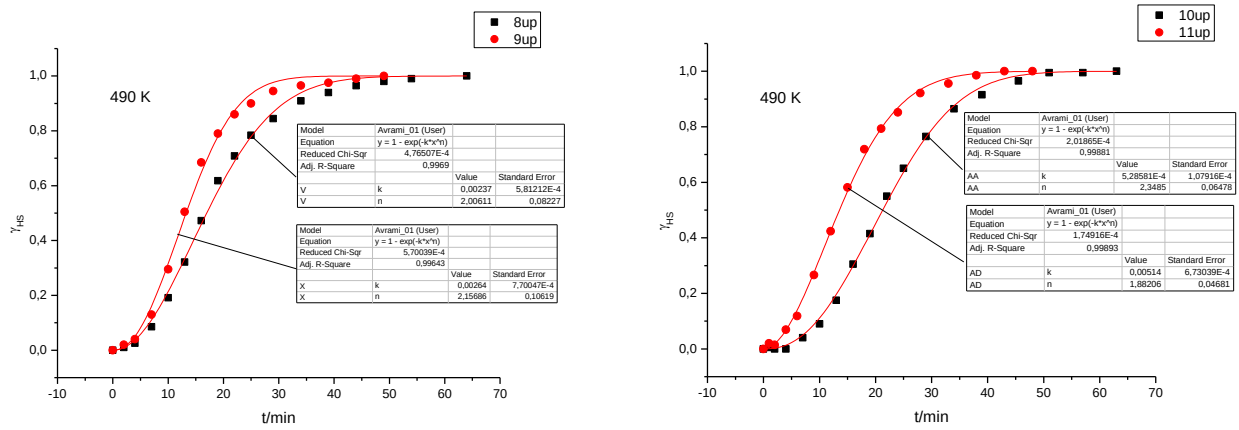

Figure S138. Fitting of kinetic curves for **12-1** using the JMAK model (LS → HS; left: cycles 8, 9; right: cycles 10, 11).

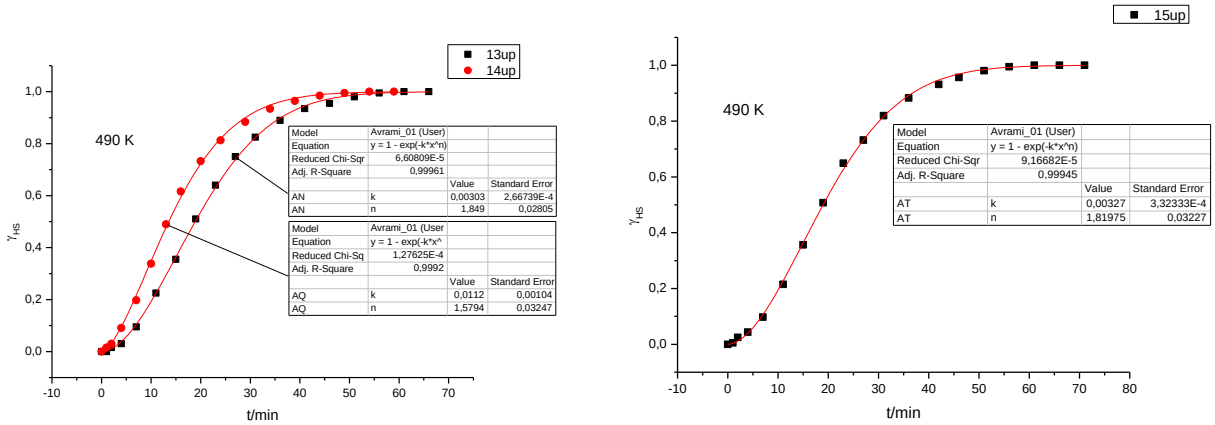

Figure S139. Fitting of kinetic curves for **12-1** using the JMAK model (left: cycles 13, 14; right: cycle 15).

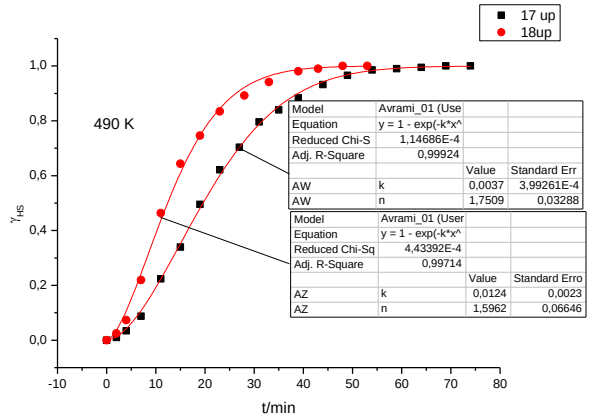

Figure S140. Fitting of kinetic curves for **12-1** using the JMAK model (LS → HS; cycles 17, 18).

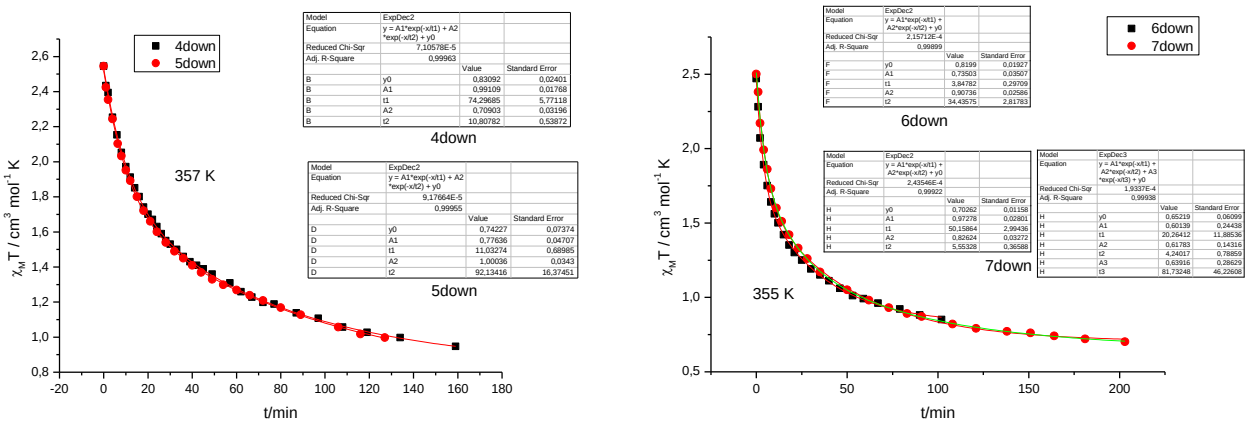

Figure S141. Fitting of kinetic curves for **12-1** using bi- and tri-exponential approximations (HS → LS; left: cycles 4, 5; right: cycles 6, 7).

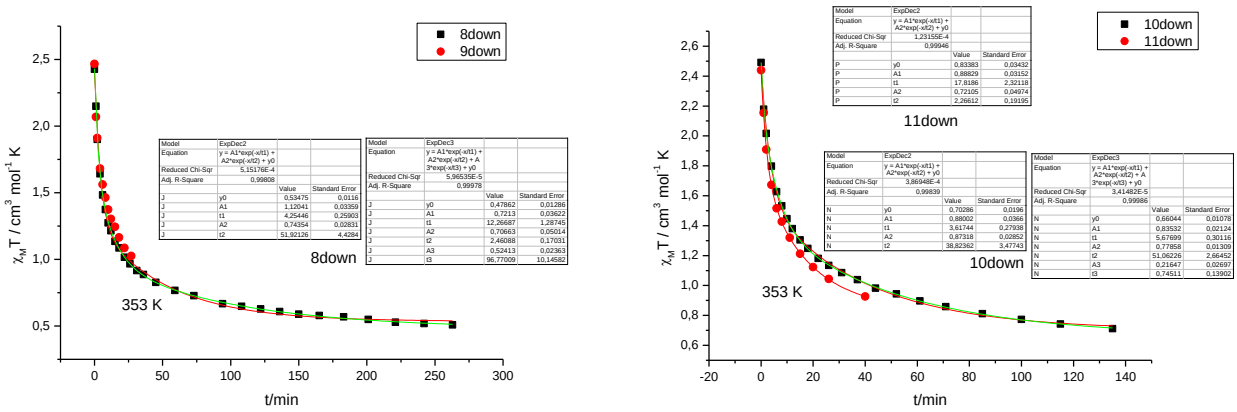

Figure S142. Fitting of kinetic curves for **12-1** using bi- and tri-exponential approximations (HS → LS; left: cycles 8, 9; right: cycles 10, 11).

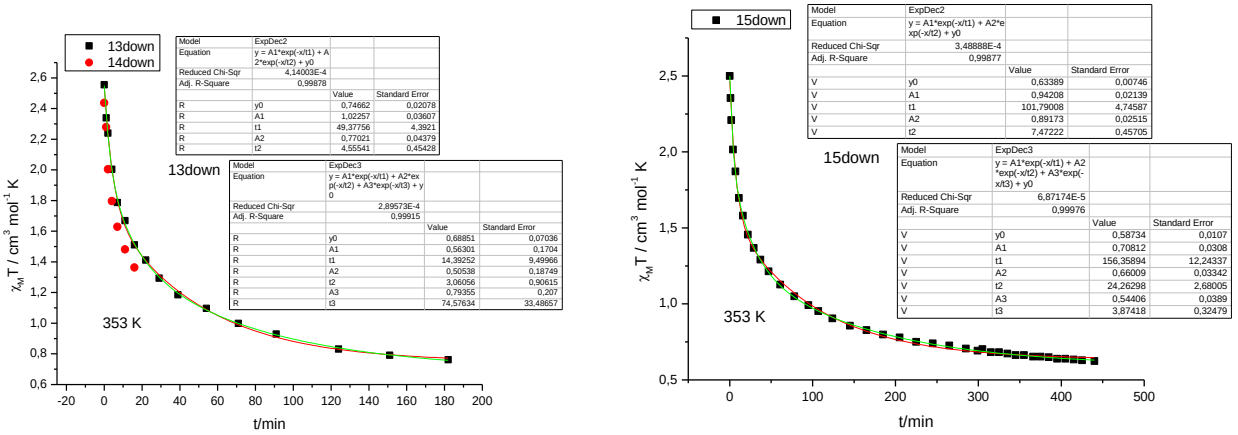

Figure S143. Fitting of kinetic curves for **12-1** using bi- and tri-exponential approximations (HS → LS; left: cycle 13; right: cycle 15).

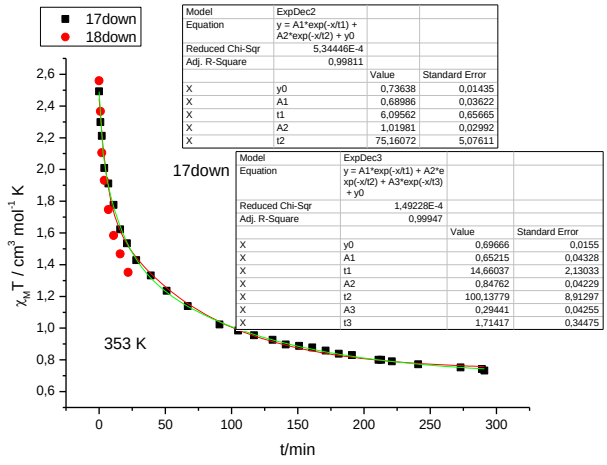

Figure S144. Fitting of kinetic curves for **12-1** using bi- and tri-exponential approximations (HS → LS; cycle 17).

Sample 13

Parent phase $\mathbf{1}^{\mathbf{A/LS}}$ after XRPD. This sample of the phase $\mathbf{1}^{\mathbf{A/LS}}$ was obtained from the phase $\boldsymbol{\alpha}$-$\mathbf{1}^{\mathbf{LS}}$.$\boldsymbol{x}\mathbf{H_2O}$ [see ref. 29, electronic supporting information, Figure S8]. The formation of the phase $\mathbf{1}^{\mathbf{A/LS}}$ was confirmed by X-ray powder diffraction. This sample of the phase $\mathbf{1}^{\mathbf{A/LS}}$ was placed in a quartz ampoule, exposed to water vapor for 1 h (mass of the sample did not change) and sealed.

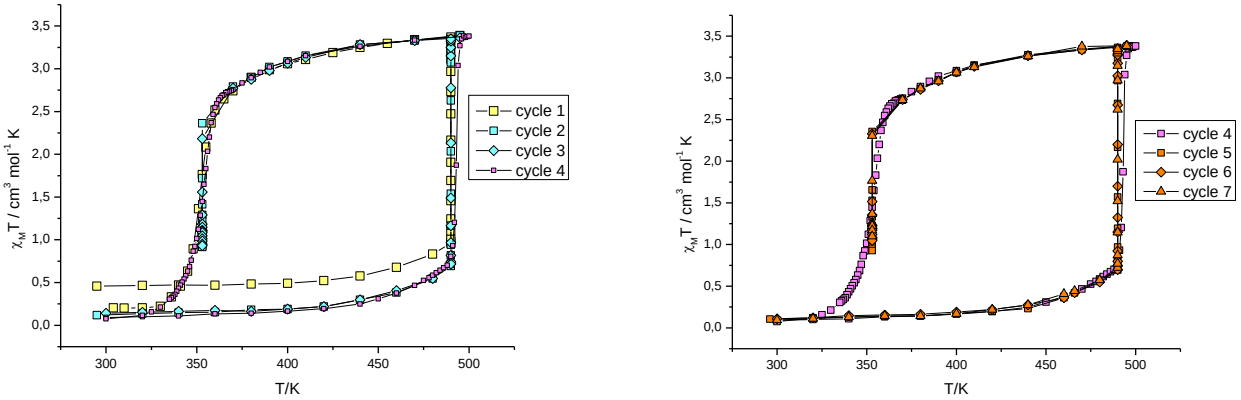

Figure S145. Sample **13**. Thermal cycles 1 – 4 (left) and 4 – 7 (right).

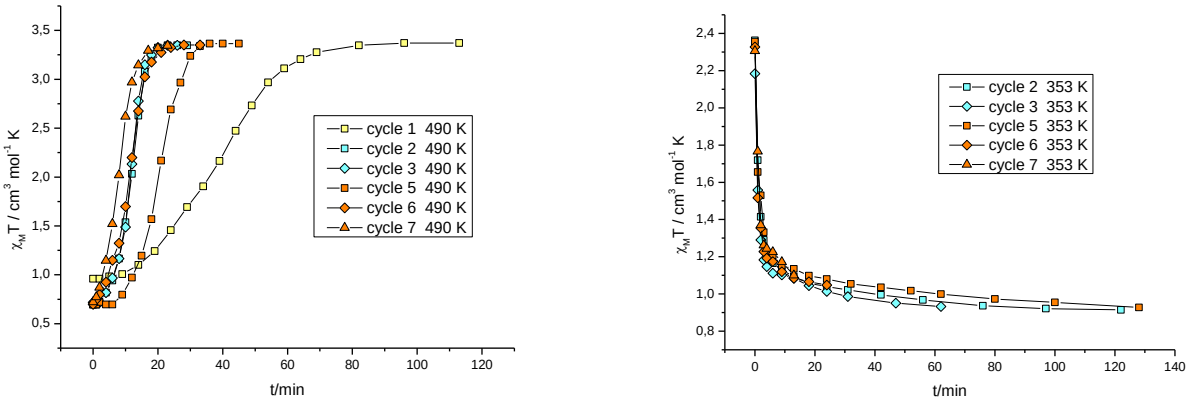

Figure S146. Sample **13**. Left: kinetic curves for the cycles 1 – 3 and 5 – 7 (LS → HS). Right: kinetic curves for the cycles 2, 3, 5 – 7 (HS → LS).

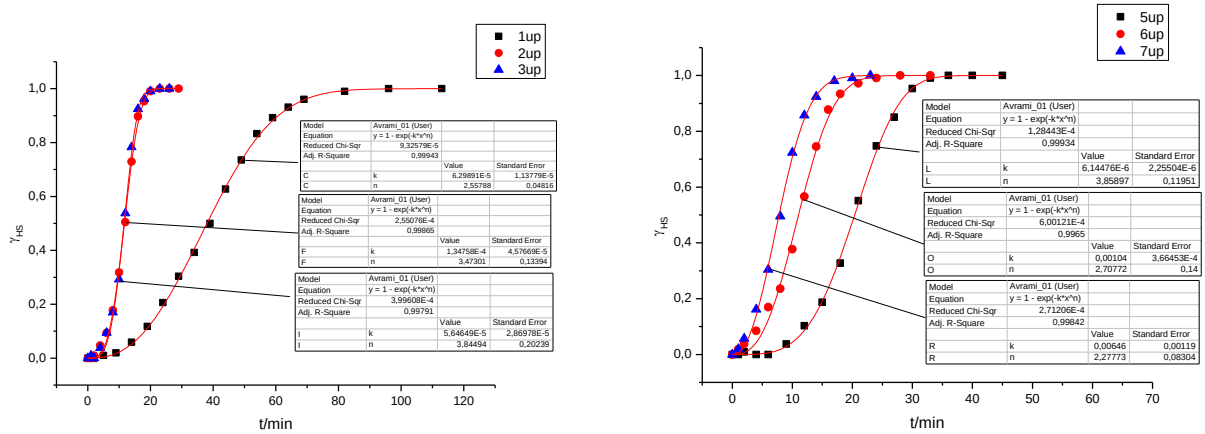

Figure S147. Fitting of kinetic curves for **13** using the JMAK model (LS → HS; left: cycles 1 – 3; right: cycles 5 – 7).

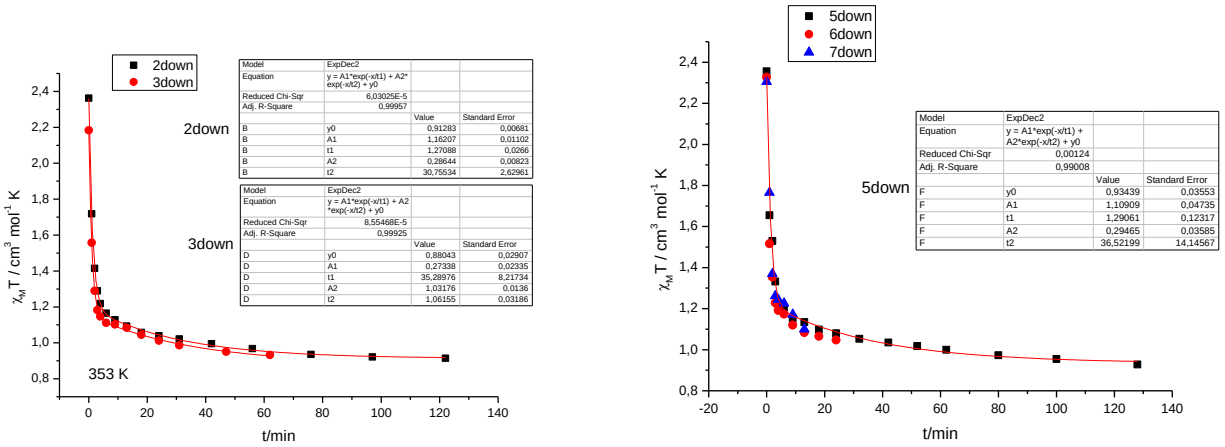

Figure S148. Fitting of kinetic curves for **13** in bi-exponential approximation (HS → LS; left: cycles 2 and 3; right: cycle 5).

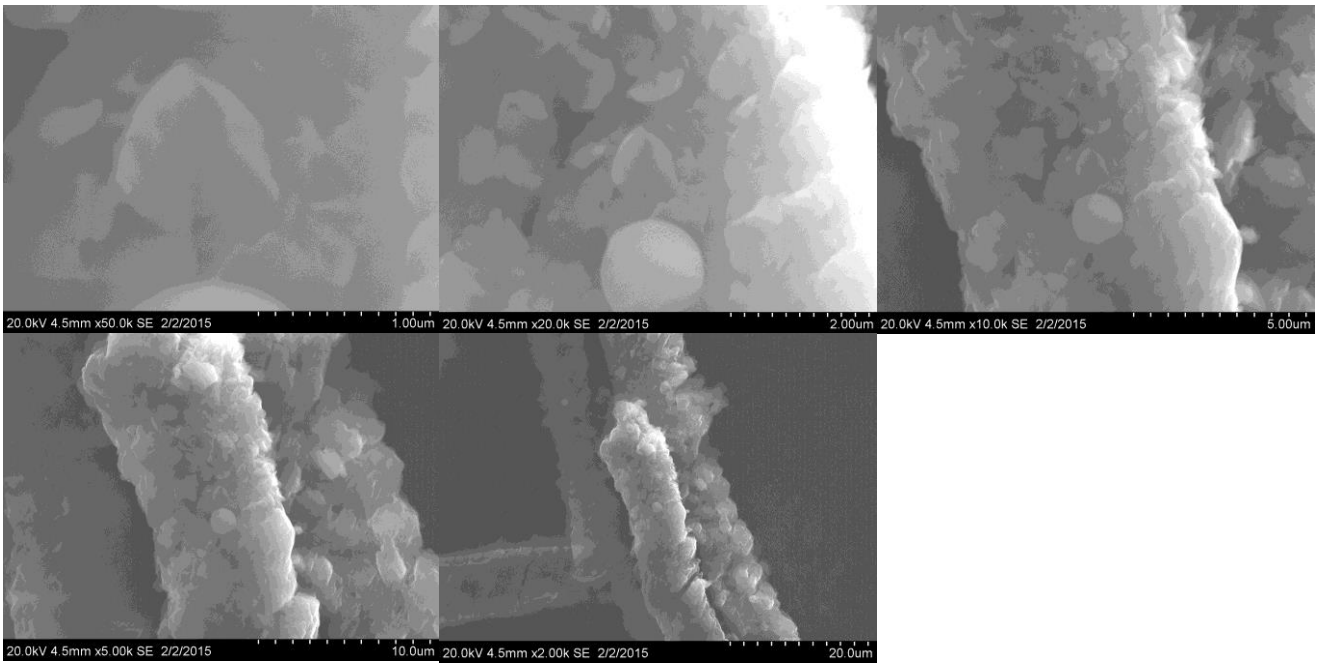

Figure S149. SEM images of the sample **13** after thermal cycling.

Samples 14 and 14-1

Sample 14

Cycles 1 – 6. Parent phase $\mathbf{1}^{\mathbf{LS}} \cdot \mathbf{EtOH} \cdot \mathbf{H_2O}$. A single crystal of the phase $\mathbf{1}^{\mathbf{A/LS}}$ suitable for X-ray analysis was taken from the sealed ampoule after the cycles 1 – 6 had been done.

Sample 14-1

Cycles 7 – 14. Parent phase $\mathbf{1}^{\mathbf{A/LS}}$. This sample of the phase $\mathbf{1}^{\mathbf{A/LS}}$ was taken from the experiment **14**, exposed to water vapor for 1 h (no change in the mass was observed) and sealed.

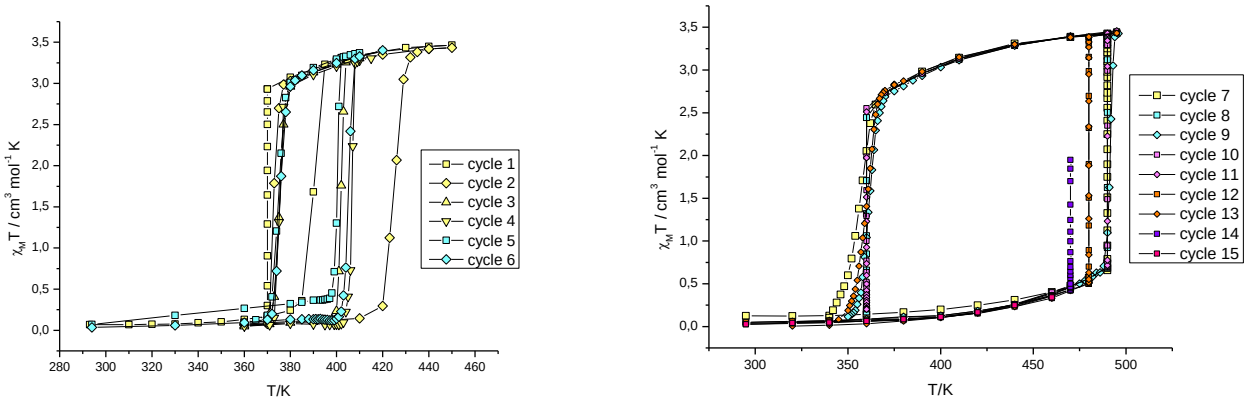

Figure S150. Left: sample **14**. Thermal cycles 1 – 6. Right: sample **14-1**. Thermal cycles 7 – 14.

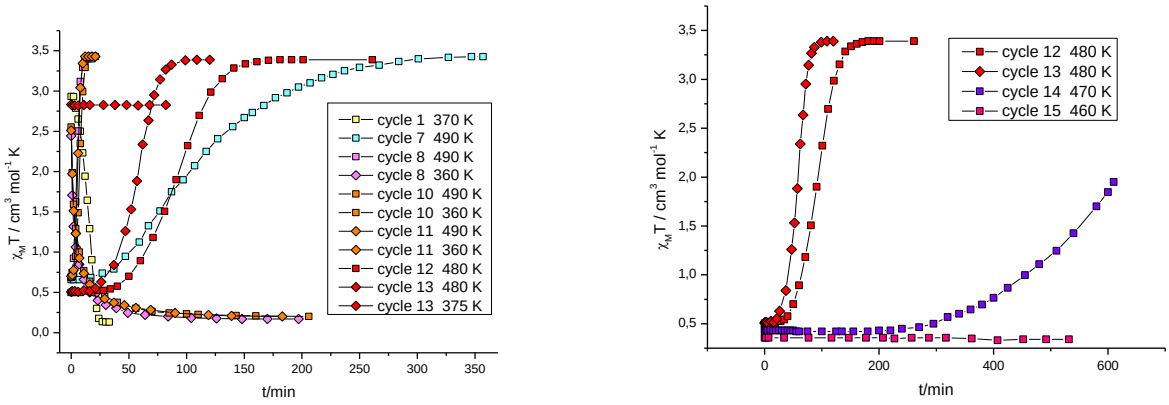

Figure S151. Kinetic curves for the samples **14** and **14-1** (LS → HS and HS → LS).

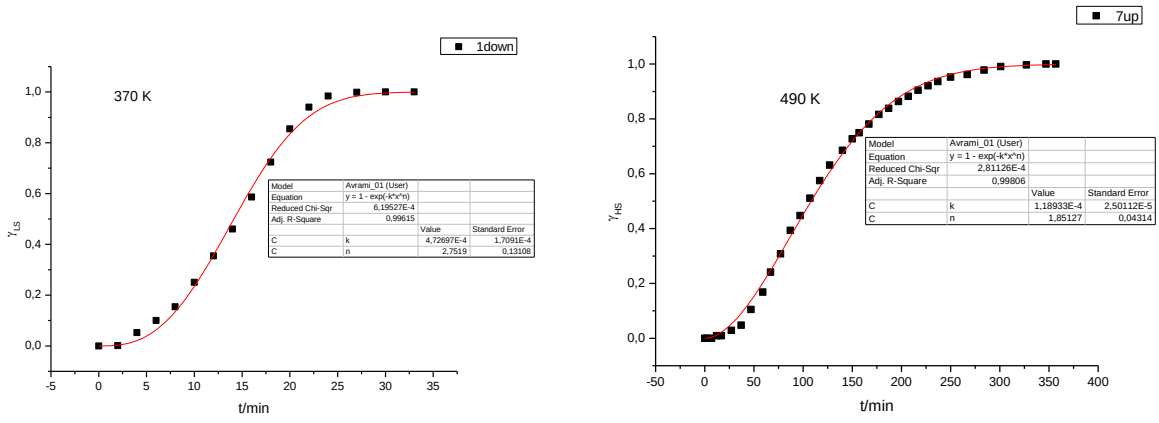

Figure S152. Fitting of kinetic curves for **14** and **14-1** using the JMAK model (LS → HS; left: cycle 1; right: cycle 7).

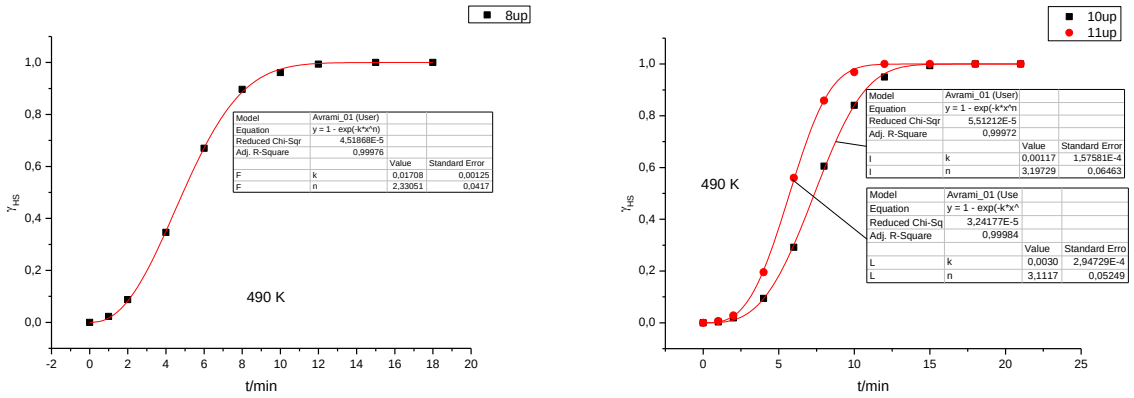

Figure S153. Fitting of kinetic curves for **14-1** using the JMAK model (LS → HS; left: cycle 8; right: cycles 10 and 11).

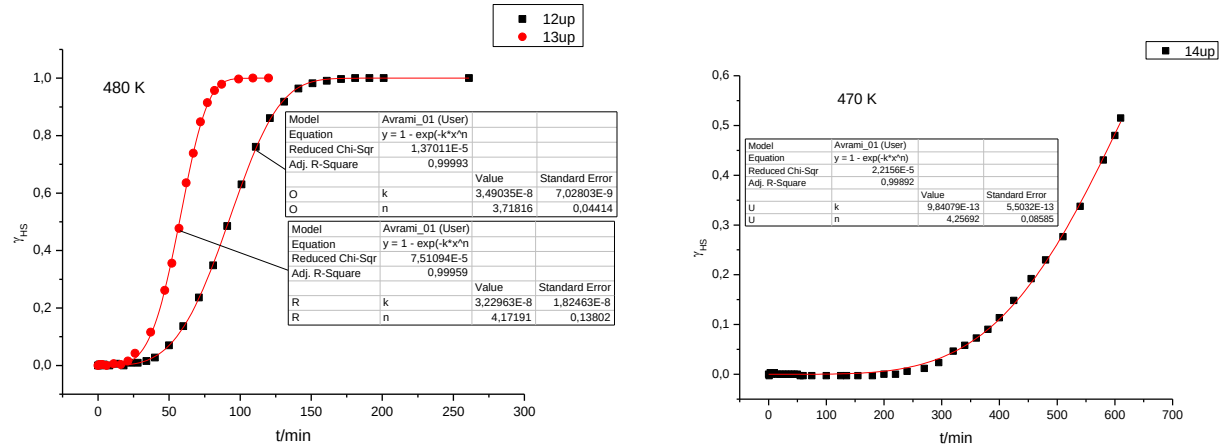

Figure S154. Fitting of kinetic curves for **14-1** using the JMAK model (LS → HS; right: cycles 12 and 13; left: cycle 14).

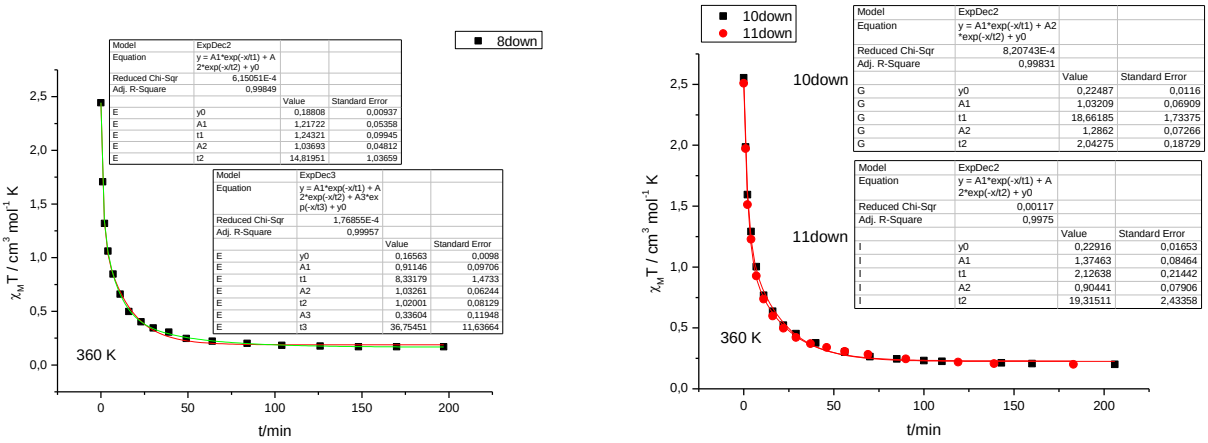

Figure S155. Fitting of kinetic curves for **9** in bi- and triexponential approximations (HS → LS left: cycle 8; right: cycles 10 and 11).

Sample 15

Parent phase $\mathbf{1^{LS} \cdot EtOH \cdot H_2O}$.

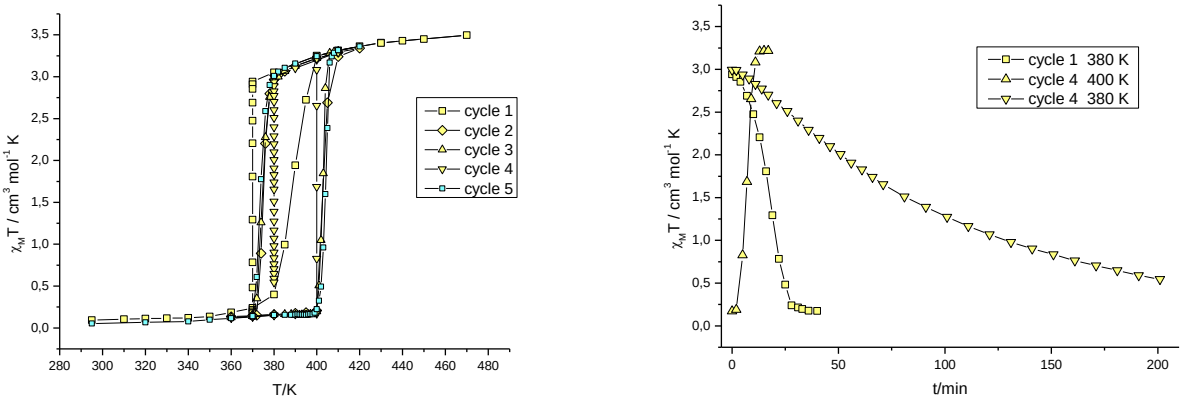

Figure S156. Sample **15**. Thermal cycles 1 – 5 (left) and kinetic curves for the cycles 1 and 4 (LS → HS and HS → LS; right).

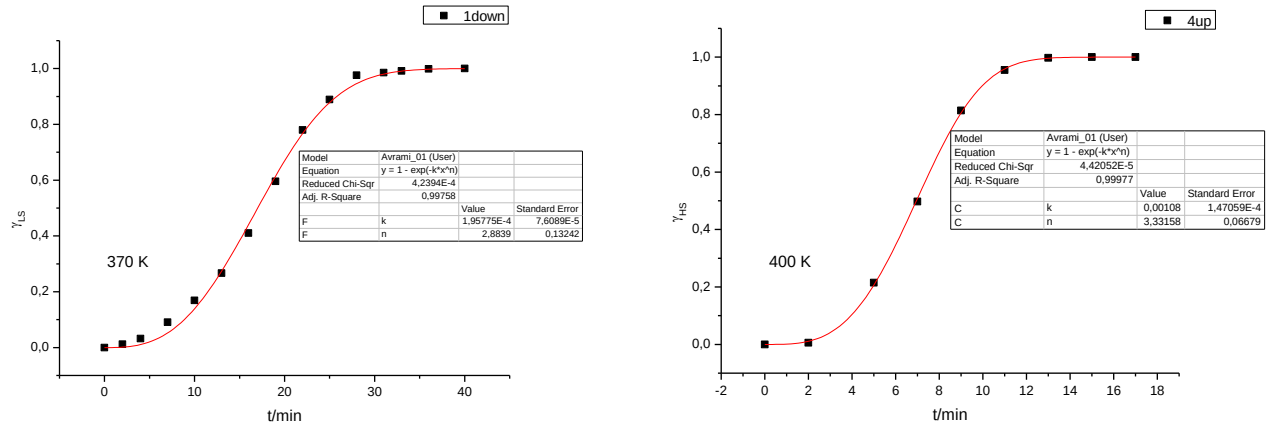

Figure S157. Fitting of kinetic curves for **15** using the JMAK model (left: cycle 1, HS → LS; right: cycle 4, LS → HS).

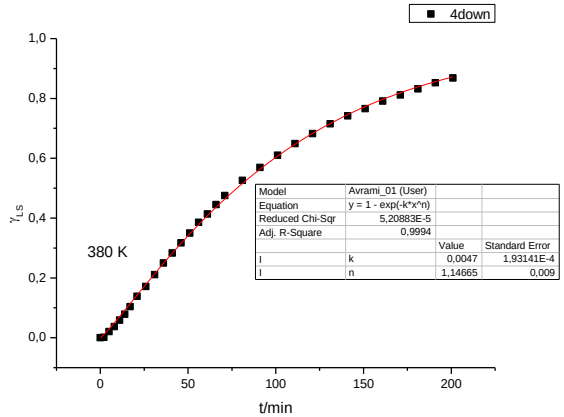

Figure S158. Fitting of a kinetic curve for **15** using the JMAK model (cycle 4, HS → LS).

Sample 16

Parent phase **β-1^{LS}·*x*H$_2$O**. The phase was exposed to water vapor for 2 days. Very slight increase of the mass was detected (*ca*. 1.0 %).

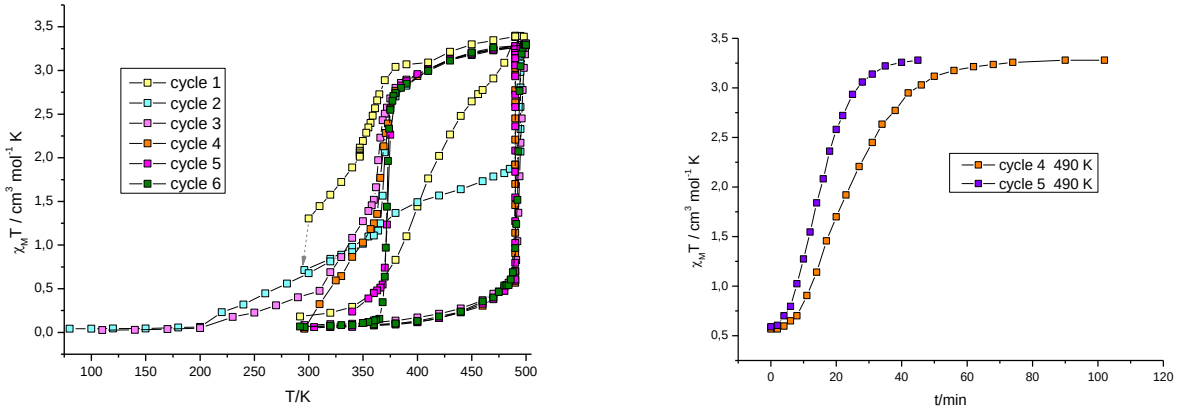

Figure S159. Sample **16**. Thermal cycles 1 – 6 (left) and kinetic curves for the cycles 4 and 5 (LS → HS transformation, right).

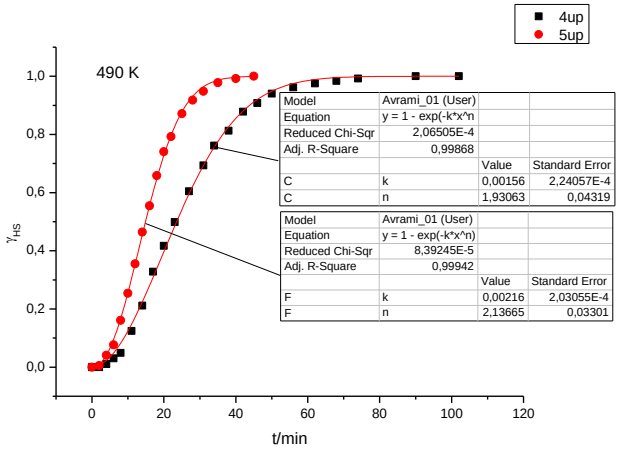

Figure S160. Fitting of kinetic curves for **16** using the JMAK model (LS → HS; cycles 4 and 5).

Sample 17

Parent phase **β-1^{LS}·*x*H$_2$O**. X-ray powder diffraction pattern of the product was recorded immediately after the cycle 1 had been done. It corresponds to the **1^{D}** (see Figure S20).

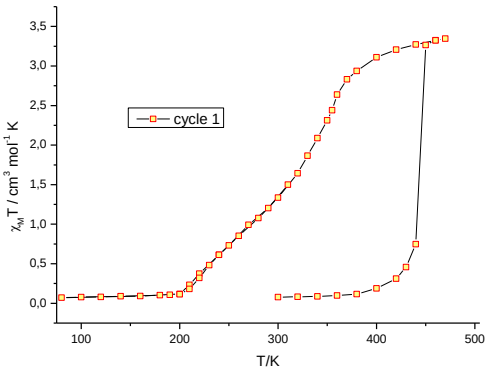

Figure S161. Sample **17**. Thermal cycle 1.

Sample 18

Parent phase **β-1^{LS}·*x*H$_2$O**. X-ray powder diffraction pattern of the product was taken in two days after cycle 1 had been done. It corresponded to a mixture of phases **1^{D}** and **1$^{A/LS}$** (see Figure S20).

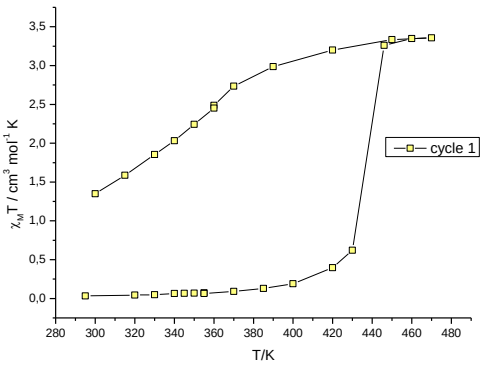

Figure S162. Sample **18**. Thermal cycle 1.

Sample 19

Parent phase $\mathbf{1^{LS}\cdot EtOH\cdot H_2O}$. Magnetic measurements were made under vacuum. X-ray powder diffraction pattern of the product corresponds to the phase $\mathbf{1^{F}}$ (see Figure S20). Weight loss of 8.0 % is consistent with the removal of EtOH and H_2O molecules (calc. for $\mathbf{1^{LS}\cdot EtOH\cdot H_2O}$: 7.8 %)

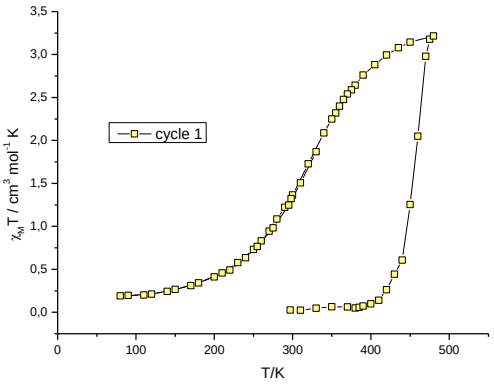

Figure S163. Sample **19**. Thermal cycle 1.

Sample 20

Parent phase $\mathbf{\beta\text{-}1^{LS}\cdot \mathit{x}H_2O}$. Magnetic measurements were made under vacuum. X-ray powder diffraction pattern of the product corresponds to the phase $\mathbf{1^{F}}$. Weight loss of 2.4 % is consistent with the H_2O molecules (calc. for $\mathbf{\beta\text{-}1^{LS}\cdot \mathit{x}H_2O}$ (x = 1): 2.3 %)

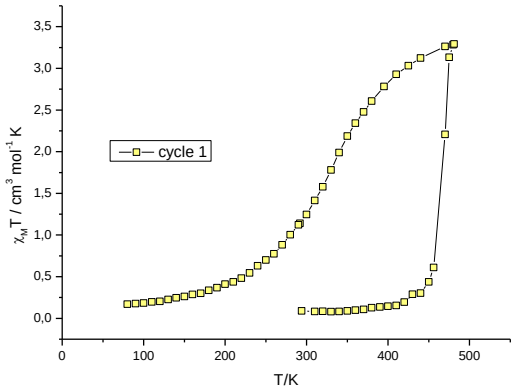

Figure S164. Sample **20**. Thermal cycle 1.

Sample 21

Parent phase **β-1^{LS} · *x*H$_2$O**. The phase was exposed to ethanol vapor for 48 h (mass increase: 4.5 %).

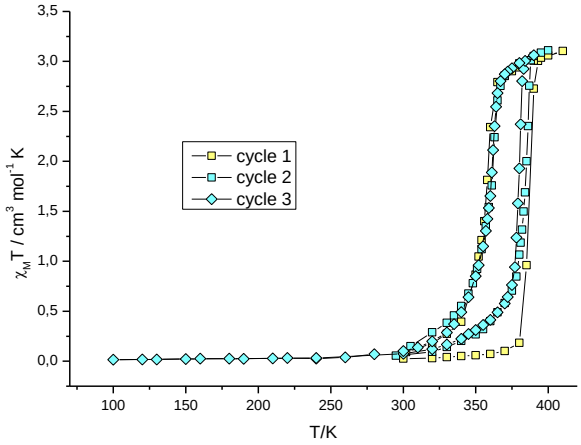

Figure S165. Sample **21**. Thermal cycles 1 – 3.

Elemental analysis of the sample after thermal cycling (%), calcd for $C_{30.8}H_{33.2}N_{10}B_2F_8FeO_{0.8}$ ($[FeL_2](BF_4)_2 \cdot 0.4EtOH \cdot 0.4H_2O$, 785.75): C 47.1, H 4.3, N 17.8; found C 46.5, H 4.0, N 17.3.

A single crystal of the phase **1$^{E/LS}$ · *y*EtOH · *z*H$_2$O** (y = 0.41, z = 0.40) suitable for X-ray analysis was taken from this sample.

Sample 22

Parent phase **1$^{A/LS}$**. Magnetic measurements were made under vacuum.

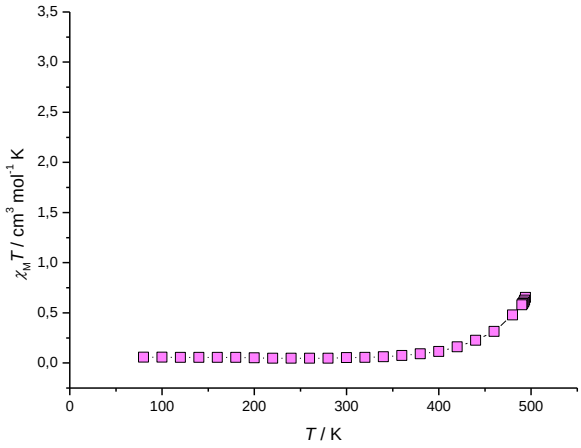

Figure S166. Thermal cycle for the sample **22**. This result agrees with the fact that in TGA experiments made under helium flow the phase **1$^{A/LS}$** shows an endothermic peak only at 529 K (Figure S32).

Sample 23

Parent phase **1**$^{\mathbf{A/LS}}$. Phase purity of the sample was confirmed by XRPD. After that, this sample was kept in dry atmosphere. Measurements were performed in a sealed ampoule.

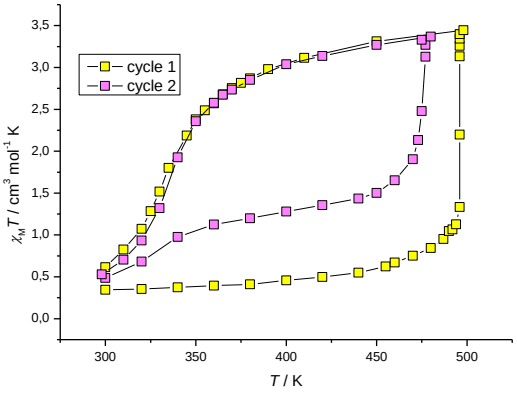

Figure S167. Sample **23**. Thermal cycles 1 and 2. After that, a mixture of the phases **1**$^{\mathbf{A/LS}}$ and **1**$^{\mathbf{B}}$ was detected by XRPD. This behavior is analogous to the behavior of the sample **2-2**. In the first cycle the sample shows high residual magnetic moment in the LS state due to X-ray irradiation (see also samples **12** and **13**).

8. MAGNETIC DATA: MISCELLANEA

Table S2. The *m/V* values (mg/μL), information about thermal cycling, temperatures $T_c\uparrow$ and $T_c\downarrow$ (K), hysteresis loop width ΔT (K) and kinetic parameters for the LS → HS and the HS → LS transitions (JMAK model and biexponential approximation). The spin transition temperatures $T_c\uparrow$ and $T_c\downarrow$ were determined in "dynamic" experiments by the maximum value of $d(\chi_M T)/dT$; the temperatures at which kinetic measurements have been done are marked by "kin". The hysteresis loop widths are given only for the cycles when both heating and cooling were done in "dynamic" mode.

Sample	*m/V*	**cycle**	day	$T_c\uparrow$, **K**	*n*	*k*, s^{-n}	*k*, s^{-1}	$T_c\downarrow$, **K**	$A_1\tau_1$, %	τ_1, s	$A_2\tau_2$, %	τ_2, s	*n*	*k*, s^{-n}	*k*, s^{-1}	**Δ*T***
1	0.0617	**1**	1st	**-**				**360 kin**					2.81	8.40×10^{-10}	5.88×10^{-4}	
		2	1st	**400 kin**	2.29	7.08×10^{-6}	5.65×10^{-3}	**375 kin**	28.3	3.91×10^{2}	71.7	1.86×10^{3}				
		3	1st	**395 kin**	1.90	2.28×10^{-5}	3.63×10^{-3}	**380/379 kin**								
		4	2nd	**399 kin**	2.09	1.68×10^{-5}	5.20×10^{-3}	**374**								
		5	2nd	**395 kin**	1.80	2.13×10^{-5}	2.57×10^{-3}	**374**								
		6	10th	**432**				**366**								**66**
		7	10th	**400**				**370**								**30**
		8	10th	**397 kin**	3.37	1.43×10^{-9}	2.39×10^{-3}	**370**								
		9	137th	**446**				**365**								**81**
		10	137th	**397**				**370**								**27**
		11	137th	**397 kin**	3.06	1.05×10^{-8}	2.47×10^{-3}	**374 kin**	4.0	6.59×10^{1}	96.0	9.85×10^{2}				
		12	259th	**458**				**364**								**94**
		13	259th	**397**				**369**								**28**
		14	259th	**400**				**371**								**29**
		15	343rd	**430**				**367**								**63**
		16	343rd	**399**				**371**								**28**
		17	343rd	**ca. 433**				**366**								**67**
		18	343rd	**399**				**371**								**28**
2	0.0482	**1**	1st	**ca. 385**				**360 kin**					3.18	2.71×10^{-10}	9.83×10^{-4}	
		2	1st	**432**				**371**								**61**
		3	1st	**412 kin**	2.51	1.03×10^{-8}	6.50×10^{-4}	**370 kin**					1.74	2.10×10^{-4}	7.78×10^{-3}	
2-1	0.0374	**4**	7th	**498 kin**	2.42	6.25×10^{-10}	1.56×10^{-4}	**345 kin**								
		5	8th	**475 kin**				**345 kin**								
		6	54th	**476**				**345 kin**								
2-2	0.0330	**7**	56th	**476**				**370**								**106**
		8	57th	**472 kin**	2.90	1.51×10^{-10}	4.15×10^{-4}	**370 kin**					1.58	1.22×10^{-4}	3.39×10^{-3}	
		9	57th	**472 kin**	2.98	2.29×10^{-9}	1.28×10^{-3}	**370 kin**					1.53	2.06×10^{-4}	3.87×10^{-3}	
		10	77th	**472 kin**	3.22	2.14×10^{-10}	9.99×10^{-4}	**370 kin**					1.52	2.69×10^{-4}	4.40×10^{-3}	
		11	77th	**472 kin**	3.13	1.51×10^{-9}	1.53×10^{-3}	**370 kin**					1.50	2.71×10^{-4}	4.27×10^{-3}	

2-3	0.0188	**12**	83rd	**490 kin**	2.71	2.14×10^{-11}	1.15×10^{-4}	**356**								
		13	84th	**490 kin**	3.02	1.11×10^{-8}	2.30×10^{-3}	**360 kin**	2.1	8.75×10^{1}	97.9	2.15×10^{3}				
		14	205th	**494**				**359**								**135**
2-4	0.0152	**1**	97th	**490 kin**	1.74	1.18×10^{-7}	1.02×10^{-4}	**360**								
		2	98th	**490 kin**	2.79	1.30×10^{-8}	1.49×10^{-3}	**360 kin**	4.7	6.96×10^{1}	95.3	2.41×10^{3}				
		3	98th	**490 kin**	2.46	2.95×10^{-7}	2.19×10^{-3}	**365 kin**	5.9	3.91×10^{1}	94.1	1.72×10^{3}				
		4	204th	**495**				**367**								**128**
3	0.0362	**1**	1st	**ca. 385**				**360 kin**					4.40	1.69×10^{-14}	7.37×10^{-4}	
		2	1st	**467 kin**	1.76	7.44×10^{-7}	3.24×10^{-4}	**370 kin**					3.17	4.56×10^{-10}	1.14×10^{-3}	
		3	1st	**467 kin**	1.72	4.91×10^{-6}	8.30×10^{-4}	**370 kin**					3.52	2.90×10^{-11}	1.00×10^{-3}	
		4	4th	**450 kin**	1.73	2.65×10^{-6}	6.08×10^{-4}	**370 kin**					2.47	2.77×10^{-7}	2.22×10^{-3}	
		5	4th	**450 kin**	2.18	5.66×10^{-8}	4.67×10^{-4}	**370 kin**					2.99	2.84×10^{-9}	1.40×10^{-3}	
		6	4th	**467 kin**	2.14	8.79×10^{-7}	1.49×10^{-3}	**370 kin**					3.10	2.68×10^{-10}	8.13×10^{-4}	
		7	9th	**450 kin**	1.77	2.29×10^{-6}	6.60×10^{-4}	**370 kin**					2.47	1.35×10^{-7}	1.67×10^{-3}	
		8	38th	**440 kin**	1.84	6.09×10^{-7}	4.15×10^{-4}	**370 kin**					1.75	2.78×10^{-5}	2.52×10^{-3}	
		9	38th	**467 kin**	1.99	2.12×10^{-6}	1.43×10^{-3}	**370 kin**					2.68	1.17×10^{-8}	1.11×10^{-3}	
		10	39th	**464**				**365**								**99**
		11	86th	**450 kin**	1.97	5.06×10^{-7}	6.30×10^{-4}	**370 kin**					1.69	2.24×10^{-5}	1.77×10^{-3}	
		12	86th	**450 kin**	2.15	8.82×10^{-7}	1.54×10^{-3}	**370 kin**					2.00	2.72×10^{-6}	1.64×10^{-3}	
		13	218th	**466**				**366**								**100**
		14	218th	**460**				**366**								**94**
		15	218th	**460**				**367**								**93**
		16	253rd	**450 kin**	2.06	3.15×10^{-7}	7.10×10^{-4}	**370 kin**					1.46	5.20×10^{-5}	1.17×10^{-3}	
		17	253rd	**450 kin**	2.08	1.79×10^{-7}	5.66×10^{-4}	**370 kin**					2.00	7.76×10^{-6}	2.83×10^{-3}	
4	0.0304	**1**	1st	**ca.445**				**340 kin**					1.31	8.65×10^{-6}	1.39×10^{-4}	
		2	1st	**491 kin**	2.26	7.92×10^{-8}	7.23×10^{-4}	**365 kin**								
		3	6th	**490 kin**	1.85	1.39×10^{-5}	2.35×10^{-3}	**370 kin**	14.9	8.23×10^{1}	85.1	7.62×10^{2}				
		4	6th	**486 kin**	2.07	5.28×10^{-6}	2.83×10^{-3}	**376**								
		5	11th	**481 kin**	2.12	9.74×10^{-7}	1.46×10^{-3}	**376 kin**	7.3	1.57×10^{2}	92.7	1.51×10^{3}				
		6	11th	**480 kin**	2.68	1.24×10^{-8}	1.12×10^{-3}	**382 kin**	2.7	2.86×10^{2}	97.3	3.02×10^{3}				
		7	12th	**480 kin**	1.85	1.38×10^{-5}	2.39×10^{-3}	**377 kin**	11.0	9.52×10^{1}	89.0	2.28×10^{3}				
		8	60th	**480 kin**	3.14	4.43×10^{-10}	1.06×10^{-3}	**377 kin**	9.9	5.88×10^{1}	90.1	6.67×10^{2}				
		9	60th	**480 kin**	3.45	7.99×10^{-11}	1.18×10^{-3}	**377 kin**	20.8	1.37×10^{2}	79.2	1.37×10^{3}				
		10	66th	**484**				**373**								**111**
		11	67th	**476 kin**	2.66	1.43×10^{-8}	1.13×10^{-3}	**377 kin**	2.2	2.05×10^{2}	97.8	2.27×10^{3}				
		12	67th	**476 kin**	2.27	3.13×10^{-7}	1.35×10^{-3}	**377 kin**	18.2	1.00×10^{2}	81.8	1.20×10^{3}				
		13	238th	**484**				**374**								**110**
		14	262nd	**476 kin**	3.51	8.22×10^{-12}	6.89×10^{-4}	**377 kin**	4.0	1.46×10^{2}	96.0	1.79×10^{3}				
		15	262nd	**476 kin**	3.39	2.49×10^{-11}	7.47×10^{-4}	**377 kin**	7.9	1.57×10^{2}	92.1	1.64×10^{3}				
		16	262nd	**476 kin**	3.42	2.20×10^{-11}	7.60×10^{-4}	**377 kin**								
		17	304th	**483**				**373**								**110**
		18	305th	**476 kin**	3.45	4.42×10^{-11}	9.93×10^{-4}	**377 kin**	4.2	1.99×10^{2}	95.8	2.00×10^{3}				

		19	305th	**476 kin**	3.29	1.11×10^{-10}	9.40×10^{-4}	**377 kin**	5.1	8.31×10^{1}	94.9	1.63×10^{3}				
5	0.0388	**1**	1st	**ca. 440**				**ca. 320**								
		2	18th	**ca. 320**				**ca. 320**								
5-1	0.0293	**3**	23rd	**493**				**353**								**140**
		4	25th	**490 kin**	2.16	2.53×10^{-6}	2.57×10^{-3}	**370 kin**			100	6.26×10^{3}				
		5	26th	**486 kin**	2.09	2.51×10^{-6}	2.08×10^{-3}	**366 kin**	6.8	3.30×10^{2}	93.2	2.89×10^{3}				
		6	26th	**482 kin**	3.15	1.22×10^{-10}	7.17×10^{-4}	**370**								
		7	28th	**482 kin**	3.51	2.52×10^{-12}	4.98×10^{-4}	**370**								
		8	28th	**482 kin**	3.82	1.12×10^{-13}	4.10×10^{-4}	**370**								
		9	131st	**486 kin**	3.77	4.89×10^{-13}	5.48×10^{-4}	**373 kin**	16.9	5.19×10^{1}	83.1	4.88×10^{2}				
		10	131st	**486 kin**	3.92	6.28×10^{-13}	7.64×10^{-4}	**373 kin**	32.0	9.35×10^{1}	68.0	1.07×10^{3}				
		11	131st	**486 kin**	3.99	9.61×10^{-14}	5.49×10^{-4}	**373 kin**								
		12	168th	**494**				**370**								**124**
		13	309th	**486 kin**	4.00	1.17×10^{-13}	5.84×10^{-4}	**373 kin**	29.8	1.96×10^{2}	70.2	1.50×10^{3}				
		14	309th	**486 kin**	3.65	8.24×10^{-13}	4.84×10^{-4}	**373 kin**	25.5	2.39×10^{2}	74.5	1.67×10^{3}				
		15	388th	**491**				**371**								**120**
		16	393rd	**487**				**372**								**115**
6	0.0279	**1**	1st	**ca. 400**			**-**									
		2	2nd	**-**			**-**									
		3	3rd	**486**				**367**								**119**
		4	3rd	**477**				**369**								**108**
		5	3rd	**471**				**369**								**102**
		6	34th	**450 kin**	1.87	1.47×10^{-6}	7.60×10^{-4}	**374 kin**					1.88	6.71×10^{-6}	1.78×10^{-3}	
		7	34th	**450 kin**	2.14	1.12×10^{-7}	5.64×10^{-4}	**374 kin**					2.04	2.51×10^{-6}	1.78×10^{-3}	
		8	152th	**467**				**368**								**99**
		9	153rd	**450 kin**	1.94	1.05×10^{-6}	8.27×10^{-4}	**374 kin**					1.71	1.16×10^{-5}	1.30×10^{-3}	
		10	153rd	**450 kin**	2.31	3.00×10^{-8}	5.56×10^{-4}	**374 kin**					1.89	3.28×10^{-6}	1.24×10^{-3}	
		11	153rd	**470**				**368**								**102**
7	0.0273	**1**	1st	**-**				**360 kin**					1.56	1.89×10^{-5}	9.45×10^{-4}	
		2	1st	**490 kin**	2.37	1.60×10^{-7}	1.37×10^{-3}	**363 kin**					1.87	7.69×10^{-5}	6.24×10^{-3}	
		3	1st	**490 kin**	1.87	1.14×10^{-5}	2.30×10^{-3}	**365 kin**					2.82	1.30×10^{-7}	3.65×10^{-3}	
		4	3rd	**480 kin**	2.09	1.47×10^{-6}	1.59×10^{-3}	**370 kin**					2.58	4.60×10^{-8}	1.42×10^{-3}	
		5	4th	**472 kin**	2.52	2.19×10^{-8}	9.26×10^{-4}	**372 kin**					1.35	1.16×10^{-4}	1.20×10^{-3}	
		6	4th	**472 kin**	2.32	1.07×10^{-7}	9.79×10^{-4}	**370 kin**					1.56	1.29×10^{-4}	3.18×10^{-3}	
		7	11th	**476**				**367**								**109**
		8	12th	**475**				**367**								**108**
		9	13th	**460 kin**	1.97	5.74×10^{-7}	6.77×10^{-4}	**373 kin**					1.42	4.72×10^{-6}	1.72×10^{-4}	
		10	13th	**460 kin**	2.14	3.56×10^{-8}	3.33×10^{-4}	**371 kin**					2.16	4.67×10^{-8}	4.07×10^{-4}	
		11	210th	**460 kin**	2.19	2.66×10^{-8}	3.51×10^{-4}	**370 kin**					2.34	3.11×10^{-6}	4.41×10^{-3}	
		12	210th	**460 kin**	2.27	1.75×10^{-8}	3.81×10^{-4}	**370 kin**					2.50	7.55×10^{-7}	3.59×10^{-3}	
8	0.0226	**1**	1st	**-**				**ca. 360**								
		2	1st	**490 kin**	1.88	1.83×10^{-6}	8.80×10^{-4}	**370 kin**					1.15	5.88×10^{-4}	1.54×10^{-3}	

		3	3rd	**490 kin**	1.85	5.58×10^{-6}	1.43×10^{-3}	**370 kin**					3.28	6.46×10^{-10}	1.57×10^{-3}	
		4	3rd	**490 kin**	2.09	9.76×10^{-6}	3.98×10^{-3}	**370 kin**					2.79	1.45×10^{-8}	1.57×10^{-3}	
		5	3rd	**490 kin**	1.35	1.54×10^{-3}	8.18×10^{-3}	**370 kin**					2.83	8.00×10^{-9}	1.38×10^{-3}	
		6	3rd	**487**				**367**								**120**
9	0.0181	**1**	1st	**ca. 450**				**350**								
		2	2nd	**494 kin**	2.20	6.89×10^{-8}	5.63×10^{-4}	**365 kin**								
		3	2nd	**490 kin**	2.37	1.38×10^{-6}	3.40×10^{-3}	**372**								
		4	8th	**492 kin**	3.16	3.62×10^{-10}	1.03×10^{-3}	**370 kin**	2.3	5.61×10^{1}	97.7	1.47×10^{3}				
		5	9th	**492 kin**	3.30	1.03×10^{-10}	9.40×10^{-4}	**367**								
		6	116th	**492 kin**	2.77	6.64×10^{-9}	1.12×10^{-3}	**370 kin**	1.9	3.07×10^{1}	98.1	1.12×10^{3}				
		7	117th	**492 kin**	3.67	4.34×10^{-11}	1.51×10^{-3}	**370 kin**	1.8	3.64×10^{1}	98.2	1.18×10^{3}				
		8	117th	**492 kin**	2.45	1.38×10^{-6}	4.07×10^{-3}	**370 kin**	3.8	4.37×10^{1}	96.2	9.74×10^{2}				
		9	117th	**490 kin**	2.26	4.05×10^{-6}	4.15×10^{-3}	**370 kin**	5.1	5.07×10^{1}	94.9	1.01×10^{3}				
		10	118th	**490 kin**	3.50	8.44×10^{-11}	1.31×10^{-3}	**370 kin**	8.2	2.31×10^{2}	91.8	1.86×10^{3}				
		11	118th	**490 kin**	2.44	1.25×10^{-6}	3.78×10^{-3}	**370 kin**	3.5	3.87×10^{1}	96.5	9.40×10^{2}				
		12	123rd	**490 kin**	3.98	5.35×10^{-12}	1.47×10^{-3}	**370 kin**	5.3	9.43×10^{1}	94.7	1.46×10^{3}				
		13	123rd	**490 kin**	3.56	4.80×10^{-10}	2.42×10^{-3}	**370 kin**	4.8	8.24×10^{1}	95.2	1.59×10^{3}				
		14	171st	**494**				**367**								**127**
		15	173rd	**490 kin**	3.63	5.61×10^{-11}	1.50×10^{-3}	**370 kin**	7.4	6.53×10^{2}	92.6	5.54×10^{3}				
		16	173rd	**490 kin**	3.05	4.05×10^{-8}	3.80×10^{-3}	**367 kin**	6.6	4.96×10^{1}	93.4	9.76×10^{2}				
		17	173rd	**490 kin**	2.91	2.49×10^{-7}	5.35×10^{-3}	**368 kin**	3.9	2.89×10^{1}	96.1	9.38×10^{2}				
		18	174th	**490 kin**	3.51	2.60×10^{-10}	1.85×10^{-3}	**368 kin**	5.7	1.67×10^{2}	94.3	2.19×10^{3}				
		19	174th	**490 kin**	3.28	2.69×10^{-9}	2.42×10^{-3}	**368 kin**								
		20	175th	**486 kin**	3.52	1.27×10^{-11}	8.00×10^{-4}	**366 kin**	2.8	3.21×10^{1}	97.2	1.32×10^{3}				
		21	175th	**486 kin**	3.14	3.66×10^{-10}	9.91×10^{-4}	**366 kin**	5.1	7.03×10^{1}	94.9	1.95×10^{3}				
		22	203th	**490 kin**	3.00	2.23×10^{-9}	1.30×10^{-3}	**370 kin**	1.2	1.21×10^{2}	98.8	3.23×10^{3}				
		23	203th	**490 kin**	2.40	4.08×10^{-7}	2.18×10^{-3}	**370 kin**	1.9	3.26×10^{1}	98.1	1.87×10^{3}				
		24	208th	**482 kin**	3.71	7.10×10^{-14}	2.83×10^{-4}	**366 kin**	6.0	5.65×10^{1}	94.0	1.61×10^{3}				
		25	208th	**482 kin**	2.75	1.47×10^{-9}	6.14×10^{-4}	**366 kin**	5.4	3.02×10^{1}	94.6	1.26×10^{3}				
		26	211th	**488 kin**	1.80	9.12×10^{-6}	1.60×10^{-3}	**366 kin**	4.5	4.78×10^{1}	95.5	1.60×10^{3}				
		27	211th	**488 kin**	1.75	3.00×10^{-5}	2.60×10^{-3}	**366 kin**	2.5	3.38×10^{1}	97.5	2.24×10^{3}				
		28	327th	**493**				**364**								**129**
		29	373rd	**486 kin**	2.75	3.79×10^{-9}	8.55×10^{-4}	**366 kin**	3.8	5.77×10^{1}	96.2	1.89×10^{3}				
		30	373rd	**486 kin**	1.80	1.11×10^{-5}	1.75×10^{-3}	**366 kin**	3.6	3.79×10^{1}	96.4	1.63×10^{3}				
		31	373rd	**486 kin**	1.69	4.21×10^{-5}	2.61×10^{-3}	**366 kin**								
		32	450th	**482 kin**	3.20	8.94×10^{-12}	3.53×10^{-4}	**370 kin**	0.5	5.90×10^{1}	99.5	5.82×10^{3}				
		33	450th	**482 kin**	2.16	1.29×10^{-7}	6.49×10^{-4}	**370 kin**	2.1	5.93×10^{1}	97.9	2.95×10^{3}				
		34	491st	**493**	2.75	3.79×10^{-9}		**363**								**130**
		35	527th	**484 kin**	2.50	5.99×10^{-9}	5.14×10^{-4}	**370 kin**	0.6	3.20×10^{1}	99.4	5.34×10^{3}				
		36	527th	**484 kin**	2.21	2.22×10^{-7}	9.92×10^{-4}	**370 kin**								
10	0.0354	**1**	1st	**ca. 405**				**353**								**52**
		2	3rd	**374**				**350**								**24**

		3	5th	**378**				**355**								**23**
10-1	0.0162	**4**	30th	**ca. 420**				**ca. 320**								
		5	37th	**490 kin**	2.56	4.46×10^{-9}	5.42×10^{-4}	**377**								
		6	37th	**490 kin**	3.31	1.16×10^{-9}	1.98×10^{-3}	**378**								
		7	39th	**490 kin**	2.56	3.63×10^{-8}	1.24×10^{-3}	**378**								
		8	40th	**490 kin**	3.65	2.05×10^{-11}	1.18×10^{-3}	**377 kin**	6.8	3.93×10^{1}	93.2	8.06×10^{2}				
		9	40th	**490 kin**	4.07	2.69×10^{-12}	1.44×10^{-3}	**377 kin**	12.4	5.93×10^{1}	87.6	7.69×10^{2}				
		10	45th	**495**				**377**								**118**
11	0.0137	**1**	1st	**ca. 395**				**ca. 355**								
		2	5th	**ca. 405**				**ca. 360**								
		3	6th	**490 kin**	1.94	4.96×10^{-7}	5.60×10^{-4}	**370 kin**	2.4	8.14×10^{1}	97.6	4.07×10^{2}	0.83	7.03×10^{-3}	2.47×10^{-3}	
		4	6th	**490 kin**	1.90	1.11×10^{-5}	2.47×10^{-3}	**370 kin**	56.3	1.14×10^{2}	43.7	4.55×10^{2}	0.88	1.26×10^{-2}	7.15×10^{-3}	
		5	6th	**490 kin**	1.92	1.87×10^{-5}	3.45×10^{-3}	**370 kin**	35.3	6.46×10^{1}	64.7	2.30×10^{2}	0.73	3.29×10^{-2}	9.46×10^{-3}	
		6	6th	**488**				**371**								**117**
12		**1**	1st	**ca. 455**				**ca. 330**								
12-1	0.0128	**2**	281st	**490 kin**	1.63	1.23×10^{-7}	5.76×10^{-5}	**350**								
		3	282nd	**490 kin**	1.96	5.55×10^{-9}	6.20×10^{-5}	**354**								
		4	283rd	**490 kin**	2.00	2.31×10^{-6}	1.52×10^{-3}	**357 kin**	9.4	6.49×10^{2}	90.6	4.46×10^{3}				
		5	283rd	**490 kin**	2.24	1.66×10^{-7}	9.51×10^{-4}	**357 kin**	8.5	6.62×10^{2}	91.5	5.53×10^{3}				
		6	284th	**490 kin**	2.48	1.91×10^{-8}	7.62×10^{-4}	**355 kin**	8.3	2.31×10^{2}	91.7	2.07×10^{3}				
		7	284th	**490 kin**	2.13	2.46×10^{-7}	8.03×10^{-4}	**355 kin**	8.6	3.33×10^{2}	91.4	3.01×10^{3}				
		8	290th	**490 kin**	2.01	6.42×10^{-7}	8.19×10^{-4}	**353 kin**	11.0	2.55×10^{2}	89.0	3.12×10^{3}				
		9	290th	**490 kin**	2.16	3.86×10^{-7}	1.06×10^{-3}	**353 kin**								
		10	369th	**490 kin**	2.35	3.52×10^{-8}	6.71×10^{-4}	**353 kin**	8.6	2.17×10^{2}	91.4	2.33×10^{3}				
		11	369th	**490 kin**	1.88	2.31×10^{-6}	1.01×10^{-3}	**353 kin**								
		12	393rd	**495**				**350**								**145**
		13	409th	**490 kin**	1.85	1.56×10^{-6}	7.24×10^{-4}	**353 kin**	6.5	2.73×10^{2}	93.5	2.96×10^{3}				
		14	409th	**490 kin**	1.58	1.74×10^{-5}	9.69×10^{-4}	**353 kin**								
		15	466th	**490 kin**	1.82	1.90×10^{-6}	7.18×10^{-4}	**353 kin**	6.5	4.48×10^{2}	93.5	6.11×10^{3}				
		16	473rd	**495**				**350**								**145**
		17	553rd	**490 kin**	1.75	2.85×10^{-6}	6.81×10^{-4}	**353 kin**	5.2	3.66×10^{2}	94.8	4.51×10^{3}				
		18	553rd	**490 kin**	1.60	1.80×10^{-5}	1.06×10^{-3}	**353 kin**								
		19	609th	**491**				**351**								**140**
		20	609th	**490**				**351**								**139**
		21	613th	**488**				**350**								**138**
13	0.0075	**1**	1st	**490 kin**	2.56	1.78×10^{-9}	3.80×10^{-4}	**353**								
		2	2nd	**490 kin**	3.47	9.01×10^{-11}	1.28×10^{-3}	**353 kin**	14.4	7.63×10^{1}	85.6	1.85×10^{3}				
		3	2nd	**490 kin**	3.84	8.22×10^{-12}	1.31×10^{-3}	**353 kin**	10.2	6.37×10^{1}	89.8	2.12×10^{3}				
		4	29th	**493**				**355**								**138**
		5	42nd	**490 kin**	3.86	8.44×10^{-13}	7.44×10^{-4}	**353 kin**	11.7	7.75×10^{1}	88.3	2.19×10^{3}				
		6	42nd	**490 kin**	2.71	1.59×10^{-8}	1.32×10^{-3}	**353 kin**								
		7	42nd	**490 kin**	2.28	5.75×10^{-7}	1.82×10^{-3}	**353 kin**								

14	0.0545	**1**	1st	**ca. 390**				**370 kin**					2.75	6.04×10^{-9}	1.03×10^{-3}	
		2	1st	**425**				**372**								**53**
		3	1st	**402**				**375**								**27**
		4	1st	**407**				**375**								**32**
		5	134th	**401**				**374**								**27**
		6	134th	**405**				**375**								**30**
14-1	0.0177	**7**	179th	**490 kin**	1.85	6.08×10^{-8}	1.26×10^{-4}	**358**								
		8	180th	**490 kin**	2.33	1.22×10^{-6}	2.91×10^{-3}	**360 kin**	9.2	7.46×10^{1}	90.8	8.89×10^{2}				
		9	180th	**492**				**361**								**131**
		10	187th	**490 kin**	3.20	2.42×10^{-9}	2.02×10^{-3}	**360 kin**	12.0	1.23×10^{2}	88.0	1.12×10^{3}				
		11	187th	**490 kin**	3.11	8.78×10^{-9}	2.58×10^{-3}	**360 kin**	14.3	1.28×10^{2}	85.7	1.16×10^{3}				
		12	242nd	**480 kin**	3.72	8.54×10^{-15}	1.64×10^{-4}									
		13	242nd	**480 kin**	4.17	1.23×10^{-15}	2.67×10^{-4}	**362**								
		14	256th	**470 kin**	4.26	2.65×10^{-20}	2.52×10^{-5}									
		15	263rd	**460 kin**												
15	0.0521	**1**	1st	**390**				**380 kin**					2.88	1.46×10^{-9}	8.63×10^{-4}	
		2	1st	**403**				**375**								**28**
		3	1st	**403**				**374**								**29**
		4	1st	**400 kin**	3.33	1.28×10^{-9}	2.15×10^{-3}	**380 kin**					1.15	4.31×10^{-5}	1.55×10^{-4}	
		5	14th	**405**				**374**								**31**
16	0.0217	**1**	1st	**ca. 400**												
		2	7th	**495**				**368**								**127**
		3	10th	**495**				**364**								**131**
		4	11th	**490 kin**	1.93	5.75×10^{-7}	5.86×10^{-4}	**366**								
		5	12th	**490 kin**	2.14	3.42×10^{-7}	9.43×10^{-4}	**372**								
		6	282nd	**493**				**372**								**121**

Table S3. HS → LS transitions. Triexponential approximation. Selected curves.

Sample	Cycle	$A_1\tau_1$, %	τ_1, s	$A_2\tau_2$, %	τ_2, s	$A_3\tau_3$, %	τ_3, s
12-1	**7**	3.9	2.54×10^{2}	18.2	1.22×10^{3}	77.9	4.90×10^{3}
	10	0.4	4.47×10^{1}	10.6	3.41×10^{2}	89.0	3.06×10^{3}
	13	2.2	1.84×10^{2}	11.8	8.63×10^{2}	86.0	4.47×10^{3}
	15	1.6	2.30×10^{2}	12.4	1.46×10^{3}	85.9	9.38×10^{3}
	17	0.5	1.03×10^{2}	10.1	8.80×10^{2}	89.4	6.01×10^{3}
9	**32**	0.1	3.49×10^{1}	2.0	8.56×10^{2}	97.9	1.18×10^{4}
	33	0.1	4.43×10^{1}	6.3	7.14×10^{2}	93.6	6.22×10^{3}
2-3	**13**	0.2	2.09×10^{1}	6.8	4.43×10^{2}	93.0	3.91×10^{3}
2-4	**2**	1.5	4.81×10^{1}	5.9	4.08×10^{2}	92.7	5.03×10^{3}
	3	2.0	3.44×10^{1}	9.5	6.40×10^{2}	88.5	5.83×10^{3}

Evolution of the Avrami exponent

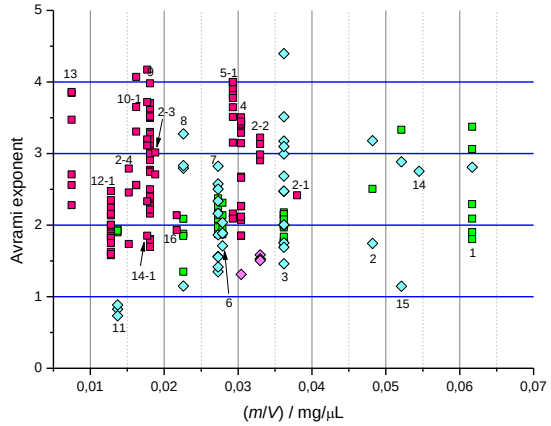

Figure S168. Values of the Avrami exponent *n* for the $\mathbf{1}^{\mathbf{A/LS}} \rightarrow \mathbf{1}^{\mathbf{A/HS}}$ (squares) and $\mathbf{1}^{\mathbf{A/HS}} \rightarrow \mathbf{1}^{\mathbf{A/LS}}$ (diamonds) transitions. Pink and light pink: parent phases $\boldsymbol{\beta}\textbf{-}\mathbf{1}^{\mathbf{LS}} \cdot \boldsymbol{x}\mathbf{H_2O}$ and $\mathbf{1}^{\mathbf{A/LS}}$. Green and cyan: parent phase $\mathbf{1}^{\mathbf{LS}} \cdot \mathbf{EtOH} \cdot \mathbf{H_2O}$.

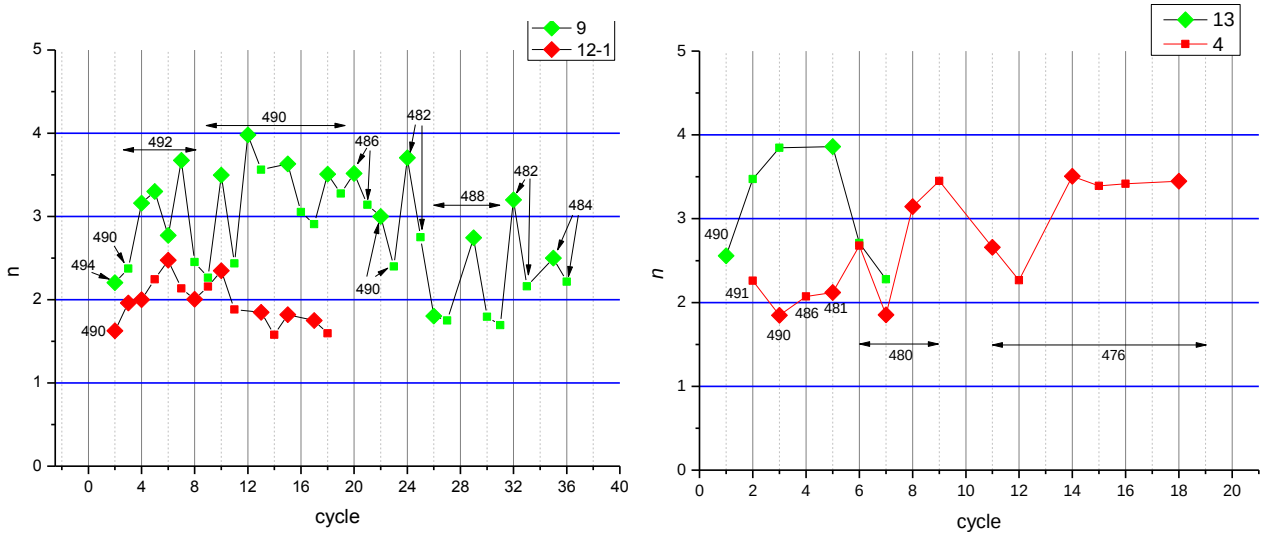

Figure S169. Evolution of the Avrami exponent *n* for the $\mathbf{1}^{\mathbf{A/LS}} \rightarrow \mathbf{1}^{\mathbf{A/HS}}$ transition (samples **9**, **12-1**, **13** and **4**; diamands: the first cycle a day (or the sole cycle)).

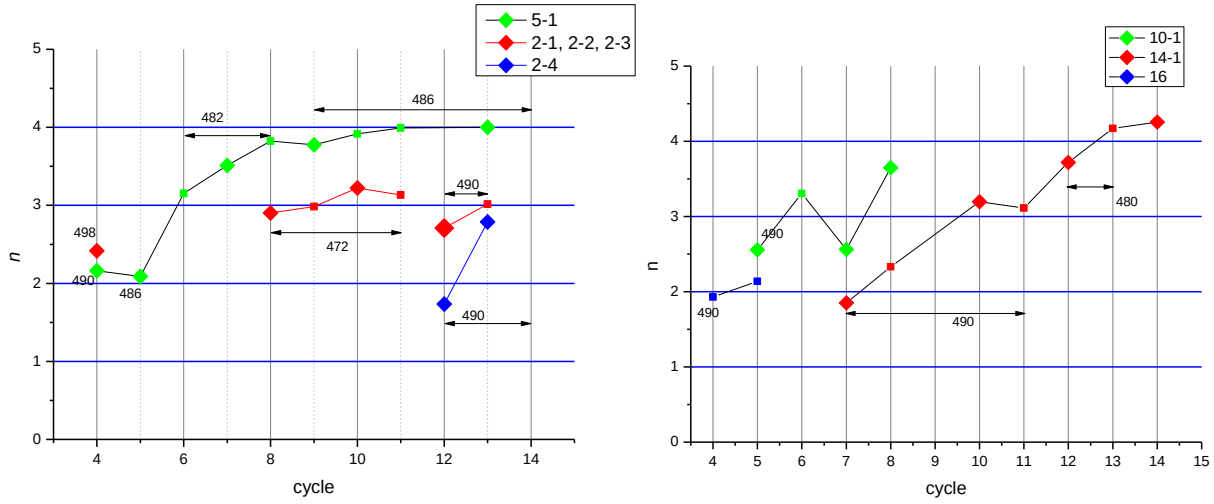

Figure S170. Evolution of the Avrami exponent *n* for the $\mathbf{1}^{\mathbf{A/LS}} \rightarrow \mathbf{1}^{\mathbf{A/HS}}$ transition (samples **5-1**, **2-1**, **2-2**, **2-3**, **2-4**, **10-1**, **14-1** and **4**; diamands: the first cycle a day (or the sole cycle)).

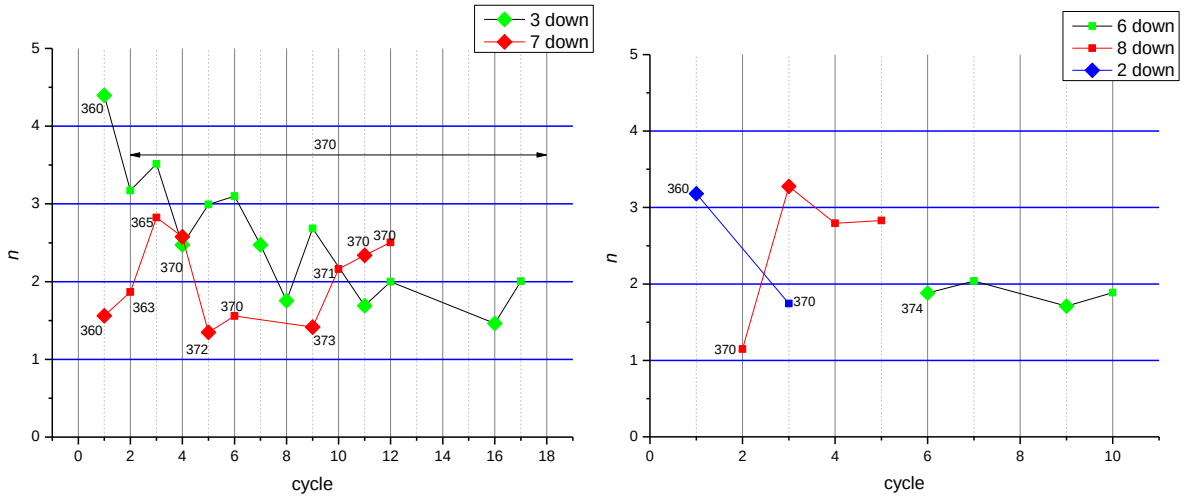

Figure S171. Evolution of the Avrami exponent *n* for the $\mathbf{1}^{\mathbf{A/HS}} \rightarrow \mathbf{1}^{\mathbf{A/LS}}$ transition (samples **3**, **7**, **2-2**, **6**, **8** and **2**; diamands: the first cycle a day (or the sole cycle)).

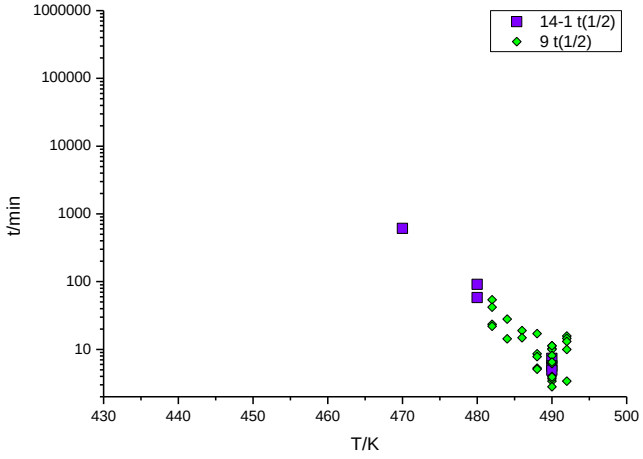

Figure S172. Half-time–Temperature–Transformation diagram for the $\mathbf{1}^{\mathbf{A/LS}} \rightarrow \mathbf{1}^{\mathbf{A/HS}}$ conversion (the samples **9** and **14-1**).

Activation energy

1) Magnetochemistry: Kinetic analysis under isothermal conditions

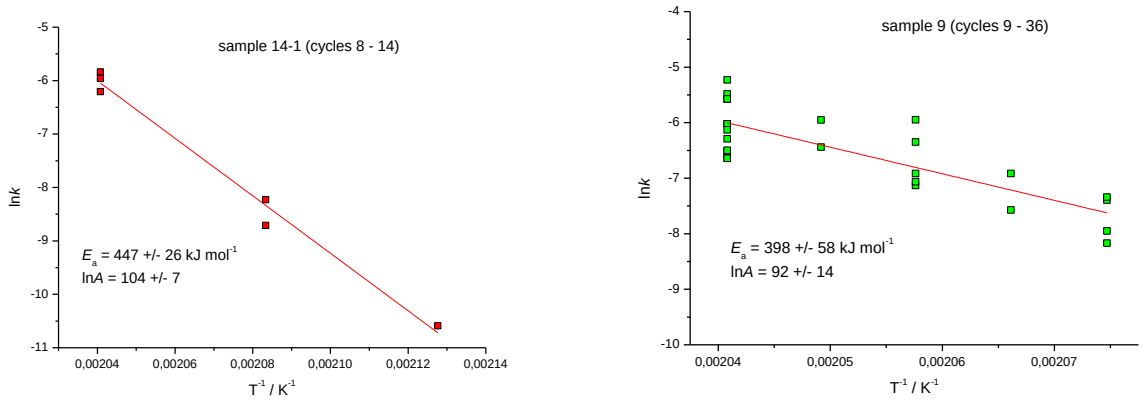

Figure S173. Left: Arrhenius plot for the sample **14-1**. Right: Arrhenius plot for the sample **9**.

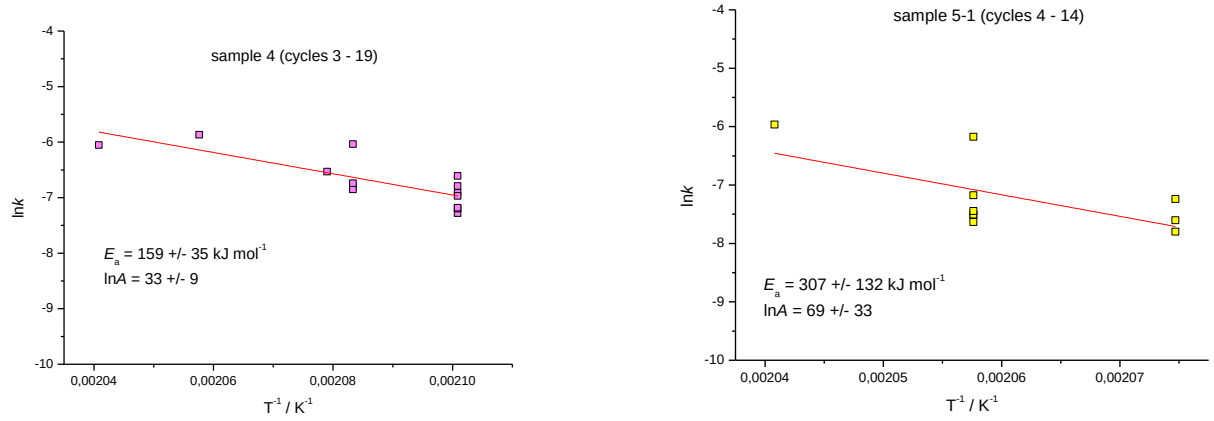

Figure S174. Left: Arrhenius plot for the sample **4**. Right: Arrhenius plot for the sample **5-1**.

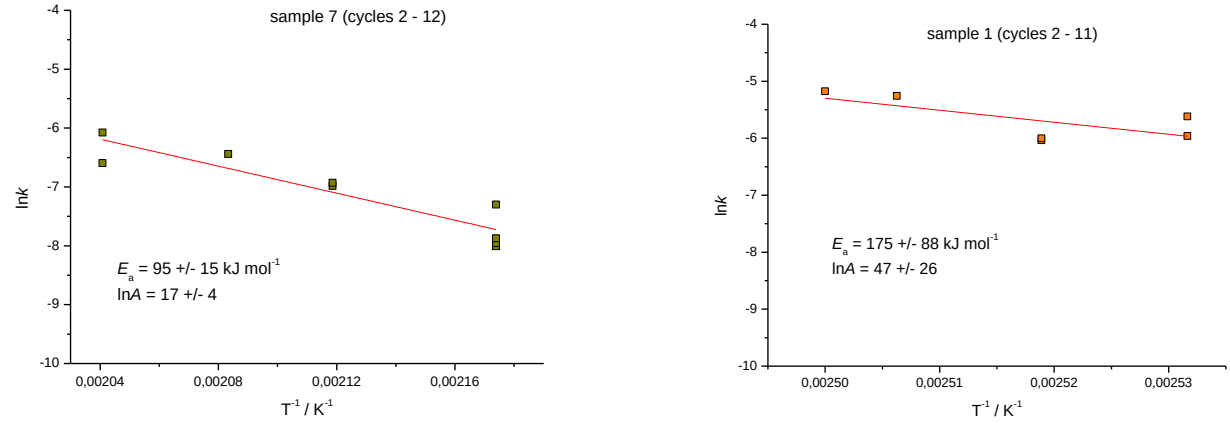

Figure S175. Left: Arrhenius plot for the sample **7**. Right: Arrhenius plot for the sample **1**.

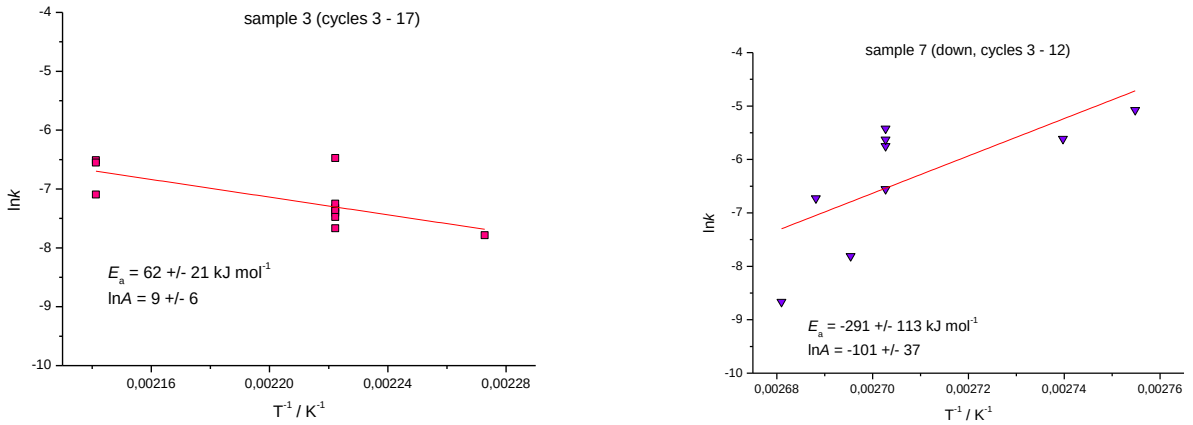

Figure S176. Left: Arrhenius plot for the sample **3**. Right: Arrhenius plot for the sample **7** (HS → LS).

2) Magnetochemistry: Kinetic analysis under non-isothermal conditions

In principle, the activation energy of the spin transition can be estimated using various methods of kinetic analysis of non-isothermal data (*e.g.* the Ozawa model, the Kissinger model, the Friedman model, *etc*). In this case the heating runs should be performed at several different heating rates varying from slow (from *ca*. 1 K min^{-1}) to fast ones (up to 10 – 40 K min^{-1}). Although we made a series of measurements at three different slow scan rates not exceeding 0.9 K min^{-1} only (which may lead to high errors when estimating the activation barrier height) we roughly estimated the activation energy of the $\mathbf{1}^{\mathbf{A/LS}} \rightarrow \mathbf{1}^{\mathbf{A/HS}}$ transition for the samples **5-1** and **12-1** using the Ozawa equation[S3]

$$ln\beta = const - 1.052\frac{E_a}{R}\frac{1}{T_c}$$

where β is heating rate and T_c is the spin transition temperature determined by the maximum value of $d(\chi_M T)/dT$. The activation energy appeared to be *ca*. 340 – 350 kJ mol^{-1} for both samples. This value is in good agreement with the values calculated using isothermal magnetic data.

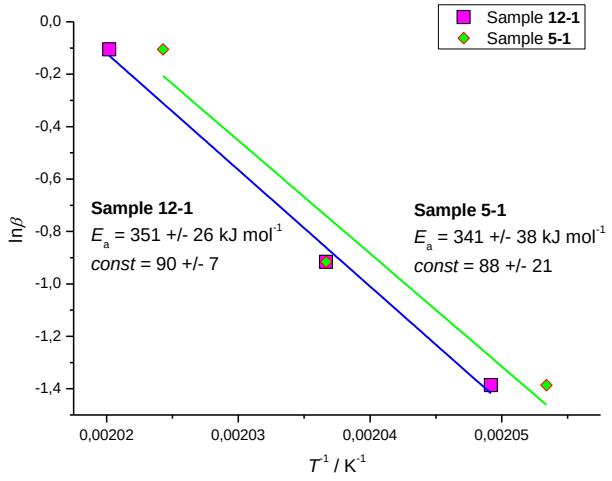

Figure S177. Ozawa plot for the samples **5-1** and **12-1**.

S3 T. Ozawa, *J. Therm. Anal.*, 1970, **2**, 301 – 324.

3) DSC: Kinetic analysis under non-isothermal conditions

DSC data were processed with the computer program Netzsch Thermokinetics 2 (Version 2004.05).[S3] We used the experimental DSC data to search for the corresponding topochemical equation (the selection was made from different equations: chemical reaction at the interface, nucleation and diffusion). This calculation was made by the improved differential procedure of Borchardt–Daniels.[S4,S5] The *F* test[S4] was used to search for the best kinetic description and for statistical control of the obtained equation. It tests the residual variance of individual models against one another and answers the question of whether the models differ significantly (statistically) or not. The statistical quantile F_{crit} is obtained for a level of significance of 0.05.

The first three equations: CnB, C1B and B1 (Table S4) describe the processes with the acceleration.

Table S4.

F_{crit}	F_{exp}	F_{act}	Equation
1.23	1.00	260	CnB
1.23	1.16	261	C1B
1.23	2.45	260	Bna
1.23	3.63	261	Fn
1.23	3.65	261	An
1.23	6.56	262	D3
1.23	6.88	262	B1
1.23	14.78	262	D4
1.23	51.18	262	D1

The used topochemical equations are: reactions with autocatalysis (CnB and C1B), different type of diffusion (D1, D3, D4), *n*-th order (Fn), Avrami-Erofeev (An), Prout–Tompkins (BnA and B1) equations.[S4]

Data on the *F* test of fit quality was considered and partially used to identify the best kinetic description.

The best description is the equation CnB:

$f(\alpha) = (1–\alpha)^{0.9}\cdot(1 + 14\cdot\alpha)$. $E = 427 \pm 1$ kJ mol^{-1}; lg $A = 42.9 \pm 1$.

Corr. coeff. = 0.998770.

The best description is the equation C1B:

$f(\alpha) = (1–\alpha)\cdot(1 + 7\cdot\alpha)$. $E = 552 \pm 1$ kJ mol^{-1}; lg $A = 56.5 \pm 1$.

Corr. coeff. = 0.998564.

We observed high values of the pre-exponential factor. In this context it should be noted that for such phase transformations as the phase transformation monoclinic sulfur → rhombic sulfur or the recrystallization of Al the amount of instantly reacting molecules is estimated as 10^7, and the reacting crystal volume is estimated as 10^{-15} cm^3.[S6] This can explain the high values of calculated pre-exponential factors for the phase transformation $\mathbf{1}^{\mathbf{A/LS}} \rightarrow \mathbf{1}^{\mathbf{A/HS}}$.

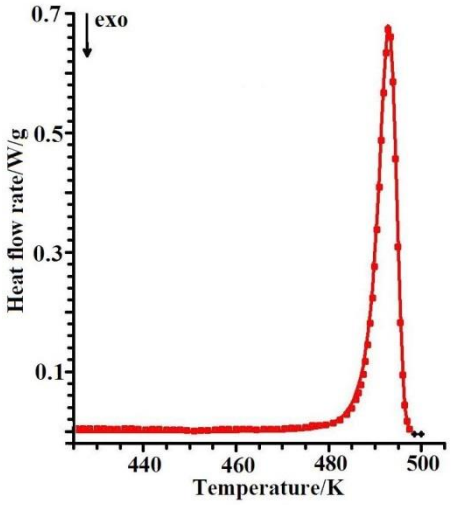

Figure S178. Data processing for the thermal phase transformation. DSC curve fitting of linear regression, simulated with single-step reaction (CnB). The *points* are the experimental data; the *lines* are the calculated data. The heating rate was 6 K min^{-1}.

S4 Netzsch Thermokinetics. http://www.netzsch-thermal-analysis.com/us/products-%20%20solutions/advanced-software/thermokinetics.html

S5 H. J. Borchard and F. Daniels, The application of differential thermal analysis to the study of reaction kinetics. *J. Am. Chem. Soc*., 1957, **79**, 41–46.

S6 N. N. Hartshorne, *Discuss. Faraday Soc*., 1945, **5**, 149.

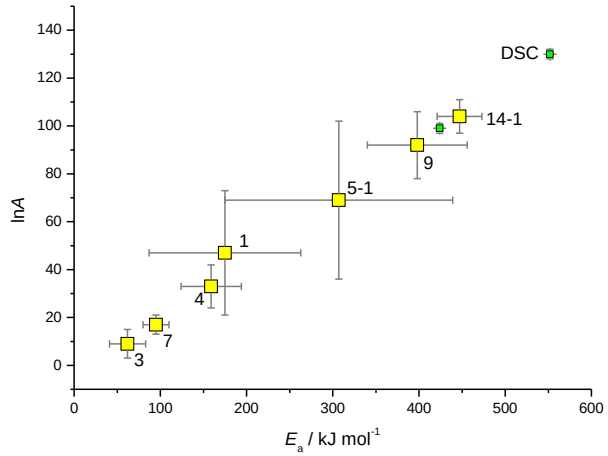

Figure S179. Compensation effect for the transition $\mathbf{1}^{\mathbf{A/LS}} \rightarrow \mathbf{1}^{\mathbf{A/HS}}$. Yellow: isothermal magnetic data. Green: non-isothermal DSC data.

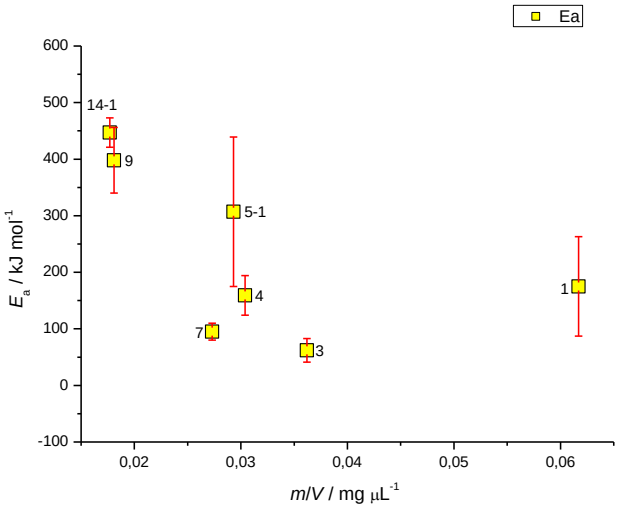

Figure S180. Dependence of the activation energy on the m/V ratio.